2006/2 vol.3

ACTA GEOTECHNICA SLOVENICA

2006/2

ISSN 1854-0171

ACTA GEOTECHNICA SLOVENICA

ISSN: 1854-0171

ustanovitelji | **founders**

Univerza v Mariboru, Fakulteta za gradbeništvo
University of Maribor, Faculty of Civil Engineering

Univerza v Ljubljani, Fakulteta za gradbeništvo in geodezijo
University of Ljubljana, Faculty of Civil
and Geodetic Engineering

Univerza v Ljubljani, Naravoslovnotehniška fakulteta
University of Ljubljana, Faculty of Natural
Sciences and Engineering

Slovensko geotehniško društvo
Slovenian Geotechnical Society

Društvo za podzemne in geotehniške konstrukcije
Society for Underground and Geotechnical
Constructions

izdajatelj | **publisher**

Univerza v Mariboru, Fakulteta za gradbeništvo
University of Maribor, Faculty of Civil Engineering

odgovorni urednik | **editor-in-chief**

Ludvik Trauner
Univerza v Mariboru

urednika | **co-editors**

Stanislav Škrabl
Univerza v Mariboru
Bojan Žlender
Univerza v Mariboru

tehnična urednika | **desk editors**

Bojana Dolinar
Univerza v Mariboru
Borut Macuh
Univerza v Mariboru

lektorica | **proof-reader**

Metka Brkan

naklada | **circulation**

500 izvodov - issues

tisk | **print**

Tercia tisk d.o.o. Ptuj

Revija redno izhaja dvakrat letno. Članki v reviji so recenzirani s strani priznanih mednarodnih strokovnjakov. Baze podatkov v katerih je revija indeksirana: ICONDA - The international Construction database, GeoRef
Pri financiranju revije sodeluje Javna agencija za raziskovalno dejavnost republike Slovenije.

uredniški odbor | **editorial board**

naslov uredništva | **address**

ACTA GEOTECHNICA SLOVENICA
Univerza v Mariboru, Fakulteta za gradbeništvo
Smetanova ulica 17
2000 Maribor
Slovenija
Telefon / Telephone: +386 (0)2 22 94 300
Faks / Fax: +386 (0)2 25 24 179
E-pošta / E-mail: ags@uni-mb.s

spletni naslov | **web address**

http://www.fg.uni-mb.si/journal-ags

The journal is published twice a year. Papers are peer reviewed by renowned international experts. Indexation data bases of the journal: ICONDA - The International Construction Database, GeoRef
Financially supported also by Slovenian Research Agency.

VSEBINA

CONTENTS

UVODNIK

Mednarodna revija Acta Geotechnica Slovenica, ki redno izhaja že tri leta, postaja vedno bolj odmevna tako doma kot v tujini, k čemer pripomore tudi dejstvo, da jo sedaj lahko nejdemo v različnih specializiranih bazah podatkov kot sta Iconda – The International Construction database in GeoRef.

Druga številka tretjega letnika prinaša štiri zelo zanimive prispevke domačih in tujih avtorjev.

V prvem članku A. Štrukelj, A. Umek in T. Pliberšek predstavljajo inženirsko smiselno transformacijo površinskih pomikov horizontalno slojevitega polprostora, kjer so prikazani tipi valov, ki nastopajo v polprostoru. Pokazano je, da so površinski valovi izraženi kot residumi izračunani v poljih integranda, volumski valovi pa so izraženi kot integrali vzdolž razvejiščnih rezov. Singularnost, ki se v osnovni singularni rešitvi v elastodinamiki pojavlja vedno, je eksaktno izločena. V drugem delu prispevka je detajlno obdelan problem pojava in obnašanja Stonely-jevih valov.

Drugi članek J. Klopčiča J. Logarja, T. Ambrožiča, A. Štimulaka, A. Marjetiča, S. Bogatin in B. Majesa predstavlja projekt predora Šentvid ter metodo 3D meritev pomikov z rezultati teh meritev. Pridobljeni rezultati so interpretirani skladno z ugotovljeno geološko sestavo hribine s poudarkom na parametrih, ki so pomembni za bolj zanesljivo uporabo pomikovne funkcije.

V tretjem prispevku avtorja B. Žlender in L. Trauner obravnavata mineraloške in fizikalne lastnosti melja (polžarice z Ljubljanskega barja) in njihov vpliv na vrednosti parametrov geomehanskih lastnosti. Rezultati raziskave kažejo na sovisnost geomehanskih lastnosti in poroznosti. Odnose lahko izrazimo kot funkcije gostote oz. poroznosti ali vlažnosti. Iz rezultatov je razvidno, da so spremembe vodoprepustnosti, konsolidacije in stisljivosti nelinearno odvisne od sprememb poroznosti. Spremembe mehanskih parametrov kot so elastični modul, Poissonov količnik in strižni kot, so pri manjših spremembah poroznosti neizrazite in skoraj linearne.

Avtorji J. Zhu, S. Semprich, E. Bauer, C. Yuan in D. Sun v četrtem prispevku podajajo teoretične osnove ter rezultate terenskih raziskav o pronicanju vode skozi valjani beton, ukrepih za doseganje vodotesnosti, drenaži, optimalnem načrtovanju in nadzoru pronicanja. Rezultati prikazane študije so bili koristno uporabljeni pri izgradnji in povratnih analizah številnih jezov. Članek podrobno opisuje raziskovalne dosežke študije, teoretske osnove ter njihovo praktično uporabo pri visokih gravitacijskih jezovih iz valjanega betona.

Ludvik Trauner
Glavni urednik

EDITORIAL

The international journal Acta Geotechnica Slovenica, which has now been published for three years, is acquiring increasing national and worldwide reputation. An indication of its success may also be seen the fact that the journal is being abstracted in different specialized databases such as Iconda, the International Construction Database, and GeoRef.

The second issue of Year 3 contains four interesting articles authored by home and foreign contributors.

A. Štrukelj, A. Umek, and T. Pliberšek describe an engineeringly reasonable transformation of surface displacements of a horizontally layered half-space, where different types of waves are present. It is shown that surface waves are expressed through residues in poles of the integrand and the volume waves are expressed as integrals along corresponding branch cuts. The singularity which always appears in the basic singular solution in elastodynamics is explicitly excluded in this case. In the second part of this article, the appearance and behaviour of Stonely waves are investigated in greater detail.

The second article by J. Klopčič, J. Logar, T. Ambrožič, A. Štimulak, A. Marjetič, S Bogatin, and B. Majes presents the Šentvid tunnel project, the method of 3D displacement measurements, the results of these measurements and their interpretation according to the geological structure of the site. The emphasis is placed on items which play an important role for a more efficient application of the displacement function.

B. Žlender and L. Trauner describe mineralogical and physical characteristics of snail soil in the Ljubljana marsh and their influence on parameter values of geomechanical characteristics. The results of the tests show that interdependency exists between geomechanical characteristics and porosity. These relationships can be expressed as functions of density, porosity or water content. It is evident from the results that changes of the coefficient of permeability, the coefficient of consolidation, and the coefficient of volume compressibility are non-linear with respect to changes of porosity. Changes of mechanical parameters, such as Young modulus, Poisson ratio, and friction angle are indistinct and almost linear at lower changes of porosity.

J. Zhu, S. Semprich, E. Bauer, C. Yuan, and D. Sun describe theoretical bases and the results of field tests performed on roller-compacted concrete tested for water seepage. Water-tightness measures, drainage and optimal design and control of seepage are presented. The results of this study have been successfully applied in construction and in back analyses of several dams. The article describes the research findings in detail, focusing on theoretical bases and their applications in high roller-compacted gravity dams.

Ludvik Trauner
Editor–in–chief

INOVATIVNI PRISTOPI K REŠEVANJU VALOVNIH PROBLEMOV V HORIZONTALNO SLOJEVITEM POLPROSTORU

ANDREJ ŠTRUKELJ, ANDREJ UMEK IN TOMAŽ PLIBERŠEK

o avtorjih

Andrej Štrukelj
Univerza v Mariboru,
Fakulteta za gradbeništvo
Smetanova ulica 17, 2000 Maribor, Slovenija
E-pošta: andrej.strukelj@uni-mb.si

Andrej Umek
Univerza v Mariboru,
Fakulteta za gradbeništvo
Smetanova ulica 17, 2000 Maribor, Slovenija
E-pošta: umek@uni-mb.si

Tomaž Pliberšek
Univerza v Mariboru,
Fakulteta za gradbeništvo
Smetanova ulica 17, 2000 Maribor, Slovenija
E-pošta: tomaz.plibersek@uni-mb.si

izvleček

V članku je predstavljena inženirsko smiselna transformacija površinskih pomikov horizontalno slojevitega polprostora, kjer so prikazani tipi valov, ki nastopajo v polprostoru. Pokazano je, da so površinski valovi izraženi kot residui izračunani v polih integranda, volumski valovi pa so izraženi kot integrali vzdolž razvejiščnih rezov. Singularnost, ki se v osnovni singularni rešitvi v elastodinamiki pojavlja vedno, je eksaktno izločena. V drugem delu prispevka je detejlno obdelan problem pojava in obnašanja Stonely-jevih valov. Pokazano je, da v primeru slojev končne debeline njihov pojav in hitrosti ne zavisijo le od materialnih karakteristik sosednjih slojev, ampak tudi od njihove debeline.

ključne besede

horizontalno slojeviti polprostor, volumski valovi, površinski valovi, Stonely-jevi valovi, Green-ova funkcija

INOVATIVE SOLUTION PRINCIPLES OF WAVE PROBLEMS IN HORIZONTALY LAYERED MEDIAS

ANDREJ ŠTRUKELJ, ANDREJ UMEK and TOMAŽ PLIBERŠEK

About the authors

Andrej Štrukelj
University of Maribor,
Faculty of Civil Engineering
Smetanova ulica 17, 2000 Maribor, Slovenia
E-mail: andrej.strukelj@uni-mb.si

Andrej Umek
University of Maribor,
Faculty of Civil Engineering
Smetanova ulica 17, 2000 Maribor, Slovenia
E-mail: umek@uni-mb.si

Tomaž Pliberšek
University of Maribor,
Faculty of Civil Engineering
Smetanova ulica 17, 2000 Maribor, Slovenia
E-mail: tomaz.plibersek@uni-mb.si

Abstract

The paper represents engineeringly reasonable transformation of surface displacements of horizontaly layered half-space. The latter shows in the half-space present types of waves. It is shown that surface waves are expressed through residues in poles of the integrand and the volume waves are expressed as integrals along corresponding branch cuts. The singularity which always appears in the basic singular solution in elastodynamics is in this case exactly excluded. In the second part of the paper the appearance and behaviour of Stonely waves is investigated in greater detail. It is shown that in the case of layers of finite thickness their appearance and velocities depends not only on the material characteristics of neighbouring layers but also on their thickness.

Keywords

horizontaly layered half-space, volume waves, surface waves, Stonely waves, Green's function

1 INTRODUCTION

Waves, which are generated in the source of vibrations due to natural (f. ex. earthquakes), technical (f. ex. railway traffic, pilot driving) and man-made agitations, are propagated through the soil and disturb the functioning of sensitive instruments, cause human discomfort, and can possibly lead to structural damage. Investigating wave propagation is one of the main interests of applied mechanics and civil engineering because of its importance for dynamic structure-soil interaction, foundation engineering, seismology, and geophysical methods for determining the structure of foundation soils. As a rule, the soil is modeled as a half space in all problems displaying local soil characteristics or soil movement in the immediate vicinity of the selected point. The problematic nature of soil propagation in three-dimensional homogeneous and mainly layered half-space mainly has aroused significant scientific attention.

Knowledge of soil propagation in a layered half-space is thus of key importance and has always attracted much scientific attention. Bromwich [1] was the first to investigate wave propagation in half-continuous solid medium covered with a solid layer of continuous thickness. His work, which refers to standing waves with wave lengths greater than the thickness of the top layer, was continued by Love [2] who also investigated waves with equal or smaller lengths than the thickness of the top layer. Sezawa [3] studied the dispersion of elastic waves which propagate on the surface of layered bodies and on curved surfaces, whilst Thomson [4] investigated the transmission of elastic waves through a layered solid medium. Dispersion of surface waves in a multi-layered medium was studies by Haskell [5]. The classical work by Ewing, Jardetzky and Press [6], which also summarized contributions of several other authors, must also be mentioned in this review.

The authors of this contribution have chosen Green's function as a starting point for wave propagation in horizontally layered half-space. They [7] first formulated Green's function for the elastic layer loaded on the

surface with concentrated harmonic force of a general direction. Then, by taking into account the findings of Kobayashi [8], they expressed Green's function of a half-space, i. e. a layer of continuous thickness described with integrals for a half-continuous integration field, with integrals along suitably chosen branch cuts and residues in the poles of integrands. The solutions described in this article lead to the exact solution of Green's function of a horizontally layered half-space described in the article [9].

It results from the above quoted works that it is possible to express the displacements on the surface of a horizontally layered half-space as a sum of products of integrals and corner functions due to a concentrated time-dependent force of general direction acting on the surface. The concentrated force of general direction can namely be presented with two components, i. e. a vertical and a horizontal one. The fact that the solution of integrals using discreet Fourier-Bessel transformation does not provide satisfactory accuracy and convergence near the source point especially motivated the authors to adopt an alternative three-step approach to the solution of the integrals. As shown in this article, after the adoption of three steps, the integrals in the form that does not observe the singularity where it exists are written as integrals along branch cuts and residues in the poles of the integrand. This confirms the facts originating in the theory of elastodynamics, namely that it is possible to express surface waves in an elastic medium with poles and that volume waves are given with integrals along nodal cuts.

This approach has opened completely new possibilities to study surface waves. This article presents the results of the new approach.

In passing from a homogenous half-space to a horizontally layered half-space, Stonely waves can be generated besides Rayleigh waves. The magnitude of the system of equations for determining integration constants quickly increases with the increase of the number of layers, which is evident from the article by [9]. This also means that Stonely poles can occur beside Rayleigh poles in solutions. It is thus reasonable to investigate the phenomenon of singularity in the integrand more in detail. In the continuation, the article will show at which ratios of thickness and shear modulus of two adjoining layers Stonely waves occur and how the thickness of layers affects the speed of Stonely and Rayleigh waves.

2 THREE STEP SOLUTION

The thesis that it is engineeringly reasonable to transform surface displacements of a layered half-space into the from which is easy to calculate and which clearly shows wave types present in the half-space, is emphasized in the works [10], [11], [9]. For an axis-symmetrical example of vertically concentrated load [9] exerted on the surface of a top layer, as well as for a tangentially loaded layered half-space [11], displacements are expressed as a sum of integrals:

$$I(r) = \int_0^\infty F(\eta) \cdot J_n(\eta \cdot r) \cdot d\eta \qquad (1)$$

multiplied with adequate trigonometric functions with a circumferential coordinate as an argument. In these integrals, J is the Bessel function of the first kind of order and n is the order of the function which can adopt the values of 0, 1 and 2. It is known from scientific literature that the evaluation of these integrals with discrete Fourier-Bessel transformation does not lead to required accuracy and stability, especially when the integrals become singular at $r \to 0$. Mathematical analysis and mechanical understanding of the problem result in an alternative approach to the evaluation of the integrals shown in [11]. The authors evaluated the integrals of type (1) in three steps using the so-called method of the »expected shape«. The first step is the extraction of singularity. In an innovative way and observing the fact that

$$\lim_{r\to 0} I(r) = \lim_{r\to 0} \int_0^\infty F(\eta) \cdot J_0(\eta \cdot r) \cdot d\eta = \qquad (2)$$

$$= \int_0^\infty \lim_{\eta\to\infty} F(\eta) \cdot J_0(\eta \cdot r) \cdot d\eta = C \cdot \int_0^\infty J_0(\eta \cdot r) \cdot d\eta = \frac{C}{r}$$

the integrals which contain singularity are divided into two parts: a regular integral and a singular integral:

$$I(r) = \frac{1}{r} \cdot C + I_1(r) \ , \qquad (2a)$$

where $I_1(r)$ is:

$$I_1(r) = \int_0^\infty \Big[F(\eta) - C\Big] \cdot J_0(\eta \cdot r) \cdot d\eta \ . \qquad (3)$$

A singular integral has a simple integrand so that it can be analytically solved, whilst regular integrals are better to be calculated using discrete Fourier-Bessel transformation. The next step leads to their even simpler

calculation. It is namely evident that the below functions are present in the function $F(\eta)$ of the integrand:

$$\alpha_i = \sqrt{\eta^2 - \gamma_i^2} \quad , \quad \beta_i = \sqrt{\eta^2 - \vartheta_i^2} \quad , \qquad e^{\pm\alpha_i \cdot h_i} \quad , \quad e^{\pm\beta_i \cdot h_i} \tag{4}$$

where

$$\gamma_i = \frac{k_{Li}}{k_{T1}} \quad ; \quad \vartheta_i = \frac{k_{Ti}}{k_{T1}} \tag{4a}$$

k_{Li} or k_{Ti}, respectively, are wave numbers of longitudinal or transversal waves, and h_i is the thickness of the *i*-th layer.

So, it is reasonable to substitute the mechanical understanding of the function $F(\eta)$ with its analytical approach and a suitable selection of branch cuts to make the function uniform. A branch cut, which is shown in Fig. (1), was first selected inventively.

If we wish that the function $F(\eta)$ is an even function of the variable η on the real η-axis we must modify accordingly exponential functions (4) which are neither even nor odd. To make these exponential functions uniform and even they are replaced with their analytical continuation:

$$e^{\pm\alpha_i \cdot h_i} = e^{\pm\frac{\eta}{|\eta|}\alpha_i \cdot h_i} \quad ; \quad e^{\pm\beta_i \cdot h_i} = e^{\pm\frac{\eta}{|\eta|}\beta_i \cdot h_i} . \tag{5}$$

The mentioned modification, which makes the integrands even, allows the Bessel function to be divided into two parts:

$$2J_i(z) = h_i(z) + h_i(-z) \tag{6}$$

and consequently to transforms Hankel's inverse integrands, which are present in the derived components of Green's function, into integrals with the integral range from minus infinite to infinite:

$$\begin{aligned} I_1(r) &= \int_0^\infty \Big[F(\eta) - C\Big] \cdot J_i(\eta \cdot r) \cdot d\eta \\ &= \frac{1}{2} \cdot \left\{ \int_0^\infty \Big[F(\eta) - C\Big] \cdot h_i(\eta \cdot r) \cdot d\eta + \int_{-\infty}^0 \Big[F(\eta) - C\Big] \cdot h_i(\eta \cdot r) \cdot d\eta \right\} \\ &= \frac{1}{2} \cdot \int_{-\infty}^\infty \Big[F(\eta) - C\Big] \cdot h_i(\eta \cdot r) \cdot d\eta = \frac{1}{2} \cdot I_2(r) \end{aligned} \tag{7}$$

The final or the third step is the evaluation of the integral $I_2(r)$. It is shown in [11] that this integral can be evaluated with a contour integration in the complex plane of the Hankel parameter. Based on the theorem of residua [12] we obtain:

$$I_{2+} + I_{2R} + I_{2-} + I_{2b1} + I_{2r} + I_{2b2} = 2\pi i \sum res \, , \tag{8}$$

where the direction of the integration is evident from Fig. 2.

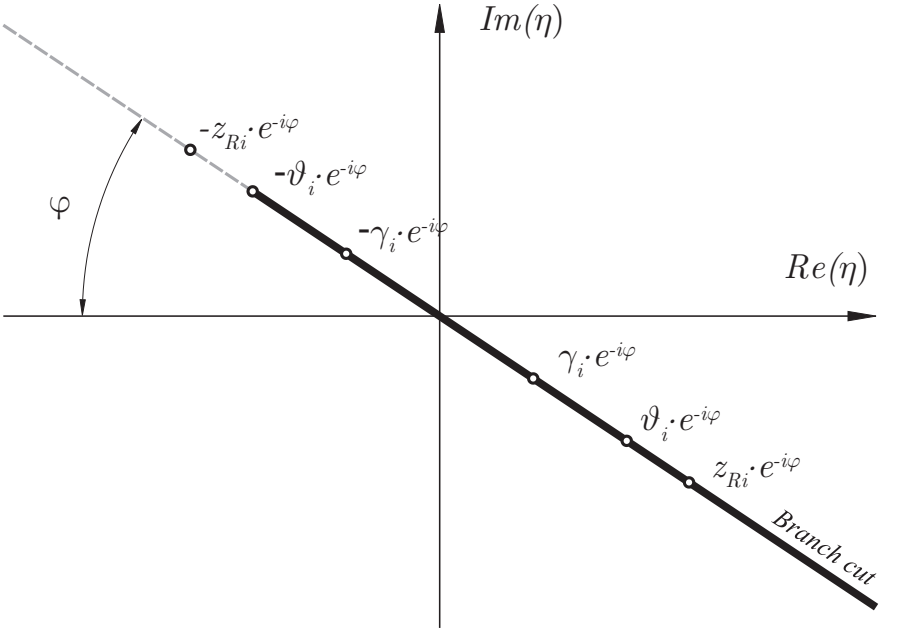

Figure 1. Branch points and poles of expressions α_i and β_i with a branch cut. For clearer presentation material damping, which is expressed with the complex shear modulus $\mu_i = \mu_{0i} \cdot e^{i\varphi}$, is considered.

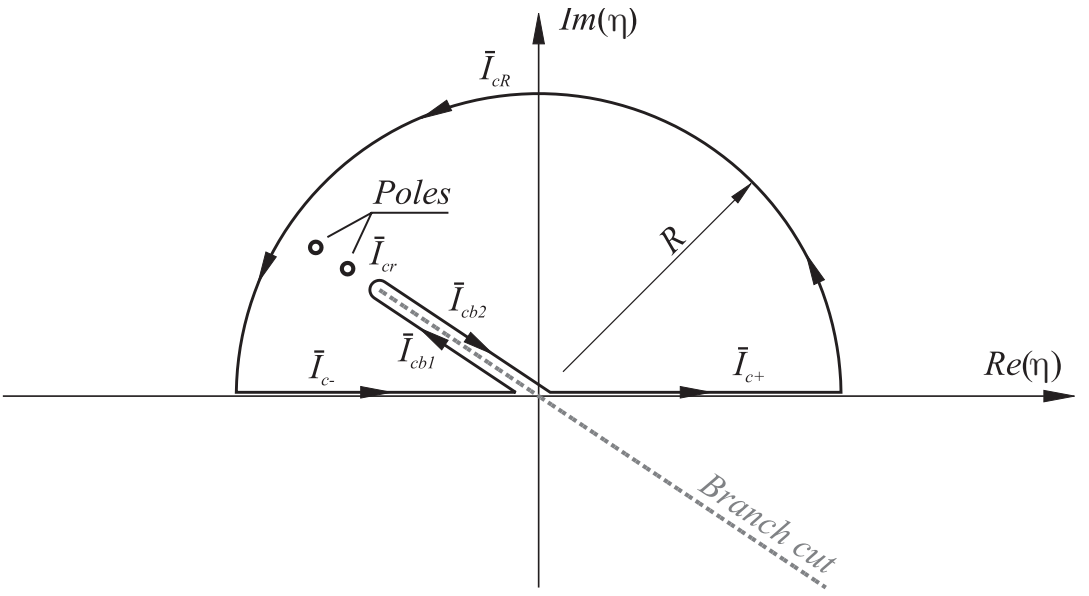

Figure 2. The integration path of the evaluation of Hankel inverse integrals which are present in the components of Green's function. The first member of the c indexes of the expressions in this figure is valid for all displacements of a horizontally layered half-space surface. Material damping is considered for clearer presentation.

Expression (8) is reasonably re-arranged:

$$I_2 = I_{2-} + I_{2+} = 2\pi i \sum res - I_{2b1} - I_{2r} - I_{2b2} \ , \quad (9)$$

or written in the form:

$$I = \frac{C}{r} + 2\pi i \sum res - I_{2b1} - I_{2r} - I_{2b2} \ . \quad (10)$$

Inverse Hankel integrals, which occur in the components of Green's function, adopt the below final form using the described alternative three-step approach:

$$I = \frac{C}{r} + 2\pi i \sum res + \sum \int_{a_i}^{b_i} \tilde{F}(\eta) \cdot J_n(\eta \cdot r) \cdot d\eta \ . \quad (11)$$

Equation (11) provides engineeringly reasonable transformation of displacements of a layered half-space surface because it transparently shows the types of waves present in the half-space. The first member presents singularity which always appears in the basic singular solution in elastodynamics and which is excluded from inverse Henkel integrals that define the components of Green's function. Linking the findings of mathematical physics with the findings in theoretic and applied mechanics leads to the conclusion that surface waves in Eq. (11) are expressed with residues in the poles of the integrand, whilst volume waves are expressed with integrals along branch cuts.

3 STONELY WAVES

In evaluating Green's function it was shown that the contribution of the second member of Eq. (11) is very important. As already said, it manifests the contribution of surface waves which is defined with the poles of integrands. In a homogenous half-space, two conjugated complex poles only appear which define the presence of Rayleigh waves. The system of equations quickly increases with the increase of the number of layers, due to the requirement that continuity conditions on contact planes of individual layers be fulfilled. So, the equation system matrix for determining unknown integration constants increases in accordance with equation $4 \cdot n + 2$ in case of vertical concentrated force acting on the surface. In case of tangential concentrated surface load, the size of the system matrix is dictated with equation $6 \cdot n + 3$. In both cases, n presents the number of layers. Besides Rayleigh waves, which always appear on the surface of a half-space, Stonely waves can also appear on contact surfaces. The presence of surface waves is defined in the system of equations with zeros of the system determinant or with singularities of integrands in integrals for the inverse transformation of expressions for individual components of Green's function. The search for the integrand singularity becomes more demanding when the system increases; yet, numerical calculation of singularity greatly reduces the speed of evaluating Green's function and hinders the automation of the calculation process. Therefore, it is sensible to investigate the process of singularity in integrands more in detail.

Rayleigh's waves always appear when the medium through which waving is propagated has an unobstructed surface. Stonely waves appear on contact surfaces between individual layers, yet only at certain ratios of thicknesses and shear modula of two neighbouring layers. The range of the appearance of Stonely waves is investigated on an example of two half-spaces.

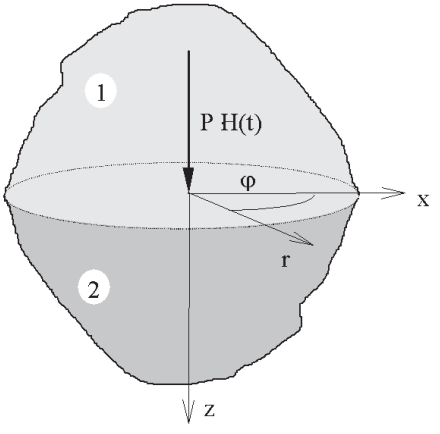

Figure 3. Model of two half-spaces.

As shown in Fig. 3, we take two homogenous elastic isotropic half-spaces with different thicknesses and different shear modula which are loaded at their contact surface with a vertical concentrated force. The problem is mathematically formulated so that the vector of displacement for each half-space is written by using potentials [13] in the form:

$$\vec{u} = \nabla \cdot \varphi + \vec{\nabla} \times \vec{\psi} \qquad (12)$$

The system of so linked partial differential equations, which presents the equations of movement,

$$\mu \cdot \nabla^2 \vec{u} + (\lambda + \mu) \cdot \vec{\nabla} \cdot \left(\vec{\nabla} \bullet \vec{u} \right) = \rho \cdot \frac{\partial^2 \vec{u}}{\partial t^2} \qquad (13)$$

disintegrates into the system of non-linked differential differential equations

$$\nabla^2 \cdot \varphi = \frac{1}{c_L^2} \cdot \frac{\partial^2 \varphi}{\partial t^2} \qquad (14)$$

$$\nabla^2 \cdot \vec{\psi} = \frac{1}{c_T^2} \cdot \frac{\partial^2 \vec{\psi}}{\partial t^2} \ , \qquad (15)$$

where c_L and c_T are the speeds of longitudinal or shear wave front, respectively. They are translated into the frequency domain with the Fourier exponential transformation $t \rightarrow \omega$. The studied elastodynamic problem is axially symmetrical, which dictates the use of the cylindrical coordinate system. Furthermore, the component of the displacement in the direction ϑ equals zero, both potentials, the scalar one φ and the vector one $\vec{\psi}$, must be independent of ϑ , and therefore the components of the vector potential $\vec{\psi}$ in the directions r and z must also equal zero. The individual components of the vector of displacement therefore resume the form:

$$\bar{\vec{u}} = \begin{Bmatrix} \dfrac{\partial \bar{\varphi}_r}{\partial r} - \dfrac{\partial \bar{\psi}_\vartheta}{\partial z} \\ 0 \\ \dfrac{\partial \bar{\varphi}_r}{\partial z} + \dfrac{1}{r} \cdot \dfrac{\partial \left(r \cdot \bar{\psi}_\vartheta \right)}{\partial r} \end{Bmatrix} \qquad (16)$$

and partial differential equations (14) and (15):

$$\frac{\partial^2 \bar{\varphi}_r}{\partial r^2} + \frac{1}{r} \cdot \frac{\partial \bar{\varphi}_r}{\partial r} + \frac{\partial^2 \bar{\varphi}_r}{\partial z^2} + \left(\frac{\omega}{c_L} \right)^2 \cdot \bar{\varphi}_r = 0 \qquad (17)$$

$$\frac{\partial^2 \bar{\psi}_\vartheta}{\partial r^2} + \frac{1}{r} \cdot \frac{\partial \bar{\psi}_\vartheta}{\partial r} + \frac{\partial^2 \bar{\psi}_\vartheta}{\partial z^2} - \frac{\bar{\psi}_\vartheta}{r^2} + \left(\frac{\omega}{c_T} \right)^2 \cdot \bar{\psi}_\vartheta = 0 \ . \qquad (18)$$

The relationship between the components of tension and displacements has the form:

$$\bar{\sigma}_z = 2 \cdot \mu \cdot \frac{\partial \bar{w}}{\partial z} - \lambda \cdot \left(\frac{\omega}{c_L} \right)^2 \cdot \bar{\varphi}_r \qquad (19)$$

$$\bar{\tau}_{zr} = 2 \cdot \mu \cdot \frac{\partial \bar{u}}{\partial z} - \mu \cdot \left(\frac{\omega}{c_T} \right)^2 \cdot \bar{\psi}_\vartheta \ . \qquad (20)$$

Partial differential equations (17) and (18) are transformed into ordinary differential equations using Hankel integral transformation $r \rightarrow \xi$:

$$\frac{d^2 \tilde{\bar{\varphi}}^0(\xi)}{dz^2} - \left[\xi^2 - \left(\frac{\omega}{c_L} \right)^2 \right] \cdot \tilde{\bar{\varphi}}^0(\xi) = 0 \qquad (21)$$

$$\frac{d^2 \tilde{\bar{\psi}}^1(\xi)}{dz^2} + \left[\xi^2 - \left(\frac{\omega}{c_T} \right)^2 \right] \cdot \tilde{\bar{\psi}}^1(\xi) = 0 \qquad (22)$$

The transformed components of the vector of displacement have the form

$$\tilde{\bar{u}}^1(\xi) = -\xi \cdot \tilde{\bar{\varphi}}^0(\xi) - \frac{d}{dz} \tilde{\bar{\psi}}^1(\xi) \qquad (23)$$

$$\tilde{\bar{w}}^0(\xi)=\frac{d}{dz}\tilde{\bar{\varphi}}^0(\xi)+\xi\cdot\tilde{\bar{\psi}}^1(\xi) \qquad (24)$$

We then also transform the expressions for normal and shear tensions:

$$\tilde{\bar{\sigma}}_z^0(\xi)=\mu\cdot\left\{\left[2\cdot\xi^2-\left(\frac{\omega}{c_T}\right)^2\right]\cdot\tilde{\bar{\varphi}}^0(\xi)+2\cdot\xi\cdot\frac{d}{dz}\tilde{\bar{\psi}}^1(\xi)\right\} \qquad (25)$$

$$\tilde{\bar{\tau}}_{rz}^1(\xi)=-\mu\cdot\left\{2\cdot\xi\cdot\frac{d}{dz}\tilde{\bar{\varphi}}^0(\xi)+\left[2\cdot\xi^2-\left(\frac{\omega}{c_T}\right)^2\right]\cdot\tilde{\bar{\psi}}^1(\xi)\right\}. \qquad (26)$$

Transformed differential Eqs. (21) and (22) for the potentials $\tilde{\bar{\varphi}}^0(\xi)$ and $\tilde{\bar{\psi}}^1(\xi)$ are ordinary homogeneous differential equations where z is the only variable. Their general solutions are:

$$\tilde{\bar{\varphi}}^0=\Phi_1\cdot\exp\left(\sqrt{\xi^2-k_L^2}\cdot z\right)+\Phi_2\cdot\exp\left(-\sqrt{\xi^2-k_L^2}\cdot z\right) \qquad (27)$$

$$\tilde{\bar{\psi}}^1=\Psi_1\cdot\exp\left(\sqrt{\xi^2-k_T^2}\cdot z\right)+\Psi_2\cdot\exp\left(-\sqrt{\xi^2-k_T^2}\cdot z\right), \qquad (28)$$

where Φ_1, Φ_2, Ψ_1 and Ψ_2 are integration constants dependent on the variable ξ, whilst the coefficients k_L and k_T are wave numbers belonging to the speed of the longitudinal or shear front, respectively. They are defined with the expressions:

$$c_L=\frac{\omega}{k_L}=\sqrt{\frac{\lambda+2\cdot\mu}{\rho}} \qquad (29)$$

$$c_T=\frac{\omega}{k_T}=\sqrt{\frac{\mu}{\rho}}\ . \qquad (30)$$

The positivity of the square root is required in the exponents of expressions (27) and (28). In case of a half-space and considering radiation condition and the selected coordinate system, it holds true that the constants Φ_1 and Ψ_1 must equal zero, or the value of the potentials would increase beyond any limit with an increasing value of the variable z. In case of a half-space, general solutions (27) and (28) for the potentials $\tilde{\bar{\varphi}}^0$ and $\tilde{\bar{\psi}}^1$ therefore equal:

$$\tilde{\bar{\varphi}}^0=\Phi_2\cdot\exp\left(-\sqrt{\xi^2-k_L^2}\cdot z\right) \qquad (31)$$

$$\tilde{\bar{\psi}}^1=\Psi_2\cdot\exp\left(-\sqrt{\xi^2-k_T^2}\cdot z\right). \qquad (32)$$

Radiation damping is considered in the studied case of two half-spaces, and the following substitutions are introduced:

$$\xi=k_{T1}\cdot\eta \qquad (33)$$

$$\frac{c_T}{c_L}=\frac{k_L}{k_T}=\sqrt{\frac{\mu}{\lambda+2\cdot\mu}}=\sqrt{\frac{1-2\cdot\nu}{2\cdot(1-\nu)}}=\gamma \qquad (34)$$

$$\vartheta_2=\frac{k_{T2}}{k_{T1}}\ . \qquad (35)$$

General solutions for individual potentials therefore are:

$$\tilde{\bar{\varphi}}_1^0=C_{1,1}\cdot\exp\left(2\cdot\pi\cdot\sqrt{\eta^2-\gamma_1^2}\cdot\zeta\right)=C_{1,1}\cdot\exp\left(2\cdot\pi\cdot\bar{\alpha}_1\cdot\zeta\right) \qquad (36)$$

$$\tilde{\bar{\psi}}_1^1=C_{1,3}\cdot\exp\left(2\cdot\pi\cdot\sqrt{\eta^2-1}\cdot\zeta\right)=C_{1,3}\cdot\exp\left(2\cdot\pi\cdot\bar{\beta}_1\cdot\zeta\right) \qquad (37)$$

$$\tilde{\bar{\varphi}}_2^0=C_{2,2}\cdot\exp\left(-2\cdot\pi\cdot\sqrt{\eta^2-\gamma_2^2}\cdot\zeta\right)=C_{2,2}\cdot\exp\left(-2\cdot\pi\cdot\bar{\alpha}_2\cdot\zeta\right) \qquad (38)$$

$$\tilde{\bar{\psi}}_2^1=C_{2,4}\cdot\exp\left(-2\cdot\pi\cdot\sqrt{\eta^2-\vartheta_2^2}\cdot\zeta\right)=C_{2,4}\cdot\exp\left(-2\cdot\pi\cdot\bar{\beta}_2\cdot\zeta\right), \qquad (39)$$

where ζ is the coordinate z standardized with respect to the wave length of shear waves of the first half-space. Four continuity conditions are available to determine unknown constants in general solutions (36) - (39). The equality of normal and shear tensions, as well as of vertical and horizontal displacements, must be assured on the contact surface of half-spaces.

$$\tilde{\bar{\sigma}}_{z,1}^0\Big|_{z=0}-\tilde{\bar{\sigma}}_{z,2}^0\Big|_{z=0}=0 \qquad (40)$$

$$\tilde{\bar{\tau}}_{zr,1}^1\Big|_{z=0}-\tilde{\bar{\tau}}_{zr,2}^1\Big|_{z=0}=0 \qquad (41)$$

$$\tilde{\bar{w}}_1^0\Big|_{z=0}-\tilde{\bar{w}}_2^0\Big|_{z=0}=0 \qquad (42)$$

$$\tilde{\bar{u}}_1^1\Big|_{z=0}-\tilde{\bar{u}}_2^1\Big|_{z=0}=0\ . \qquad (43)$$

Real zeros of the determinant of the so obtained equation system show the relationships of speeds of shear waves in the first medium and of Stoneley waves. Unlike Rayleigh waves, which are always present on the surface of a half-space, Stonely waves only appear at certain ratios of thicknesses and shear modula. The latter is represented by the graph in Fig. 4, where the abscissa is represented by the ratio of densities $\left(\rho_2/\rho_1\right)$, and the ordinate by the ratio of shear modula $\left(\mu_2/\mu_1\right)$. The range where real solutions appear (it is possible to show that there are only two), is limited with two curves. The curve A is defined with the requirement that the

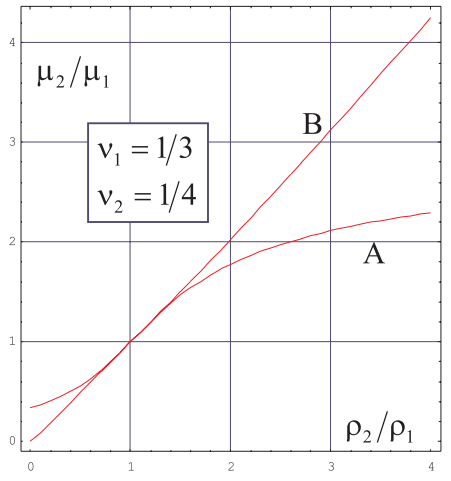

Figure 4. The range of the appearance of Stonely waves.

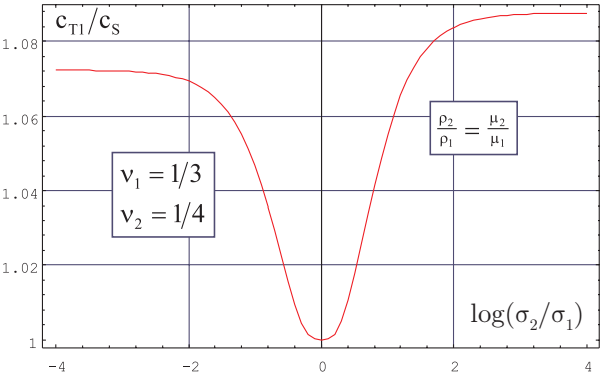

Figure 6. Speed changes of Stonely waves.

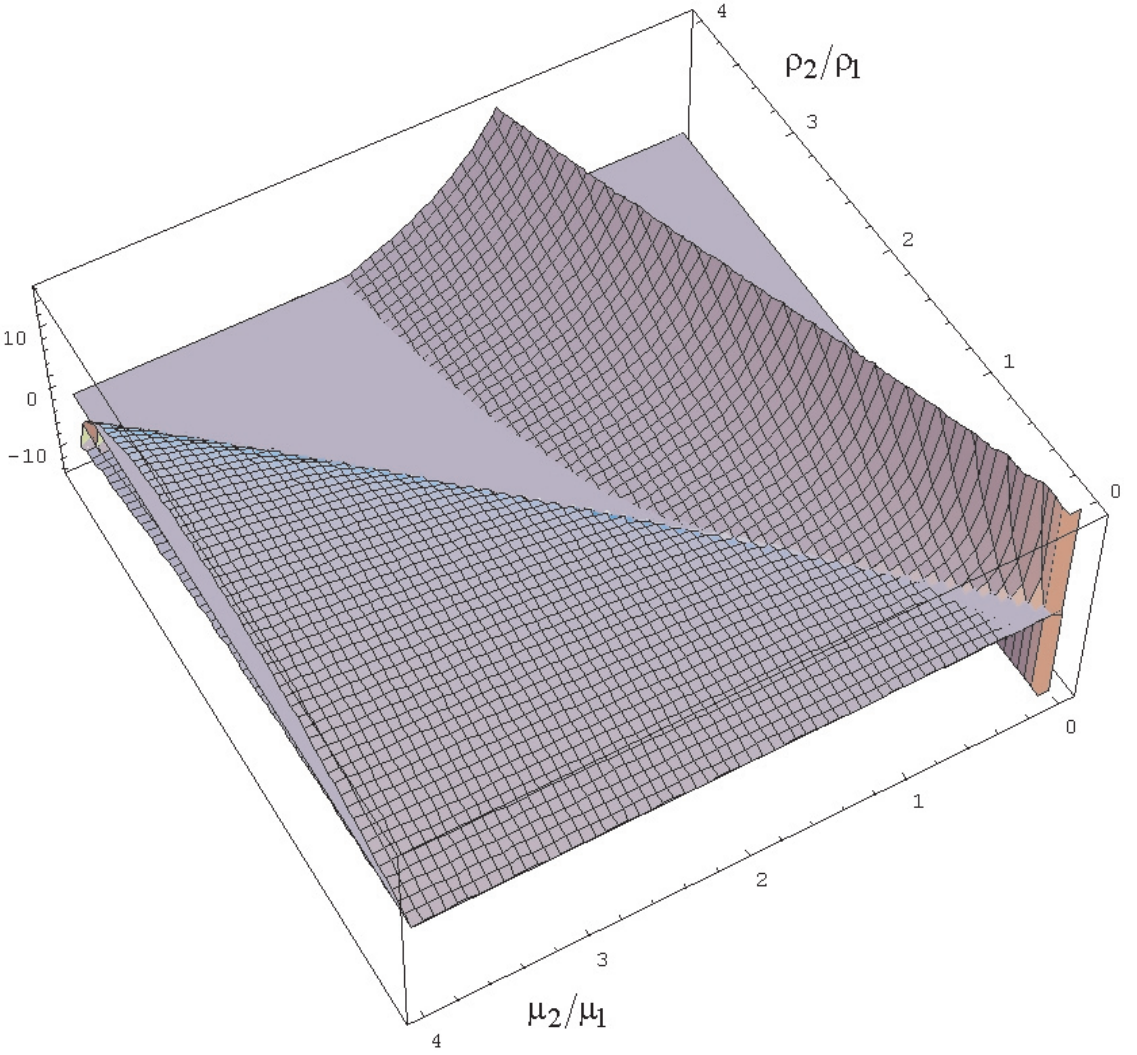

Figure 5. Three dimensional view of finding the appearance range of Stonely waves.

speed of a Stonely wave (c_S) equals the speed of a shear wave in the first medium (c_{T1}), which also physically presents one of the limits of a possible solution range. The curve B is defined with the requirement that the speed of a Stonely wave equals the speed of a shear wave in the second medium. An interesting three-dimensional view (Fig. 5) of finding the mentioned curves is presented in [10], where the author first searches for the intersection of the plane 0 and the surface defined with an equation of a determinant evaluated in $\eta = 1$, and then for the intersection of the plane 0 and the surface defined with an equation of a determinant evaluated in $\eta = \sqrt{\mu_2/\rho_2}$.

The change of speed of Stonely waves in the area where they occur is shown in Fig. 6, in which the abscissa is represented by the logarithm of the ratio of thicknesses or shear modula, respectively, and the ordinate is represented by the ratio of speeds of shear waves in the first medium and Stonely waves. To do this, we first draw a line in Fig. 4 that represents a symmetrical line of the odd quadrants $\rho_2/\rho_1 = \mu_2/\mu_1$; we then draw the change of speeds of Stonely waves along the symmetrical line. When the thickness and the shear modulus of the second medium are infinitely small, a Stonely wave is transformed into a Rayleigh wave for the first medium because this medium behaves as a homogenous half-space with a free surface. Contrary to this, a Stonely wave is transformed into a Rayleigh wave for the second medium when the thickness and the shear modulus of the first medium are infinitely small. When the thicknesses and shear modula of both media are the same, both half-spaces form a homogenous space, and a Stonely wave is transformed into a shear volume wave.

The appearance of Stonely waves does not only depend on characteristics of both media that are in contact but also on their thickness. To investigate this phenomenon it is reasonable to study the layer on an elastic homogenous half-space. In this case, general solutions (27) and (28) for individual potentials can be written in the below form considering a radiation condition and substitutions (33) - (35):

$$\tilde{\bar{\varphi}}_1^0 = C_{1,1} \cdot \exp\left(2 \cdot \pi \cdot \bar{\alpha}_1 \cdot \zeta\right) + C_{1,2} \cdot \exp\left(-2 \cdot \pi \cdot \bar{\alpha}_1 \cdot \zeta\right) \quad (40)$$

$$\tilde{\bar{\psi}}_1^1 = C_{1,3} \cdot \exp\left(2 \cdot \pi \cdot \bar{\beta}_1 \cdot \zeta\right) + C_{1,4} \cdot \exp\left(-2 \cdot \pi \cdot \bar{\beta}_1 \cdot \zeta\right) \quad (41)$$

$$\tilde{\bar{\varphi}}_2^0 = C_{2,2} \cdot \exp\left(-2 \cdot \pi \cdot \bar{\alpha}_2 \cdot \zeta\right) \quad (42)$$

$$\tilde{\bar{\psi}}_2^1 = C_{2,4} \cdot \exp\left(-2 \cdot \pi \cdot \bar{\beta}_2 \cdot \zeta\right), \quad (43)$$

where ζ represents a coordinate z standardized with respect to the length of shear waves of the first half-space.

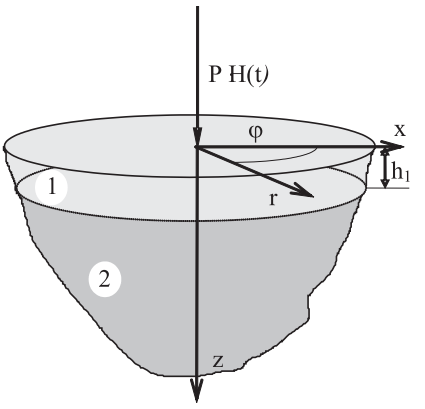

Figure 7. A model of a layer on a homogenous half-space.

To determine unknown constants in general solutions (40) - (43) two boundary conditions on a free surface $(z = 0)$ are available

$$\tilde{\bar{\sigma}}_z^0(\xi)\Big|_{z=0} = -\frac{\bar{P}(\omega)}{2 \cdot \pi} \quad (44)$$

$$\tilde{\bar{\tau}}_{zr}^1(\xi)\Big|_{z=0} = 0 \quad (45)$$

as well as four continuity conditions on the contact surface $(z = h_1)$:

$$\tilde{\bar{\sigma}}_{z,1}^0\Big|_{z_1=h_1} - \tilde{\bar{\sigma}}_{z,2}^0\Big|_{z_2=0} = 0 \quad (46)$$

$$\tilde{\bar{\tau}}_{zr,1}^1\Big|_{z_1=h_1} - \tilde{\bar{\tau}}_{zr,2}^1\Big|_{z_2=0} = 0 \quad (47)$$

$$\tilde{\bar{w}}_1^0\Big|_{z_1=h_1} - \tilde{\bar{w}}_2^0\Big|_{z_2=0} = 0 \quad (48)$$

$$\tilde{\bar{u}}_1^1\Big|_{z_1=h_1} - \tilde{\bar{u}}_2^1\Big|_{z_2=0} = 0\,. \quad (49)$$

The zeros of the determinant of the system of equations (44) - (49) represent poles of solutions of the system of equations in a transformed domain. The mentioned poles define the speeds of surface waves which appear at the surface of the total half-space and on the contact surface between a layer and a half-space.

In the studied case of an elastic layer on a homogenous half-space, we wish to investigate how the occurrence of Stonely waves depends on the thickness of the layer. To do this, we seek the zeros of the determinant of the system for different thicknesses of a layer, with a requirement that the ratio of thicknesses of both media

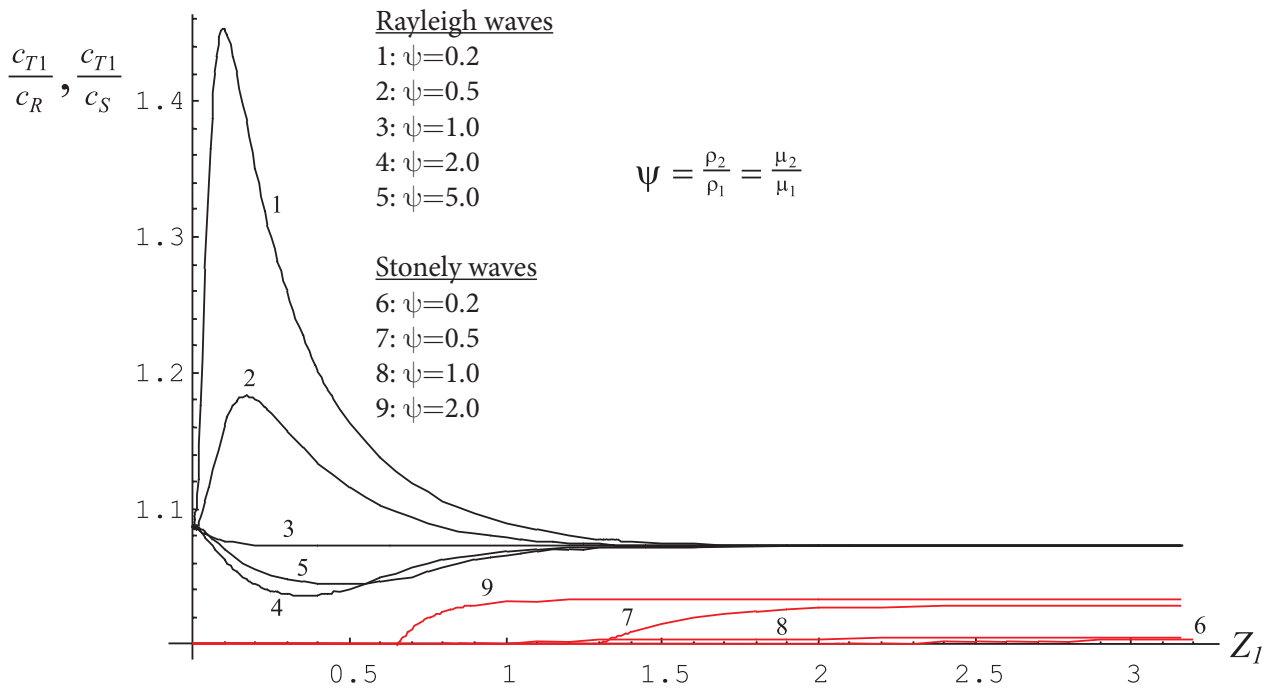

Figure 8. Dispersion diagram.

equals the ratio of their shear modula. We so obtain dispersion curves of the speed of surface waves, which are shown in Fig. 8, in which the abscissa is presented by the ratio of the layer thickness and wave length of a shear wave in the layer (Z_1), and the ordinate by the ratio of the speed of shear waves in a layer and the speed of Rayleigh waves (c_{T1}/c_R) or Stonely waves (c_{T1}/c_S), respectively. As expected, Rayleigh waves always occur without respect to the thickness of a layer. Their speed, however, quickly changes with the layer thickness when the latter is smaller than the wave length of a shear wave in a layer. Contrary to this, Stonely waves only appear at layer thicknesses that are greater than certain limit values depending on the ratio of thicknesses or shear modula, respectively, in both media. In a limit case, when the layer thickness approaches infinity, the speed of Stonely waves stabilizes at values obtained with the interaction of two half-spaces from the previous chapter. The speed of Rayleigh waves, however, approaches the values obtained for the case of a homogenous half-space with layer characteristics.

4 CONCLUSIONS

This article presents and alternative approach to the evaluation of inverse Hankel integrals which appear in the components of Green's function for a layered half-space on the surface of a top layer loaded with a concentrated force of general direction. This approach completely abolishes weak points of past procedures. After three steps of an innovative solution, described in this article, integrals pass into a form which transparently shows types of waves present in a half-space. Besides a better physical interpretation, this form allows a simple, numerically economical, and robust calculation. The results give a better physical insight into a layered half-space, which has been unknown up to the present, and open ways, due to their transparency, to studies of an inverse problem.

This article concentrates on the studies of possible appearance and behavior of Stonely waves. The appearance of Stonely and Rayleigh waves and consequently the finding of the integral poles, which is always numerical due to sophisticated expressions, is namely that segment of the Green's function solving procedure which greatly hinders the introduction of a universal algorithm for calculation. It is shown that the appearance of

Stonely waves only depends on material characteristics of both media, in case when two half-spaces are in contact. As soon as the thickness of an individual half-space becomes final, it is thickness, too, that influences the appearance and behaviour of Stonely waves. On the basis of the above procedures, we can namely fairly accurately limit the ratios of shear modula and material thicknesses of two proximate layers at which Stonely waves appear. This somehow facilitates the calculation procedure, yet the presented semi-analytical method is too sophisticated to be used for calculations in everyday engineering applications. Its advantage, however, is the accuracy of the obtained results. Taken as such, its basic aim and value lie in the comparison of engineering adequacy with other approximate methods for studying dynamic soil-structure interaction based on fundamental solutions. If we wish to obtain practical applicability of the presented method, the calculation process must be inevitably simplified, yet the simplifications must not affect the accuracy of the results. A relatively submissive behavior of roots in expressions for integrands in the complex η-plane further motivates us to consider the change of the integration path as one of possible simplifications in the calculation. In further investigations the integration path should be led so that the system of equations for integration constants could be solved numerically with optional accuracy and no longer with symbols. This would set the starting-points for an extremely fast, accurate and stabile procedure for determining a three-dimensional Green's function which, by considering the fact that it includes both, boundary and continuous conditions as well as radiation condition, presents a basis for calculating a dynamic stiffness soil matrix. This will be shown in our next articles that are in the phase of preparation.

REFERENCES

[1] Bromwich, T.J. (1898). On the influence of gravity on elastic waves, and, in particular, on the vibrations of an elastic globe, *Proc. London Math. Soc., 30:98-120*.

[2] Love, A.E.H. (1911, 1926). Some Problems of Geodynamics, *Cambridge University Press*, London.

[3] Sezawa, K. (1927). Dispersion of elastic waves propagated on the surface of stratified bodies and on curves surfaces, *Bull. Earthq. Res. Inst. Tokyo, 3:1-18*.

[4] Thomson, W.T. (1950). Transmissions of elastic waves through a stratified solid medium, *Journal Appl. Phys. 21:89-93*.

[5] Haskell, N.A. (1953). The dispersion of surface waves in multilayered media, *Bull.Seis. Soc. Amer. 43:17-24*.

[6] Ewing, W.M. and Jardetzky, W.S. and Press, F. (1957). *Elastic waves in layered media*. McGraw-Hill, New York.

[7] Pliberšek T, Štrukelj A, Umek A. (2005). Green's function for an elastic layer loaded harmonically on its surface. *Acta Geotechnica Slovenica 2: 4-21*.

[8] Kobayashi T, Sasaki F. (1991). Evaluation of Green's function on semi-infinite elastic medium. *Kajima Technical Research Institute Kajima Corporation; KICT Report No.86*.

[9] Štrukelj A, Pliberšek T, Umek A. (2006). Evaluation of Green's function for vertical point load excitation applied to the surface of a layered semi-infinite elastic medium. *Arch. appl. mech. (1991) Dec. 2006, vol. 76, no. 7/8, 465-479*.

[10] Štrukelj, A. (2001). *Prispevek k razvoju aproksimativnih metod za določevanje Green-ove funkcije za slojevit polprostor : doktorska disertacija*. Maribor VIII, 140 f., ilustr.

[11] Pliberšek, T. (2006). *Green-ova funkcija tangencialno obremenjenega slojevitega pol-prostora: doktorska disertacija*.

[12] Spiegel M.R. (1994). *Shaum's outline of theory and problems of complex variables with an introduction to conformal mapping and its applications*. New York: McGraw-Hill Book Company.

[13] Achenbach, J.D. (1973). *Wave propagation in elastic solids*. North-Holland, Amsterdam, London.

POMIKI V RAZISKOVALNEM ROVU PRED IZKOPNIM ČELOM PREDORA ŠENTVID

JURE KLOPČIČ, JANKO LOGAR, TOMAŽ AMBROŽIČ, ANDREJ ŠTIMULAK, ALEŠ MARJETIČ, SONJA BOGATIN IN BOJAN MAJES

o avtorjih

Jure Klopčič
Univerza v Ljubljani,
Fakulteta za gradbeništvo in geodezijo
Jamova 2, 1000 Ljubljana, Slovenija
E-pošta: jklopcic@fgg.uni-lj.si

Janko Logar
Univerza v Ljubljani,
Fakulteta za gradbeništvo in geodezijo
Jamova 2, 1000 Ljubljana, Slovenija
E-pošta: jlogar@fgg.uni-lj.si

Tomaž Ambrožič
Univerza v Ljubljani,
Fakulteta za gradbeništvo in geodezijo
Jamova 2, 1000 Ljubljana, Slovenija
E-pošta: tambrozi@fgg.uni-lj.si

Andrej Štimulak
DDC svetovanje inženiring d.o.o.
Kotnikova 40, 1000 Ljubljana, Slovenija
E-pošta: andrej.stimulak@ddc.si

Aleš Marjetič
Univerza v Ljubljani,
Fakulteta za gradbeništvo in geodezijo
Jamova 2, 1000 Ljubljana, Slovenija
E-pošta: amarjetic@fgg.uni-lj.si

Sonja Bogatin
Univerza v Ljubljani,
Fakulteta za gradbeništvo in geodezijo
Jamova 2, 1000 Ljubljana, Slovenija
E-pošta: sbogatin@fgg.uni-lj.si

Bojan Majes
Univerza v Ljubljani,
Fakulteta za gradbeništvo in geodezijo
Jamova 2, 1000 Ljubljana, Slovenija
E-pošta: bmajes@fgg.uni-lj.si

izvleček

Prilagajanje analitične pomikovne funkcije merjenim premikom v predoru omogoča spremljanje procesa umirjanja deformacij po izvedenem izkopu predora v območju merjenega prečnega profila ter določitev pričakovanega poteka pomikov opazovanih točk z oddaljevanjem izkopnega čela. Pomikovno funkcijo sestavljajo trije členi. Medtem ko je tretji člen pomikovne funkcije dobro določen, saj opisuje obnašanje po izkopu predora na mestu merskega profila in po vzpostavitvi meritev, pa sta prva dva člena pomikovne funkcije, ki opisujeta potek pomikov pred čelom ter med čelom ter vzpostavitvijo meritev, definirana izključno na podlagi numeričnih simulacij. Za verifikacijo privzetih analitičnih izrazov ter za definicijo potrebnih parametrov pomikovne funkcije je potrebno opraviti meritve premikov pred čelom. S 3D geodetskimi meritvami pomikov pred čelom predora v raziskovalnem rovu predora Šentvid med izkopom glavnega predora smo pridobili dragocene podatke o obnašanju sistema hribina-predor. Članek predstavi projekt predora Šentvid ter metodo 3D meritev pomikov z rezultati teh meritev. Pridobljeni rezultati so interpretirani skladno z ugotovljeno geološko sestavo hribine s poudarkom na parametrih, ki so pomembni za bolj zanesljivo uporabo pomikovne funkcije.

ključne besede

predor, raziskovalni rov, geodetske meritve pomikov, pomiki pred čelom

DISPLACEMENTS IN THE EXPLORATORY TUNNEL AHEAD OF THE EXCAVATION FACE OF ŠENTVID TUNNEL

JURE KLOPČIČ, JANKO LOGAR, TOMAŽ AMBROŽIČ, ANDREJ ŠTIMULAK, ALEŠ MARJETIČ, SONJA BOGATIN and BOJAN MAJES

about the authors

Jure Klopčič
University of Ljubljana,
Faculty of Civil and Geodetic Engineering
Jamova 2, 1000 Ljubljana, Slovenia
E-mail: jklopcic@fgg.uni-lj.si

Janko Logar
University of Ljubljana,
Faculty of Civil and Geodetic Engineering
Jamova 2, 1000 Ljubljana, Slovenia
E-mail: jlogar@fgg.uni-lj.si

Tomaž Ambrožič
University of Ljubljana,
Faculty of Civil and Geodetic Engineering
Jamova 2, 1000 Ljubljana, Slovenia
E-mail: tambrozi@fgg.uni-lj.si

Andrej Štimulak
DDC Consulting&Engineering Ltd.
Kotnikova 40, 1000 Ljubljana, Slovenia
E-mail: andrej.stimulak@ddc.si

Aleš Marjetič
University of Ljubljana,
Faculty of Civil and Geodetic Engineering
Jamova 2, 1000 Ljubljana, Slovenia
E-mail: amarjetic@fgg.uni-lj.si

Sonja Bogatin
University of Ljubljana,
Faculty of Civil and Geodetic Engineering
Jamova 2, 1000 Ljubljana, Slovenia
E-mail: sbogatin@fgg.uni-lj.si

Bojan Majes
University of Ljubljana,
Faculty of Civil and Geodetic Engineering
Jamova 2, 1000 Ljubljana, Slovenia
E-mail: bmajes@fgg.uni-lj.si

abstract

Fitting the displacement function to the measured displacements enables the assessment of the stabilization process of the observed cross section and the determination of its normal behaviour. The displacement function consists of three parts. Whilst the third part has been successfully applied for several times and thus proven to be very well defined, the first two parts were defined only on the basis of numerical simulations. To overcome this deficiency and to obtain the necessary coefficients of the pre-face part of the displacement function, the 3D displacement measurements ahead of the face due to tunneling should be performed. Such measurements were performed in the exploratory tunnel of the Šentvid tunnel during the excavation of the main tunnel. This paper presents the Šentvid tunnel project, the method of the 3D displacement measurements, the results of these measurements and their interpretation according to the geological structure of the site with an emphasis on items important for the coefficients of the displacement function.

keywords

tunnel, exploratory tunnel, geodetic displacement measurements, pre-face displacements

1 INTRODUCTION

Since the ancient times, the construction of the tunnels and underground spaces has been a big challenge to engineers. This challenge is even greater when the underground spaces are constructed in faulted and heterogeneous rock mass of low strength and of high deformability. Although a lot of time and money has been spent recently in the design stage to establish a reliable and accurate geological model of the rock mass on the site of the future project, inconvenient geological surprises still occur. To minimize the risk of such situations during the construction of tunnels and other underground spaces according to NATM, the observa-

tional approach was introduced already by Rabcewicz [1] and has been later on widely accepted as its integral part [2,3]. Geological-geotechnical monitoring typically includes geological drafts of the excavation faces, results from pressure cells built in the primary lining, measurements of the forces in rock bolts, results from the extensometer measurements of the displacements of the surrounding rock mass and systematic monitoring of absolute primary lining displacements by geodetic methods.

Based on the interpretation of these results the quality and quantity of the rock mass support, the excavation sequence and the technology foreseen by the tunnel design are checked daily and adjusted when necessary. Monitoring enables the observation of the rock mass – support system response due to the face excavation advance and time dependent effects of the surrounding rock mass and shotcrete.

The interpretation of the 3D displacement measurements of the targets in primary lining has proven to be the most convenient method for daily monitoring of the tunnel behaviour [3]. The targets are installed on the circumference of the primary lining in measuring sections, which should be arranged at a distance approximately one equivalent diameter along the tunnel axis. The 3D positions of the targets are usually recorded once a day or more often if needed. The analysis of the measured displacement allows a reliable prediction of the rock mass conditions ahead of the face and around the tunnel tube [4].

The displacement history plots are the most common plots of the measured displacements and are used for the assessment of the stabilization process of each individual cross section. The displacement rate is highest immediately after the top heading excavation and the support installation, and it decreases with the further excavation advance (Fig. 1). As soon as the bench excavation face approaches the observed cross section, the displacement rate increases again and after the closure of the support ring (execution of the invert) it reduces to zero.

The expected behaviour of the cross section is shown in Fig. 1. Stresses induced by the excavation are regularly distributed between the support and the rock mass in the way that the support is not overstressed and thus damaged. The displacement history plot in Fig. 1 indicates the proper response of the rock mass – support system.

Contrary to the behaviour shown in Fig. 1 the displacement history plot in Fig. 2 reveals the inadequate support in the vicinity of the measuring section to carry the load transferred from the surrounding rock mass. The displacement rate did not decrease after the top heading excavation or after the closure of the support ring. Fig. 3 shows the failure of the primary lining in the area of this measuring section.

Although one can clearly see that the rock mass – support system had malfunctioned, the determination of the point where loads exceeded the capacity of the support is a difficult task. What would be the adequate

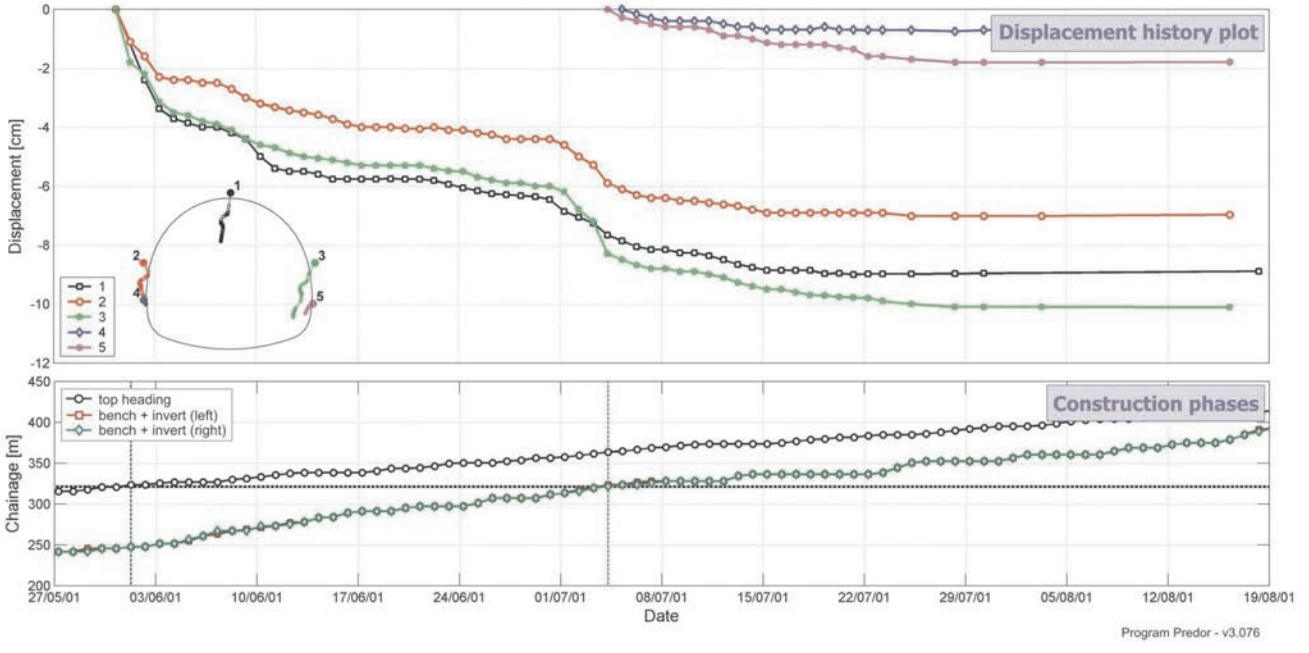

Figure 1. Regular behaviour of the cross section as shown on the displacement history plot.

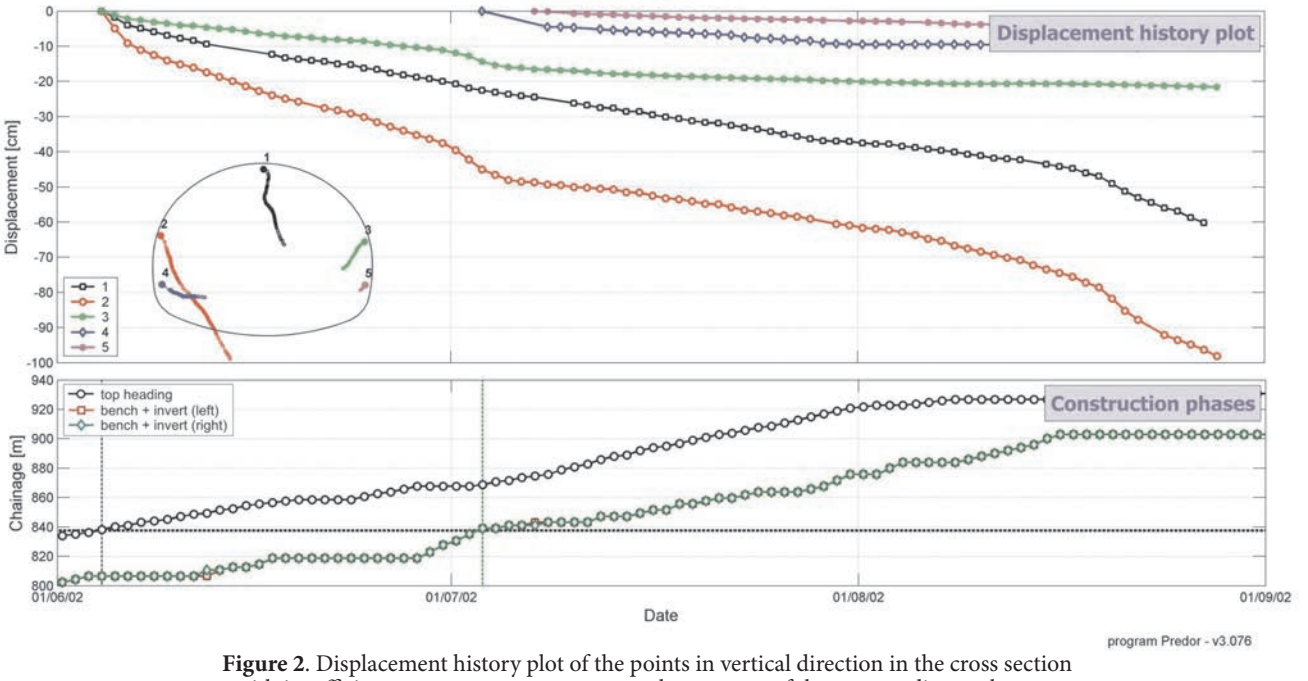

Figure 2. Displacement history plot of the points in vertical direction in the cross section with insufficient support measures to carry the pressure of the surrounding rock mass.

Figure 3. Failure of the primary lining in the parking by niche in the left tube of the Trojane tunnel at chainage km 82+295 (area of the measuring section from Fig. 2).

support measures to avoid excessive displacements and consequently the failure of the support?

There are several possibilities to answer this question. One of them is the 3D numerical analyses, which are not suitable for use on a day-to-day basis due to their inability to model complex geological structures, unreliable material parameters of the rock mass, lack of knowledge on the primary stress state and especially because they are time consuming and costly [5].

On the other hand, analytical methods with even more simplifications of the stress and rock mass conditions with limitations to two dimensional and time dependent problems do not provide the needed degree of reliability.

In the next chapter a description of a simple, but very accurate method will be given. This method is based on the fitting of the analytical function to measured displacements in order to determine the anticipated behaviour of the rock mass – support system.

2 THE DISPLACEMENT FUNCTION

2.1 BASICS OF THE DISPLACEMENT FUNCTION

The original proposal for the convergence equation was given by Guenot, Panet and Sulem [6]. This analytical function describes the displacements within a cross section of a circular tunnel with full face excavation without the installation of the support. These displacements are caused by face advance effect and time-dependent effects.

In order to overcome the limitations of the convergence equation Barlow extended the displacement function for more realistic description of the conditions during tunneling [7]. Barlow considered the support installation and the sequential excavation.

Further modifications of the displacement function were introduced by Sellner [8], which was implemented in the computer code GeoFit [9].

The displacement function as proposed by Barlow was used in this work and is expressed by the following three equations:

- the displacement that occurs ahead of the face - part 1:

$$C(x,t) = c_1(x) \cdot \left[C_{x\infty} + A \cdot c_2(t)\right] \qquad (1)$$

- the displacement that occurs between the excavation and the installation of support - part 2:

$$C(x,t) = \left[Q_1 + Q_2 \cdot C_1(x) - Q_k \cdot P_k^+(x)\right] \cdot \left[C_{x\infty} + A \cdot C_2(t)\right] \qquad (2)$$

- the displacement that occurs after the installation of support - part 3:

$$C(x,t) = \frac{\left[Q_1 + Q_2 \cdot C_1(x) + K \cdot C_s - Q_k \cdot P_k^-(x)\right]}{\left[1 + K \cdot \left(C_{x\infty} + A \cdot C_2(t)\right)\right]} \cdot \left[C_{x\infty} + A \cdot C_2(t)\right] \qquad (3)$$

with

$c_1(x)$ = time independent function (loading function)

$c_2(t)$ = time dependent function

x = distance between observed cross section and excavation face

t = elapsed time between excavation and observation time

X = curve fitting parameter describing the shape of $C_1(x)$

T = curve fitting parameter describing the shape of $C_2(t)$

$C_{x\infty}$ = curve fitting parameter describing ultimate time independent displacement

A = curve fitting parameter describing ultimate time dependent displacement

Q_1 = proportion of the total stress change due to the tunnel excavation that occurs ahead of the face

C_{pf} = proportion of the total stress change due to the tunnel excavation that occurs after the excavation face passes the monitored cross section $(Q_1+Q_2=1)$

$Q_k \cdot P_k^+(x)$ and $Q_k \cdot P_k^-(x)$ = functions that distribute the effect of the support installation on the displacements ahead of and behind the face, respectively

C_s = displacement at the time of support installation

K = parameter of the support

The main objective of this work is related to the pre-face displacements described by Eq. 1, which includes the loading function ahead of the face (C_{pf}) defined as:

$$C_{pf} = \left[\frac{X}{X + \left(x_f - x\right)}\right]^{1.2} \qquad (4)$$

where

x_f = the length of the pre-face domain (influential area ahead of the excavation face)

2.2 ADVANTAGES OF THE DISPLACEMENT FUNCTION

The simplicity of the algorithm and consequently fast calculations are the major advantages of the use of the displacement function if compared to other methods described above. Unlike the analytical methods the displacement function takes account of time effects and 3D effects of the tunnel excavation. The use of the displacement function is much more time-effective than the use of numerical calculation and does not require a large amount of parameters, the determination of which needs a lot of costly and time-consuming laboratory tests. These advantages make the displacement function suitable for the use on a day-to-day basis on construction sites [9].

To fully exploit the displacement function's advantages, computer software for fitting the function to the measured displacements is required. For this purpose the computer code Predor has been developed [10].

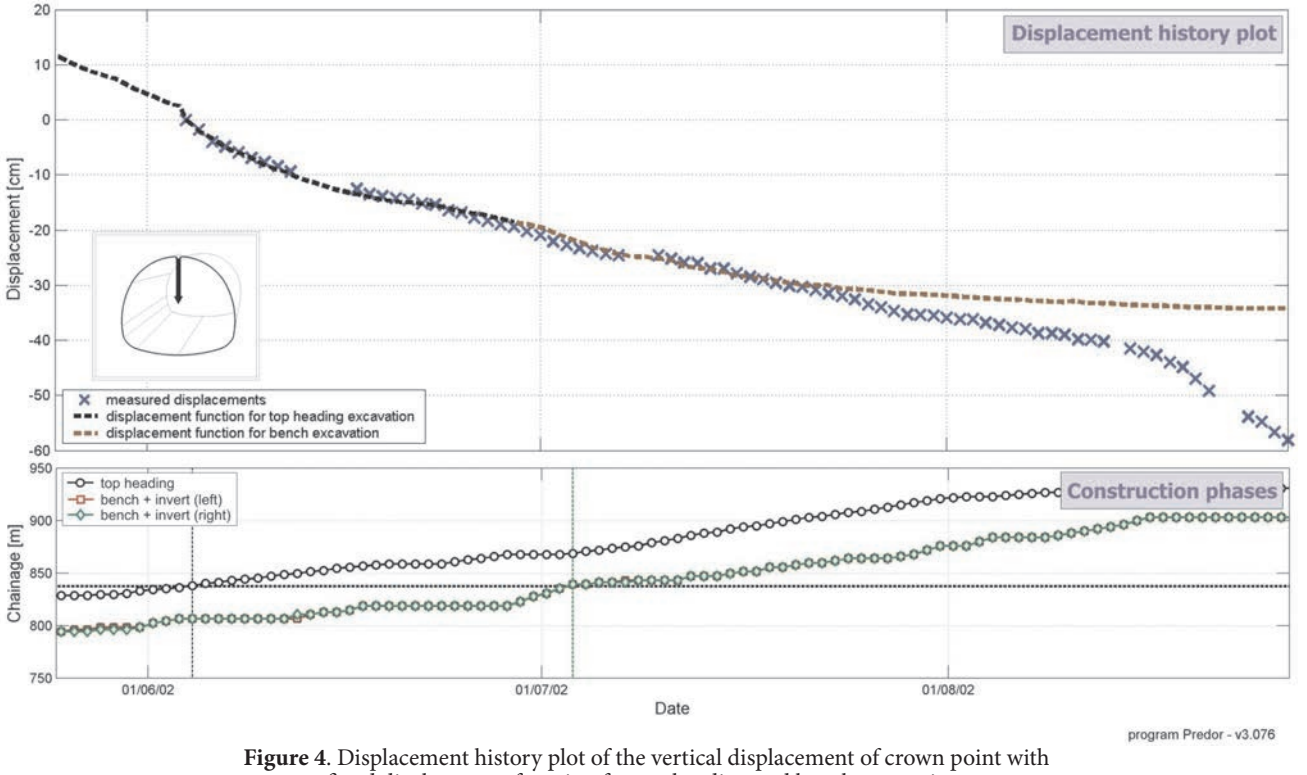

Figure 4. Displacement history plot of the vertical displacement of crown point with fitted displacement function for top heading and bench excavation.

For the case described in Fig. 2 the fitted displacement function to the measured displacements is shown in Fig. 4. The divergence of the theoretical curve and measured displacements in this case indicated the support failure in the vicinity of the measuring section (Fig. 3). According to the fitted displacement curve the failure of the cross section occurred soon after the ring closure at approximately 30 cm of vertical displacement of the crown point. At this point additional support measures should have been undertaken to avoid further disintegration of the rock mass – support system.

2.3 LIMITATIONS OF THE DISPLACEMENT FUNCTION

While part 3 of the displacement function (after the excavation face passed the observed cross section - Eq. 3) is very well defined by fitting the curve to the measured displacements, the first two parts (ahead of the face (part 1) and between the excavation and the support installation (part 2)) are determined on the basis of numerical simulations and rely on the parameters that depend on the rock mass behaviour ahead of the tunnel face:

Q_1 = proportion of the total stress change due to the tunnel excavation that occurs ahead of the face and

x_f = parameter presenting the magnitude of the pre-face domain.

The magnitude of both parameters and the shape of first two parts of the displacement function could be verified or accurately determined only by measuring the displacements within the rock mass ahead of the tunnel face. Obviously, this cannot be done in terms of ordinary geodetic methods.

In case of low overburden and provided that monitoring of the displacements is established in the tunnel as well as on the surface along and perpendicular to the tunnel axis, the amount of the displacements that occurred before the first measurement in the observed cross section can be estimated from the difference between the tunnel and the surface settlements.

Extensive monitoring of the surface displacements was established above the eastern part of the Trojane tunnel that passes the Trojane village at shallow depth. The Trojane tunnel was constructed in heavily faulted

and densely foliated rock mass of carboniferous age. The comparison of the measured displacements in the tunnel tube and above it revealed that less than 50% of the final displacement measured on the surface was only measured in the tunnel tube [11]. The rest of displacement occurred before the first measurement of the measuring cross section was performed. From the relation between the surface displacement and the distance to the approaching top heading excavation face the magnitude of the pre-face domain can also be estimated.

More reliable information on the rock mass behaviour ahead of the face and magnitude of the pre-face domain was given by the interpretation of the measurements of the horizontal inclinometer that was installed in the length of 40 m in the crown of the left tube of the Trojane tunnel under the Trojane village ([12], [13]). The crown settlements measured by the horizontal inclinometer are shown in Fig. 5 together with influence lines.

At the chainage km 80+293 a geodetic measuring cross section (marked in Fig. 5) was installed. The settlement measured by the horizontal inclinometer at the given chainage was 17.5 cm and the measured spatial displacement of the crown point in the geodetic cross section was 4.9 cm, which is less than 30 % of the final settlement. All three components of the displacement vector are drawn in Fig. 6.

The magnitude of the pre-face domain is approximately 1 - 1.5 equivalent tunnel diameter (10 - 15 m in the case of the Trojane tunnel) ahead of the face as one can observe from Fig. 5.

The advantages of measuring displacements ahead of the face with the horizontal inclinometer are the accuracy of measurements, minimum disturbance of the rock mass and the position of the inclinometer, which allows the direct comparison with the geodetically measured settlement of the crown point. The major disadvantage is the inability of measuring the 3D displacement. Only the settlement of the crown is obtained. The longitudinal component of pre-displacement might be additionally measured using deformeters, but no reports on such measurements can be presently found in literature.

3D displacements ahead of the tunnel face can be easily obtained by geodetic monitoring, when a small diameter tunnel existed within the alignment of the future tunnel with considerably larger cross section.

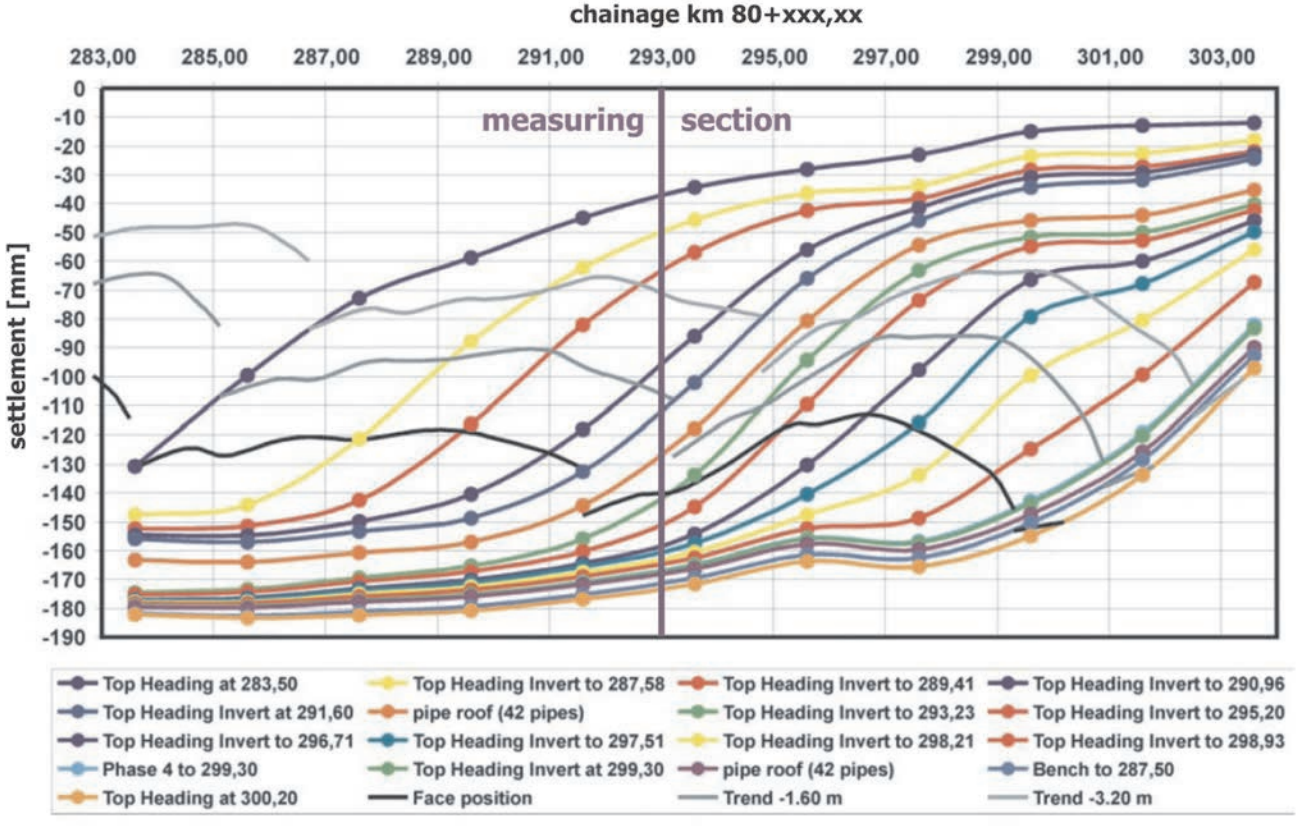

Figure 5. The influence lines of the settlements, measured by the horizontal inclinometer in the crown of the left tube of the Trojane tunnel (unpublished report by Button and Volkmann).

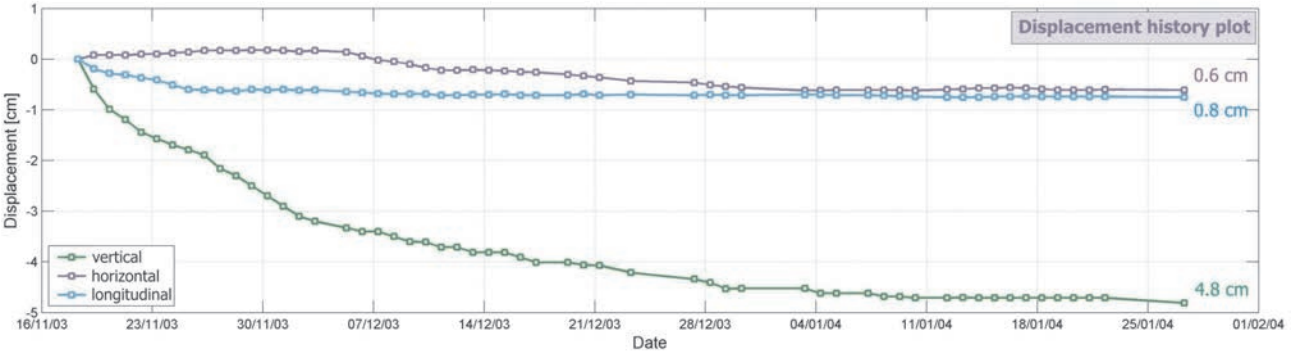

Figure 6. Displacement history plot of all three components of the crown point displacement vector (left tube of the Trojane tunnel, measuring cross section at the chainage km 80+293).

3 3D GEODETIC DISPLACEMENT MEASUREMENTS AHAED OF THE MAIN TUNNEL FACE

In the eight-month period between September 2005 and April 2006 the 3D displacement measurements were performed in the exploratory tunnel of the Šentvid motorway tunnel ahead of the main tunnel excavation face.

3.1 THE ŠENTVID TUNNEL

The Šentvid tunnel system is the missing link of the Slovenian A2 Karavanke-Ljubljana motorway to the Ljubljana ring motorway (Fig. 7).

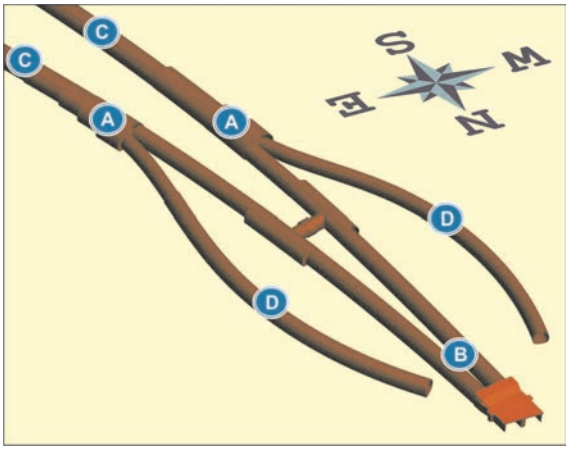

Figure 8. The scheme of the Šentvid tunnel [14].

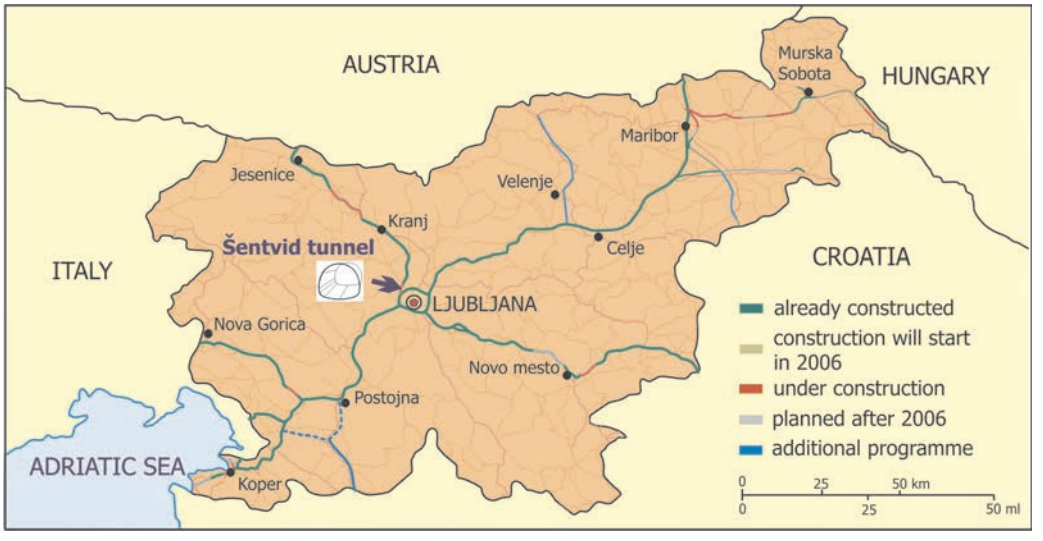

Figure 7. Slovenian road map.

An approximately 1100 m long motorway tunnel is designed as a double tube tunnel with two large merging caverns with maximum excavation cross section of approximately 330 square meters and the length of 60 m (label A in Fig. 8). The Šentvid tunnel consists of twin two lane tunnels from northern portal up to the merging caverns (label B) and twin three lane tunnels from southern portal to the merging caverns (label C). Two ramp tunnels (label D) will connect the Celovška street to the main motorway tunnel. The tunnel system is currently under construction. All underground structures are constructed following the principles of NATM. Maximum overburden reaches 115 m.

The Šentvid tunnel alignment passes through densely foliated clastic sedimentary rocks of carboniferous age, mainly sandstones, siltstones and clayey slates. The region has undergone intense tectonic deformations, presumably during several deformation phases. Due to intensive tectonics the rock is folded, fault zones are up to several meters thick and consist mainly of gouge clay. The rock mass itself is very heterogeneous and anisotropic (Fig. 9).

The quantity of water that percolates from the surface into the tunnel tube is small. Water appears mainly in fault zones. Together with deformations that occur due to tunneling this water causes the increase of the water content along the foliation and consequently the decrease of rock suction, which affects mechanical properties of the rock mass and worsens the tunneling conditions in the vicinity of fault zones.

Tunneling conditions for the Šentvid tunnel system were estimated in the range from fair to very poor [15].

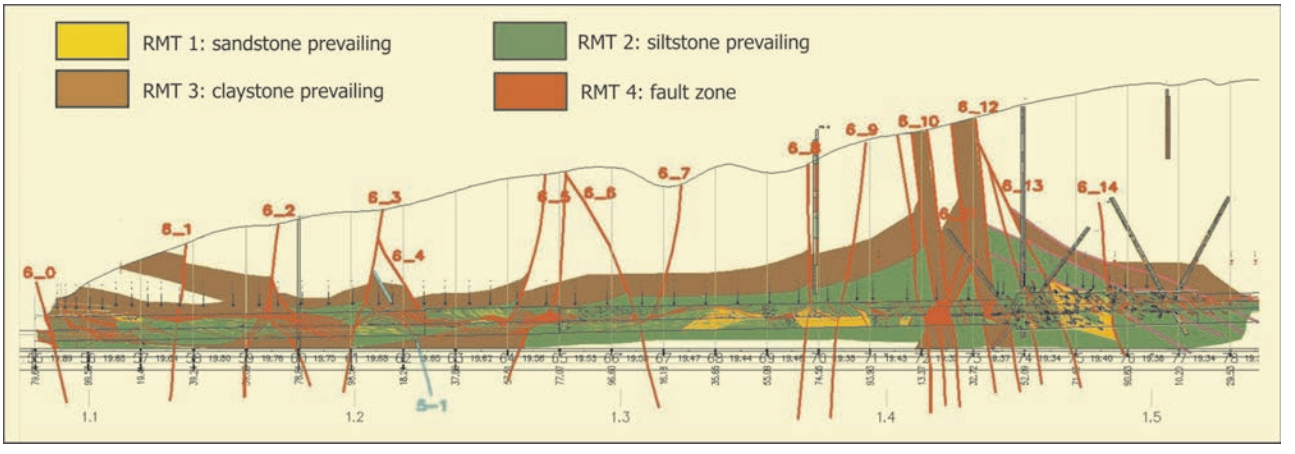

Figure 9. Geological cross section of the Šentvid hill – left tube, northern part (ELEA iC).

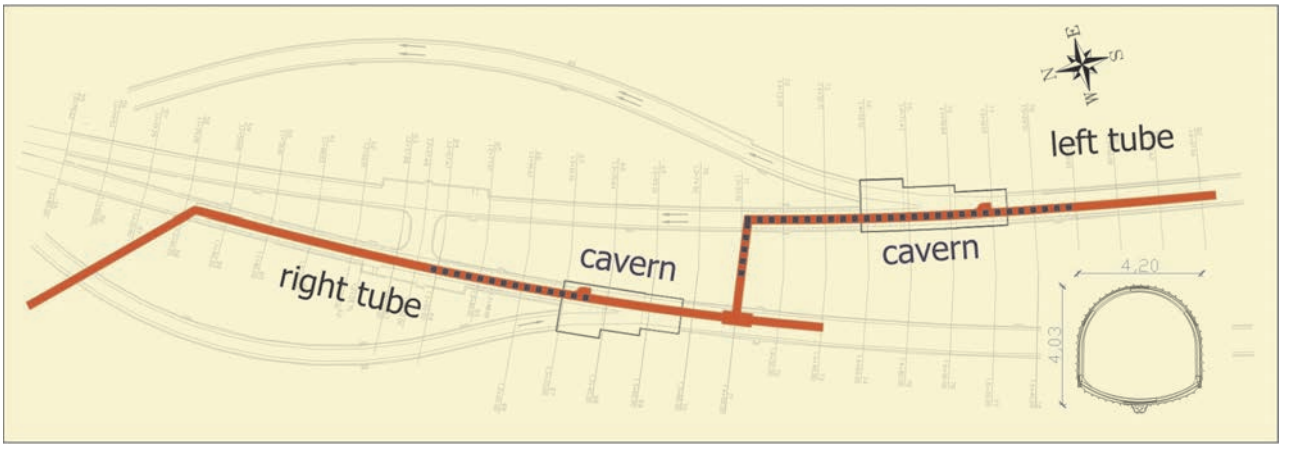

Figure 10. Ground plan and cross section of the Šentvid exploratory tunnel.

To determine the most favorable position of the caverns in terms of geological and geotechnical criteria the exploration gallery in the axis of the main tunnel was constructed in the final stage of the design. The length of the exploration gallery was approximately 655 m with a cross section of 13 m^2 (Fig. 10). Due to a small cross section the primary lining was executed as a micro fiber reinforced shotcrete with steel arches and wire mesh in the crown. No rock bolts were installed.

The exploratory tunnel allowed the establishment of a reliable geological model and enabled the in-situ geotechnical testing (core drilling, geophysical surveys, extensometers). The geodetic measurements of the 3D displacements during the exploratory tunnel construction improved the knowledge of the rock mass behaviour and its response to the tunnel excavation.

Beside all the information that contributed to the successful execution of the main tunnel, the exploration gallery enabled the observations of the rock mass – support system behaviour ahead of the face of the main tunnel during the execution of the main tunnel.

3.2 PERFORMANCE OF GEODETIC MEASUREMENTS

Continuous measurements of the primary lining were performed in both tubes of the exploratory tunnel. When the left tube of the main tunnel was approaching the intersection of the cross-passage and left tube of the exploratory tunnel (chainage km 1.3+97), the geodetic measurements of the targets were performed once a day in cross-passage, perpendicular to the main tunnel axis. These results improved the knowledge on the rock mass behaviour perpendicular to the tunnel axis.

The monitored sections are marked with a blue dotted line in Fig. 10. The lengths of the monitored sections and the number of the measuring profiles are given in Table 1.

Table 1. Chainages, lengths and number of measuring profilein monitored tunnel sections.

	chainage	section length [m]	measuring profiles
right tube	km 1.2+57 - km 1.3+32	75	37
cross-passage	km 0+20 - km 0+40	20	9
left tube	km 1.3+97 - km 1.5+44	147	72

The geodetic prisms were installed in the primary lining of the exploratory tunnel every two meters in the crown and every six meters on both side walls and ground along the tunnel axis. The 3D positions of the targets in the lining of the exploratory tunnel in front of the main tunnel face were recorded every hour by precise electronic tachymeter LEICA TCRP 1201R300.

3.3 RESULTS OF 3D DISPLACEMENT MEASUREMENTS

The magnitude of the measured displacements was in range from a few millimeters to almost 35 cm. The maximum observed displacements in each direction are given in Table 2.

Figure 11a. Electronic tachymeter and geodetic prisms installed in the primary lining and on the bottom of the exploration gallery.

Figure 11b. Position of the exploratory tunnel on the double lane tunnel top heading face.

Table 2. Maximum displacements in each direction for different points in the exploratory tunnel due to the excavation of the main tunnel.

	vertical		lateral		longitudinal	
	[cm]	dir.	[cm]	dir.	[cm]	dir.
crown	18.7	↓	6.4	←	29.3	↙
left side wall	26.5	↓	16.9	→	21.1	↙
right side wall	20.4	↓	17.1	←	21.0	↙
bottom	34.6	↑	11.3	←	6.4	↗

3.3.1 General behaviour

General behaviour of rock mass – support system that was measured in the exploratory tunnel in front of the main tunnel face is shown in Fig. 12 together with the prevailing geological scheme in monitored sections (sub-horizontal foliation in cross section with slight inclination towards left side of the tunnel and steeply inclined foliation into the excavation direction in longitudinal cross section, i.e. dip angle of the foliation is approximately 55° with relative dip direction with respect to the tunnel axis of 25° to the left).

The distinctive bilinear deformation pattern can be observed in Fig. 12 (evident in longitudinal section and cross section). The displacement vectors in cross section of the exploratory tunnel followed the direction of the rock mass foliation towards the left sidewall of the tunnel when the excavation face was far away from the observed cross section. In this first deformation phase the additional rock mass pressure onto the primary lining was small and the sliding mechanism along the foliation dominated over the radial deformation due to rock mass pressure. For this reason the left sidewall point tended vertically down and not in the radial direction. Similar explanation can be given for the longitudinal section.

As the tunnel face approached the observed cross section, the displacements due to the rock mass pressure became significantly larger than the sliding displacements along the foliation and consequently the displacement vectors changed their orientation.

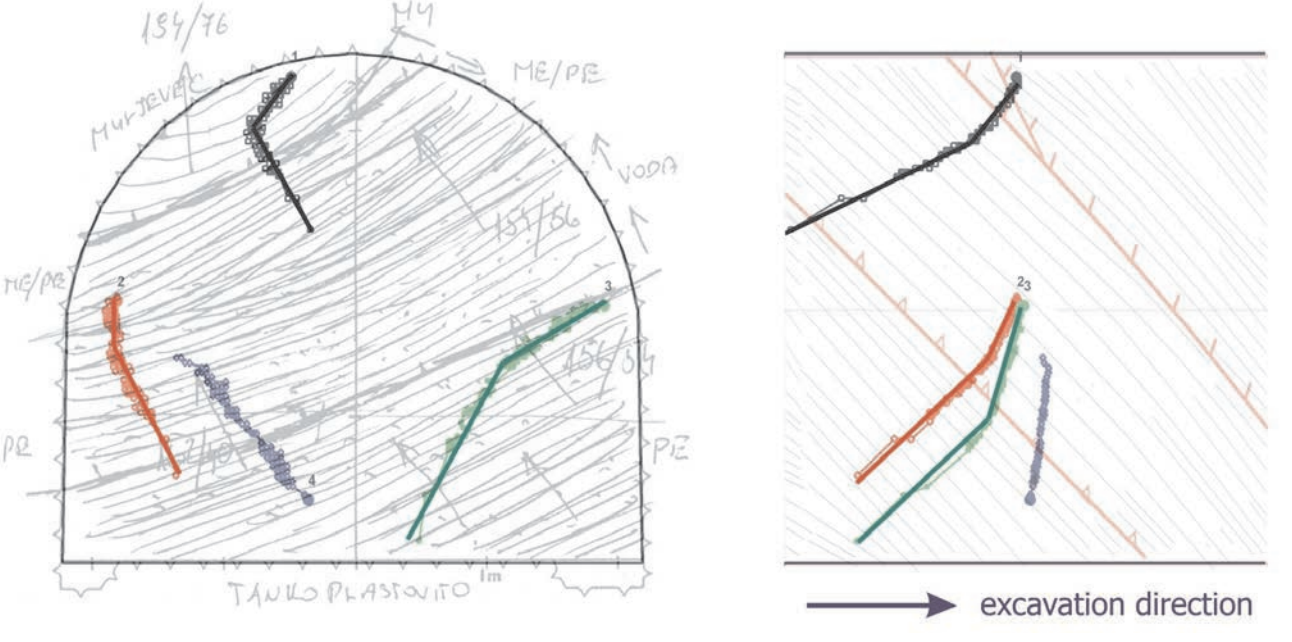

Figure 12. Bilinear displacement vectors in cross section and in longitudinal section in the left tube at chainage km 1.4+56.

The deformation mechanism changed from sliding along the foliation in the first phase to the buckling of the foliation in the second phase when the influence of the excavation face to the monitored cross section was intensified. On the basis of several monitored cross sections with similar deformation patterns we can conclude that the rock mass – support system behaviour well ahead of the face is mainly governed by the orientation of the rock mass discontinuities.

The displacement vector orientation change occurred suddenly and a turn point can be located on the plots of displacement vectors (Fig. 12). This turn point happened at a certain distance between the monitored section and the approaching face of the top heading.

If the percentage of the final measured displacement is plotted against the distance from the top heading excavation face the displacement-distance curve is obtained (Fig. 13). This curve is also bilinear and can be simply divided in two parts. The turn point for monitored cross section between both parts occurred 5.5 m ahead of the two lane tunnel excavation face and at 45 % of the final displacement for the presented measuring cross section.

The analysis of other cross sections indicates that the turn point occurs at about one half of an equivalent tunnel diameter in front of top heading face at 40-60% of final displacement. Between the measuring section and the approaching face of the top heading at the moment when the diagram in Fig. 13 exhibits the turn point there is the area of large displacements. The area further away from the tunnel face in the excavation direction can be referred to as the area of small displacements.

Observed structural damage of the primary lining coincided well with the measured displacements. In the area of small displacements only micro cracks were noticed while in the section closer to the tunnel face up to 25 cm wide cracks were registered (Fig. 14). These large cracks were formed mainly due to large longitudinal displacements. As it can be seen from displacement vectors in longitudinal section in Fig. 12, the longitudinal displacements in the first phase were much smaller than the vertical, but were greatly increased in the second phase.

In some cross sections no vertical displacements were observed in the second deformation phase, sometimes even heaving was registered.

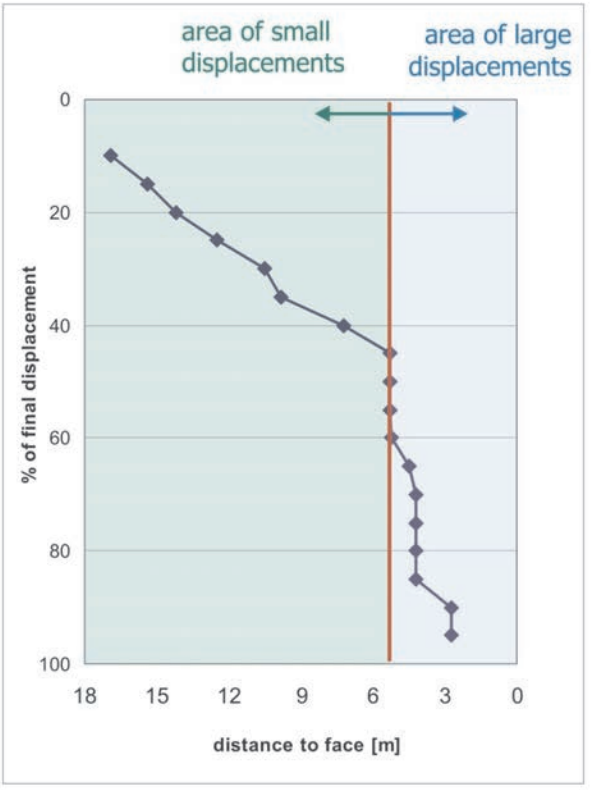

Figure 13. Relative vertical displacement of the crown point in exploratory gallery vs. distance to the top heading excavation face.

Figure 14. Large crack in primary lining of the exploration gallery due to large longitudinal displacements.

3.3.2 Area of small displacements ahead of the main tunnel top heading face

The beginning of the area of small displacements at the far end from the main tunnel face was determined at a 3 mm displacement of a particular measuring point to eliminate the measurement error (the inaccuracy of determining the position of measuring points was less than 2 millimeters [16]).

In Fig. 15 the distances from the excavation face to the measuring points at which the measured vertical displacements of a bottom and crown point reached 3 mm and 1 cm, respectively, are plotted along the monitored section of the left tube of the exploratory tunnel. It can be observed that the bottom points moved prior to the crown points. A rather stiff primary lining where the crown point was installed on one hand and no invert at the bottom of the exploratory tunnel on the other can explain such behaviour.

Area of recognizable displacements as observed on bottom points reached the length of about 18 – 25 m (2 - 2.5 equivalent tunnel diameters) for a 3 mm displacement and 10 – 20 m (1 – 2 diameters) for a 1 cm displacement in front of the face of the two lane tunnel. Due to a larger excavation cross section in the cavern with simultaneous transition into the fault zone, the uplift of the bottom was registered at larger distances from the top heading face from the chainage km 1.4+95 on. The maximum distance to the excavation face, where the measured vertical displacement of the bottom point exceeded 3 mm, reached 42 m.

Similar behaviour was observed for the crown points, only the distances to the face were considerably smaller (10 – 20 m for a 3 mm displacement and 5 – 12 m for a 1 cm displacement in front of the two lane tunnel).

3.3.3 Comparison of the displacements in the exploratory tunnel measured during the exploratory tunnel construction with the displacements measured during the main tunnel construction

As described above in chapter 3.3.1, the rock mass behaviour in the exploratory tunnel ahead of the face during the main tunnel construction is mainly governed by the orientation of the foliation. Similar dependence can also be observed at the displacements measured during the exploratory tunnel construction. Fig. 16

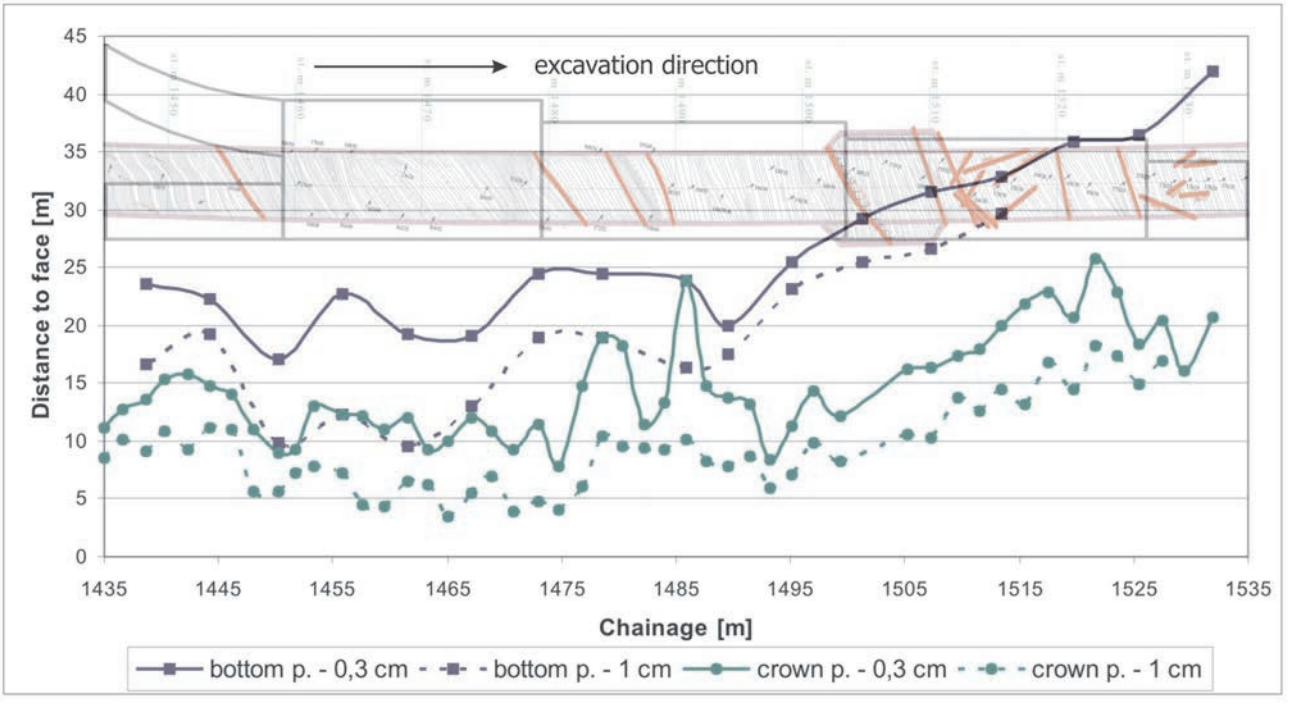

Figure 15. Distance of measuring points to the top heading face when the vertical displacement of the bottom and crown point reached 3 mm and 1 cm, respectively, plotted along the left tube of the exploratory tunnel. The scheme of the merging cavern is not in scale.

shows different behaviour of the exploratory tunnel due to two different construction activities (construction of the exploratory tunnel and construction of the main tunnel) and consequently two different load cases.

When the exploratory tunnel was under construction, the stress change rate due to the excavation was the highest in the area of the excavation face. As the excavation continued, the stress change rate around the same cross section was reduced. Consequently, the displacement rates were high during the initial phase and were close to zero later on. The displacement vector of the crown point tended perpendicularly to the foliation during the initial phase (in the area of large displacements – a blue line marked with letter L in Fig. 16) and parallel to the foliation in the second deformation phase (the area of small displacements – a purple line marked with letter S). Bilinear displacement pattern can only be seen to a limited extent because the absolute values of the measured displacements are small. This phenomenon became more evident from the displacement measurements ahead of the main tunnel excavation face, since the measured displacements were considerably larger in this case due to larger cross section of the main tunnel compared to the exploration gallery. Moreover in the latter case the entire displacement history was measured.

The behaviour ahead of the main tunnel excavation face was just the opposite of the behaviour, observed during the excavation of the exploratory tunnel. The directions of displacement vectors in both cases coincided well when the displacement rates are small (letter S in Fig. 16) and were similar in the area of large displacement rates (letter L in Fig.16). The hypothesis is proposed that the displacements parallel to the foliation dominate when stress change rates are small, while radial displacements govern the behaviour when stress change rates are high.

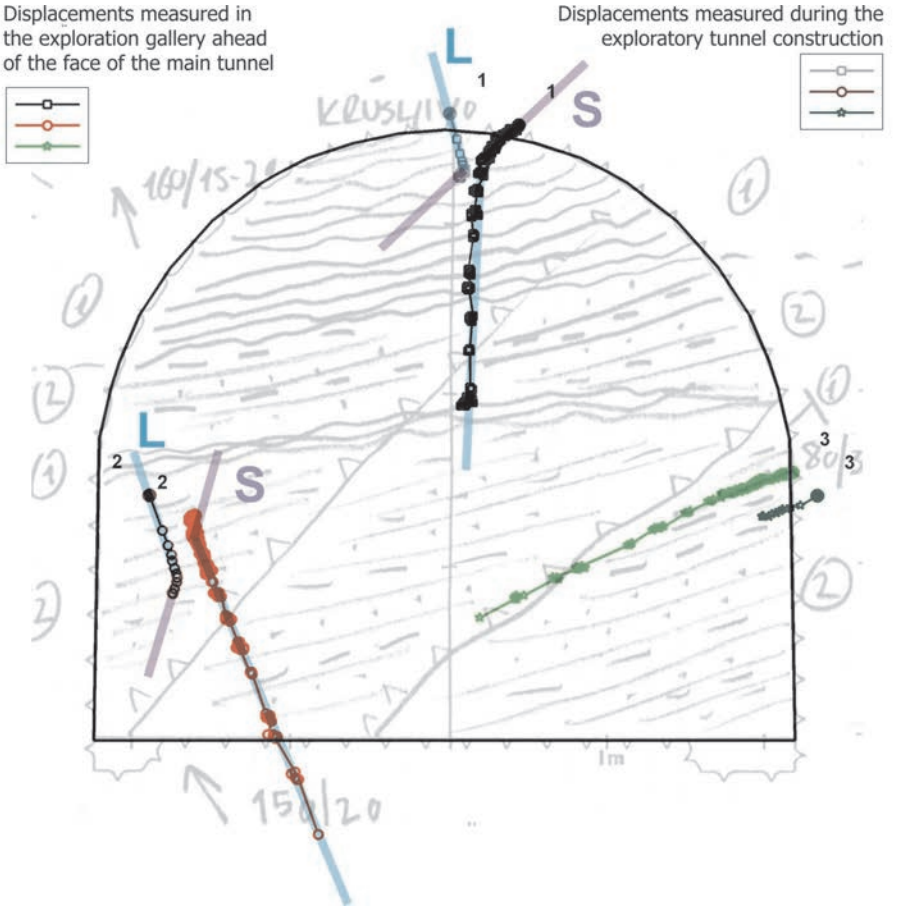

Figure 16. Comparison of the displacements during the execution of the exploration gallery and the displacements measured during the main tunnel construction in the left tube at the chainage km 1.5+17 – cross section together with a face log.

3.3.4 comparison of the displacements ahead of the face and the displacements within the main tunnel due to the main tunnel construction

The comparison of the measured displacements ahead of the face of the main tunnel with the displacements of the main tunnel at the same chainages along the tunnel axis allows the estimation of the portion of the pre-face displacements in total measured displacements and the influence of the orientation of foliation on the orientation of the displacement vectors.

The displacement vectors of the exploration gallery and of the main tunnel, caused by the execution of the main tunnel, are plotted in Fig. 17. Similar displacement patterns as described in the previous chapter can be seen. The displacement rates of the monitored cross section were largest some meters ahead (measured on the lining of the exploration gallery) and behind the top heading excavation face (measured on the lining of the main tunnel). Hence, the crown and left sidewall point's displacement vectors tended perpendicularly to the rock mass foliation. The orientation of the displacement vectors changed when the excavation face was far enough from the observed cross section (ahead or behind the face) and the rate of displacements diminished.

The magnitudes of the vertical and horizontal displacements of both sidewall points in the exploratory tunnel were approximately the same as the displacements of the sidewall points in the primary lining of the double lane tunnel. The vertical displacement of the crown point was in the exploration gallery than the vertical displacement of the crown point target in the main tunnel and reached about 35% of total measured displacement (marked with a red square in Fig. 18 for the cross section shown). Total measured displacement refers to the sum of displacements measured ahead of and behind the face of the main tunnel. The displacements caused by the exploration gallery execution are neglected. It should be also noted that the targets, where displacements were summed and compared, were not installed at the same places in the observed cross section, as can be seen in Fig. 17. The influence of these simplifications on the assessment of the pre-face portion of total displacements will be studied by numerical analyses. Preliminary numerical study by Jemec showed that the presence of the exploration gallery had limited effect on the behaviour of the main tunnel [17].

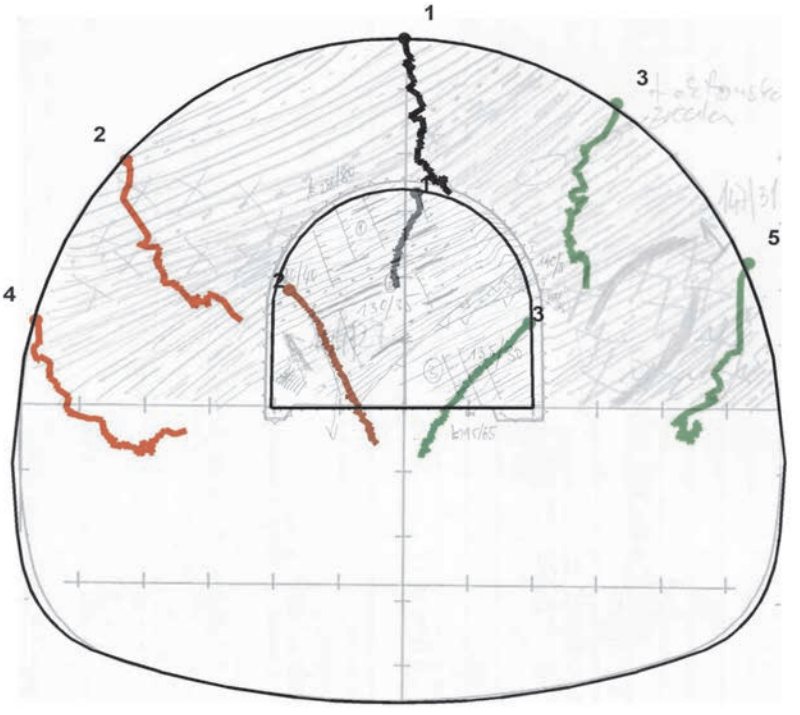

Figure 17. Comparison of the displacements ahead of the face and the displacements after the excavation of the main tunnel at chainage km 1.4+44 in the left tube of the Šentvid tunnel – displacement vectors in cross section with face log.

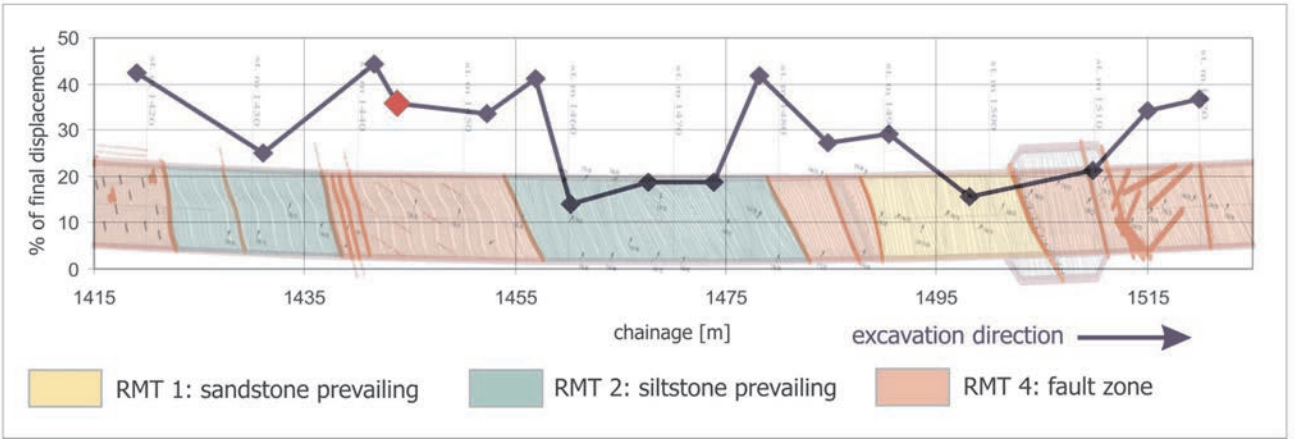

Figure 18. The portion of the vertical displacements that occurred ahead of the face for the crown point in the exploratory tunnel and for a point in the main tunnel that is situated above the exploration gallery.

In the monitored section of the left tube of the Šentvid tunnel the measured displacements ahead of the face amounted 15% to 45% of the total measured displacements in the same cross section (Fig. 18). A lower portion of the pre-face displacements was observed in stiffer and non-folded rock mass or folded to smaller extent (regions of green and yellow colour in Fig. 18), whilst in more deformable or intensively folded rock mass (regions of red colour) the percentage of the pre-face displacements was considerably higher.

The stated percentage does not take into account the displacement that occurred between the excavation and the first measurement of the newly installed measuring

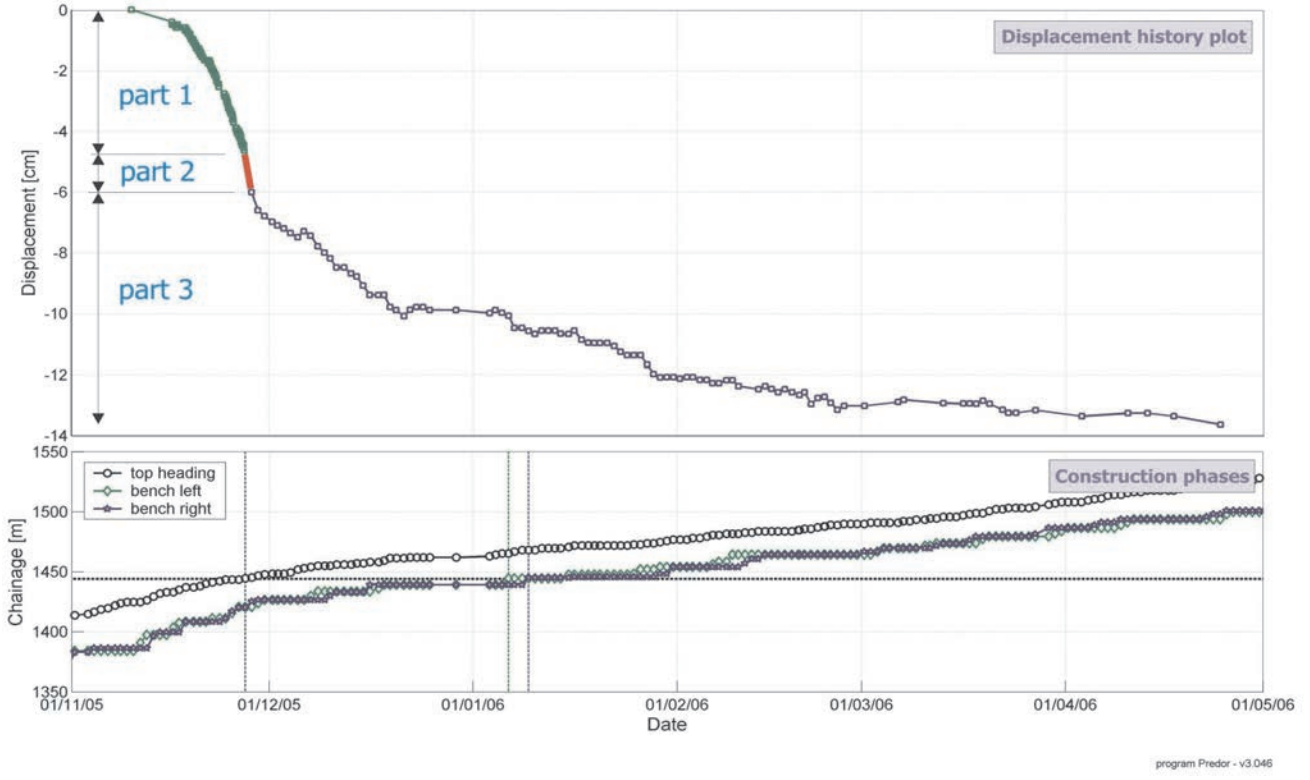

Figure 19. The complete displacement history plot of the crown point in the cross section at the chainage km 1.4+44.

section (part 2). The displacement rates in this phase are the highest because of the unsupported rock mass immediately after the excavation and low stiffness of the installed support before the shotcrete hardens. On the basis of the displacement's tangent slope close to the excavation face (some days before and after the excavation of a certain cross section) and time delay between the excavation and the first measurement, we can anticipate the course and the magnitude of the second part of the displacement function's curve (Fig. 19). The estimated portion of the displacements in part 2 is in the range from 10% – 25% of the total displacements.

From the presented cases we can deduce that 25% - 70% of displacement occurs before the first measurement of the observed cross section, depending mainly on the stiffness of the surrounding rock mass, construction sequence and the time delay of the first measurement.

4 CONCLUSION

Back analyses and interpretation of measured displacements ahead of the excavation face of the main tunnel and perpendicular to its axis and the comparison with the displacements measured during the exploratory tunnel construction as well as the main tunnel construction allow comprehensive interpretation of the rock mass – support response due to the tunnel excavation.

A large amount of data was obtained on approximately 250 m long section of the exploratory tunnel of the Šentvid tunnel system. The analyses of these data can provide the knowledge on deformation mechanisms of the rock mass – support system ahead of the tunnel face, which is essential in case of tunnel construction at low overburden under populated area. According to the presented cases one can conclude that the behaviour of the rock mass – support system strongly depends on the foliation orientation if the tunnel is constructed in foliated rock mass of low strength and stiffness like the Šentvid tunnel.

The magnitude of the displacements of the exploratory tunnel primary lining due to the main tunnel construction and its portion in all the measured displacements is strongly correlated to the stiffness of the rock mass. The comparison of the displacements ahead of the face with the displacements after the excavation of the main tunnel indicates that 15-45% of the measured displacements occur ahead of the face (less displacement in stiff rock mass that was not folded and more in worse geological – geotechnical conditions). On the basis of the measured displacements in different rock mass types we can assume the strong dependence of the portion of the stress state alternation ahead of the face (parameter Q_i) on the stiffness of the rock mass.

The geological structure ahead of the face and the size of the tunnel affect the influence area ahead of the face due to the excavation face advance or what is called pre-face domain. The analysis of the measured displacements shows that the small displacement domain can be observed approximately 2 equivalent diameters of the tube ahead of the face and the majority of the displacements occur within a half of an equivalent tube diameter from the face. The value for the parameter x_f cannot be deduced from the measured data at present time. Detailed analyses including fitting displacement function to the measured displacements ahead of the face as well as the displacements of the excavated area will define the recommended value for x_f.

The fitting of the displacement function to the displacements measured ahead of the face allows a judgment on the suitability of the first part of the proposed displacement function and possible modifications of its shape to demonstrate the observed bilinear response of the primary lining in the foliated rock mass.

To establish a reliable model for the rock mass behaviour prediction ahead of the face measured displacements will serve as an input to extensive 3D numerical simulations to confirm the suitability of the model.

If the proposed model proves to be reliable and accurate, it will be a fast and powerful tool for the prediction of the overall rock mass – support system behaviour. Such tool can contribute to better understanding of the ground behaviour around tunnels with low overburden under populated area [5]. For a given geological structure and known rock mass behaviour on some sections at the same site the displacements of further sections to be excavated can be calculated and therefore sufficient support measures can be designed to comply with the displacement tolerance in the tunnel as well as on the surface.

The knowledge on the rock mass behaviour ahead of the face can also serve for the optimization of the support, installed ahead of the face.

REFERENCES

[1] Rabcewicz L. (1964) *The New Austrian Tunnelling Method*, Part one, Water Power, November 1964, 453-457, Part two, Water Power, December 1964, 511-515.

[2] Vavrovsky, G. M. and Ayaydin N. (1987) *Die Bedeutung der vortriebsorientierten Auswertung von Messungen im oberflächennahen Tunnelbau.* STUVA-Tagung, Essen.

[3] Schubert, W. and Vavrovsky, G.M. (2003) *Innovations in Geotechnical on-site Engineering for Tunnels*. International Symposium on GeoTechnical Measurements and Modelling, Karlsruhe, 35-44.

[4] Steindorfer, A. (1998). *Short Term Prediction of Rock Mass Behaviour in Tunneling by Advanced Analysis of Displacement Monitoring Data*. PhD thesis, Technische Universität Graz.

[5] Sellner, P., Grossauer, K., Leitman, R. (2004). *How to Predict Surface Movements & Prevent Damages of Surface Structures*. Rock engineering – Theory and Practice, Proceedings of the ISRM regional symposium EUROCK 2004 & 53rd Geomechanics Colloquy. Salzburg, 7-9 October, 245-250.

[6] Guenot, A., Panet, M., Sulem, J. (1985). *A New Aspect in Tunnel Closure Interpretation*. Proc. 26th US Symposium on Rock Mechanics, Rapid City, 445-460.

[7] Barlow, J.P. (1986). *Interpretation of Tunnel Convergence Measurements*. MSc thesis, Department of Civil Engineering, The University of Alberta, Edmonton, Alberta.

[8] Sellner, P.J. (2000). *Prediction of Displacements in Tunneling*. PhD thesis, Technische Universität Graz.

[9] GeoFit homepage: http://www.geofit.3-g.at/

[10] Klopčič, J. (2004). *Visualization and analysis of the displacement monitoring data in tunneling*. BSc thesis, University of Ljubljana, Faculty of Civil and Geodetic Engineering. (in Slovene)

[11] Schubert, P., Klopčič, J., Štimulak, A., Ajdič, I., Logar, J. (2005). *Analysis of Characteristic Deformation Patterns at the Trojane Tunnel in Slovenia*. Felsbau, No.5, 25-30.

[12] Volkmann, G. and Schubert, W. (2005). *The use of horizontal inclinometers for the optimization of the rock mass – support interaction*. Underground space use: Analysis of the past and lessons for the future, World tunneling congress, Istanbul, Turkey.

[13] Likar, J., Volkmann, G., Button, E. (2004). *New Evaluation Methods in Pipe roof Supported Tunnels and its Influence on Design during Construction*. Rock engineering – Theory and Practice, Proceedings of the ISRM regional symposium EUROCK 2004 & 53rd Geomechanics Colloquy. Salzburg, 7-9 October, 277-282.

[14] Žigon, A., Proprentner M., Žibert, M. and Jemec, P. 2006: *Šentvid tunnel*. Proceedings of the XIII. Danube – European Conference on geotechnical engineering, Ljubljana. 29-31 May 2006, 2nd part, 1025-1030.

[15] Čadež, F., Genser, W., Kleberger, J. and Pöschl, I. (2004). *Šentvid motorway tunnel – Interim results from Slovenia's most recent exploration gallery*, Proceedings of the 7th international symposium on tunnel construction and underground structures, Ljubljana, 50-56.

[16] Marjetič, A., Ambrožič, T., Bogatin, S., Klopčič, J., Logar, J., Štimulak, A. and Majes, B. (2006). *Geodetic measurements in Šentvid tunnel*. Geodetski vestnik *50*, No.1, Ljubljana, 11-24. (in Slovene)

[17] Jemec, P. (2006). *Influence of the exploration gallery on the Šentvid two lane tunnel construction*. BSc thesis, University of Ljubljana, Faculty of Civil and Geodetic Engineering. (in Slovene)

VPLIV POROZNOSTI NA GEOMEHANSKE LASTNOSTI POLŽARICE IZ LJUBLJANSKEGA BARJA

BOJAN ŽLENDER IN LUDVIK TRAUNER

o avtorjih

Bojan Žlender
Univerza v Mariboru,
Fakulteta za gradbeništvo
Smetanova ulica 17, 2000 Maribor, Slovenija
E-pošta: bojan.zlender@uni-mb.si

Ludvik Trauner
Univerza v Mariboru,
Fakulteta za gradbeništvo
Smetanova ulica 17, 2000 Maribor, Slovenija
E-pošta: trauner@uni-mb.si

izvleček

Prispevek obravnava mineraloške in fizikalne lastnosti polžarice in njihov vpliv na vrednosti parametrov geomehanskih lastnosti. Polžarica, ime je dobila po vsebovanih fosilih, je tipični sloj Ljubljanskega barja. Je izrazito porozna, zasičena in se nahaja v židkem konsistentnem stanju.

V Laboratoriju za mehaniko tal (LMT), Fakultete za gradbeništvo, Univerze v Mariboru je bila izvedena raziskava polžarice s preiskavo mineraloških in fizikalnih lastnosti. Za raziskavo je bil odvzet niz vzorcev na jugozahodni lokaciji Ljubljanskega barja.

V Centru za elektronsko mikroskopijo Fakultete za strojništvo, Univerze v Mariboru sta bila raziskana kemična sestava in optični izgled. Kemična sestava je bila določena z visokoločljivim vrstičnim elektronskim mikroskopom SIRION. Optični izgled treh vzorcev polžarice je bil preiskan z okoljskim vrstičnim elektronskim mikroskopom QUANTA 200 3D. Mineralna sestava in zrnatost polžarice sta bila določena na Geološkem zavodu Slovenije. Mineralna sestava je bila določena z rentgenskim difraktometrom. Zrnatost polžarice je bila določena s pomočjo laserskega analizatorja Fritsch particle sizer analysette 22. Specifična površina je bila določena na Kemijskem inštitutu Slovenije, s pettočkovno BET metodo, za meritve je bil uporabljen avtomatski plinski adsorbcijski analizator TriStar 3000, proizvajalca Micromeritics Instrument Corporation, Norcross, ZDA. Ostale fizikalne lastnosti polžarice so bile določene v LMT.

Raziskane fizikalne lastnosti kažejo, da je polžarica v naravi zasičena, zelo porozna in skoraj tekoča meljna zemljina. Preiskava stisljivosti kaže, da je polžarica izrazito stisljiva, volumenske spremembe so velike že ob malih spremembah napetosti. Parametri trdnosti imajo značilno nizke vrednosti, ki se ujemajo s predhodnimi raziskavami.

Raziskava geomehanskih lastnosti je bila izvedena s poudarkom na sovisnosti fizikalnih lastnosti. Izveden je bil niz triosnih preizkusov polžarice različne gostote oz. vlažnosti in poroznosti. Preizkusi so bili izvedeni v triosnih aparatih na valjastih preizkušancih višine 100 mm in premera 50 mm.

Rezultati raziskave kažejo na sovisnost geomehanskih lastnosti in poroznosti. Odnose lahko izrazimo kot funkcije gostote oz. poroznosti ali vlažnosti. Iz rezultatov je razvidno, da so spremembe vodoprepustnosti, konsolidacije in stisljivosti nelinearno odvisne od sprememb poroznosti. Spremembe mehanskih parametrov kot so elastični modul, Poissonov količnik in strižni kot, so pri manjših spremembah poroznosti neizrazite in skoraj linearne.

ključne besede

polžarica, triosni preizkus, poroznost, vodoprepustnost, konsolidacija, Youngov modul, Poissonov količnik, strižni kot

THE INFLUENCE OF POROSITY ON GEOMECHANICAL CHARACTERISTICS OF SNAIL SOIL IN THE LJUBLJANA MARSH

BOJAN ŽLENDER and LUDVIK TRAUNER

about the authors

Bojan Žlender
University of Maribor,
Faculty of Civil Engineering
Smetanova ulica 17, 2000 Maribor, Slovenia
E-mail: bojan.zlender@uni-mb.si

Ludvik Trauner
University of Maribor,
Faculty of Civil Engineering
Smetanova ulica 17, 2000 Maribor, Slovenia
E-mail: trauner@uni-mb.si

abstract

This article focuses on mineralogical and physical characteristics of snail soil and their influence on parameter values of geomechanical characteristics. Snail soil, which got its name from fossil remains, is a typical layer observed in the Ljubljana marsh. It is distinctly porous, saturated and in a liquid consistency state.
Snail soil was investigated for mineralogical and physical characteristics in the Laboratory of Soil Mechanics, Faculty of Civil Engineering of the University of Maribor. Mineral and chemical composition, visual appearance, specific surface and grain property were determined. Physical characteristics show that snail soil is saturated in nature, highly porous and almost liquid.
Geomechanical characteristics were investigated for their interdependency on physical characteristics. A series of triaxial tests were performed on snail soil samples of different porosity, density and water content. Cylindrical samples of the height of 100 mm and the diameter of 50 mm were tested using three-axial testing apparatuses.
The results of the tests show that interdependency exists between geomechanical characteristics and porosity. These relationships can be expressed as functions of density, porosity or water content. It is evident from the results that changes of the coefficient of permeability, the coefficient of consolidation, and the coefficient of volume compressibility are non-linear with respect to changes of porosity. Changes of mechanical parameters, such as Young's modulus, Poisson's ratio, and friction angle are indistinct and almost linear at lower changes of porosity.

keywords

Snail soil, triaxial test, porosity, permeability, consolidation, Young's modulus, Poisson's ratio, friction angle

1 INTRODUCTION

This article focuses on mineralogical and physical characteristics of snail soil and their influence on parameter values of geomechanical characteristics. Snail soil, which got its name from fossil remains, is a typical layer observed in the Ljubljana marsh. It is distinctly porous, saturated and in a liquid consistency state.

The Ljubljana marsh is a wide tectonic sink which was formed two million years ago by a gradual depression of the area. The marsh is located in the south of Ljubljana, at the elevation of 287–290 m above the sea level, and covers the surface of 163 km^2.

The Ljubljana marsh was inhabited already thousands of years ago. Archeological findings (fascine dwellings) date from the iron, copper, and bronze periods. Later, this marshy area was invaded by the Romans who were the first to start draining the land. The contribution of fascine dwellers from the Ljubljana marsh to a wider cultural space is also proven by the recent archeological finding, i.e. a wheel and the ax of a two-wheel vehicle, which dates from about 3200 A. D. For the present, this archeological finding is known to be the oldest of its type in the world.

Today, this area is almost completely drained and urbanized. Yet, the construction of traffic ways and tall buildings presents a great challenge to construction engineers due to the softness of layers below the surface.

Geological structure of the marsh is very interesting. Ground water is located immediately below the surface. The surface layer is composed of peat of the thickness of 1 m to 8 m. The dept of the peat is nowadays essentially smaller than in a past, due to the intensive excavations in

a first half of the 20th century. Below the peat layer, there is a layer of snail soil of the thickness of a few meters at the borders to more than 10 m in the center of the marsh. The snail soil layer is distinctly porous, saturated with water and of a low-bearing capacity. There are clay and sandy-gravel layers below the snail soil layer. A layer of rocks starts at the depth of some ten meters.

Geological structure of the Ljubljana marsh has been studied by numerous experts. The oldest geological documents go back to the middle of the 19th century, when the first geological map was drawn of this region. Later, several other studies were performed. In the second half of the 20th century the researches were focused on geomechanical characteristics of the soil and detailed investigations of physical and mechanical characteristics of snail soil were performed. Strength parameters showing possible static loadings were also determined. To understand geomechanical characteristics of this marshy area it is essential to know rheological characteristics of snail soil. In 1979, in the framework of Trauner's doctoral thesis [1], slow triaxial tests were performed in the Laboratory of Soil Mechanics at the Faculty of Architecture, Geodesy and Civil Engineering of the University of Ljubljana. A similar investigation was later repeated in the Laboratory of Soil Mechanics (LSM), Faculty of Civil Engineering of the University of Maribor. A rheological model of snail soil was set which shows relationships between stresses, deformations and time [2]. The results of investigation were expressed with rheological dependencies, i.e. function relationships between rheological parameters and stress state and deformation, at void ratio e = 2.1.

An example of dependencies (Figure 1a) showing the relationship between shear stress τ and effective normal stress σ', with low value of friction angle $\varphi = 21^\circ$ and no cohesion c = 0.

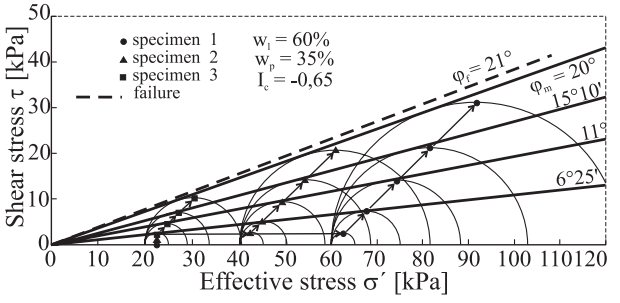

Figure 1a. Relationship between shear stress τ and effective normal stress σ'.

Fig. 1b shows a typical result obtained for the octahedral strain ε_0 depending on the octahedral shear stress τ_0 and effective octahedral stress state σ_0' of snail soil.

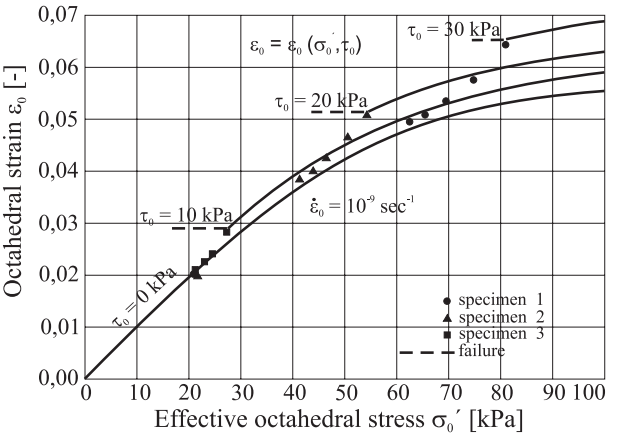

Figure 1b. Octahedral strain ε_0 vs. shear stress τ_0 for effective octahedral stress state σ_0'.

Fig. 1c shows a typical result obtained for the octahedral shear strain γ_0 depending on the octahedral shear stress τ_0 and effective octahedral stress state σ_0' of snail soil.

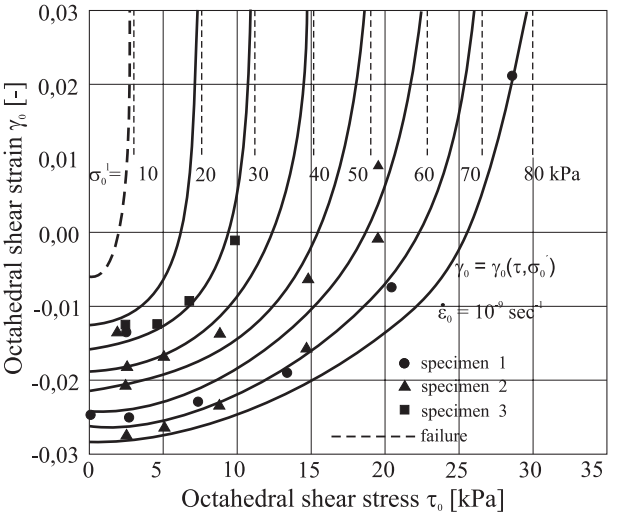

Figure 1c. Octahedral shear strain γ_0 vs. octahedral shear stress τ_0 for different effective octahedral stress state σ_0'.

Three years ago, the testing of snail soil was repeated and upgraded with the investigation of mineralogical and physical characteristics, as well as of geomechanical characteristics depending on physical characteristics. This article briefly presents researches performed and the influence of snail soil porosity on geomechanical characteristics.

2 CHARACTERISTICS OF SNAIL SOIL

A set of samples were taken on the southwest region of the Ljubljana marsh to conduct this research. Sampling was performed in the region of 3 m x 3 m at the depth of 3 m, so the ground was excavated to the depth of 2,5 m and a thin wall tube sampler (of the internal diameter of 100 mm) was forced into the ground. Samples of the diameter of 100 mm and the height of 300 mm were immediately packed after sampling. The ground water level was 1m under the surface in the region of sampling.

2.1 MINERAL COMPOSITION

The mineral composition (Table 1) was determined in the Laboratory of Geological Survey of Slovenia. The samples were scanned by X-ray diffraction technique (XRD) using a Philips PW 3710 diffractometer, a goniometer 1820, with an automatic divergence slit and a curved graphite monochromator, operating at 40 kV, 30 mA with CuK_{α} radiation and an Ni filter.

Table 1. Mineral composition of snail soil samples.

Mineral composition	Weight portion (%)
Calcite	87
Kaolinite	7
Muscovite	4
Quartz	3

2.2 CHEMICAL COMPOSITION

Chemical composition of the snail soil (Table 2) was determined at Centrum for electronic microscopy in University of Maribor. The scanning electron microscope SIRION which is equipped with the energy dispersive spectrometer EDS Oxford INCA 350, was used. The latter allows qualitative and quantitative micro chemical point and plane analyses, as well as qualitative linear analysis and determination of surface element distribution. Elements from beryllium to uranium can be analyzed.

Table 2. Chemical composition of snail soil.

Element	Average value (%)	Standard deviation (%)
C	12.15	1.49
O	48.78	1.95
Mg	0.52	0.09
Al	2.90	1.14
Si	5.34	2.25
K	0.80	0.25
Ca	29.51	5.17

2.3 VISUAL APPEARANCE

Visual appearance of snail soil samples was tested with the environmental scanning electron microscope QUANTA 200 3D, at Centrum for electronic microscopy in University of Maribor. The electron microscope is equipped with a system of double jets, i.e. electronic and ionic. The microscope is denoted with the word "environmental" or with the marking "ESEM" because it can be used at different pressures and at 100 % humidity.

The pressure in the chamber determines the types of samples to be observed.

Three operating principles are possible:

- High vacuum – It allows to observe conductive and non-conductive samples covered with a conductive coating (Au, C, Ag).
- Low vacuum – It allows to observe conductive and non-conductive samples without prior preparation.
- ESEM tape – It allows to observe all samples, also wet and greasy ones, and in-situ processes (hydration, dissolution …).

In observing the samples of snail soil, all three principles were used. Photographs were taken of damp samples and different blow ups were made; photographs of dry samples (Figure 2a), minerals in crystallized form, and remains of micro-organisms in the snail soil (Figure 2b) were also developed.

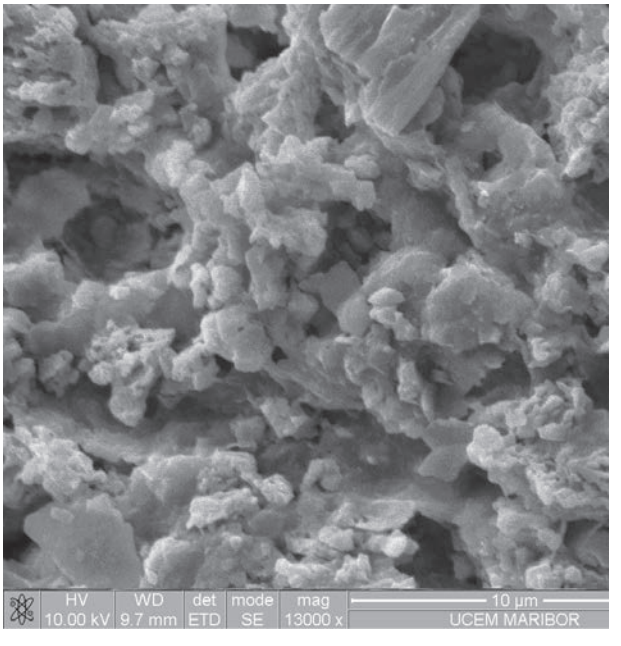

Figure 2a. A dry sample of snail soil (ESEM).

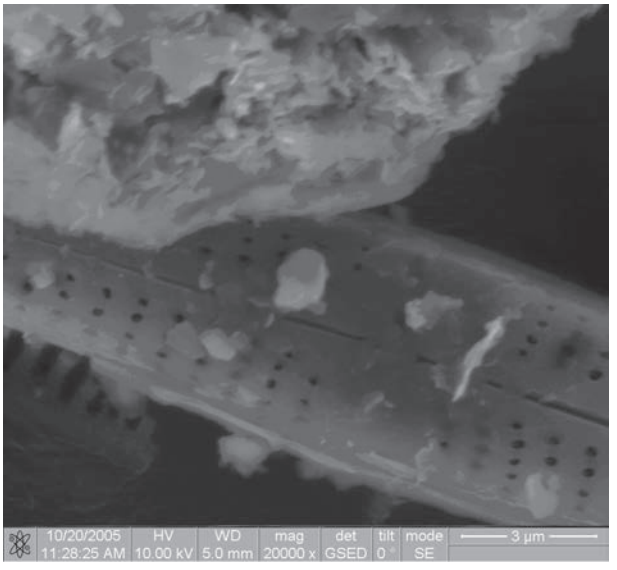

Figure 2b. Remain of micro-organism in snail soil, a dry sample (ESEM).

2.4 SPECIFIC SURFACE

Specific surface of grains is the surface of grains per unit mass. It is expressed in square meters per gram of dry substance (m^2/g). Specific surface of snail soil was determined at Chemical Institute Ljubljana, with the five-point BET method with adsorption of liquid nitrogen of 99.9% cleanliness and the temperature of 77^0 K.

The measurements were performed using the automatic TriStar 3000 gas adsorption analyzer, produced by Micromeritics Instrument Corporation, Norcross, U.S.A. The results of the test showed that snail soil has the specific surface of 5.03 ± 0.03 m^2/g.

2.5 PARTICLE SIZE DISTRIBUTION

Grain property of the snail soil sample was determined using the Fritsch Laser Particle Sizer Analysette 22 at the laboratory of Geological Survey of Slovenia. The results of the grain property analysis show (Fig. 3) that this snail soil falls within the range of silt (MH) with respect to granulometrical structure.

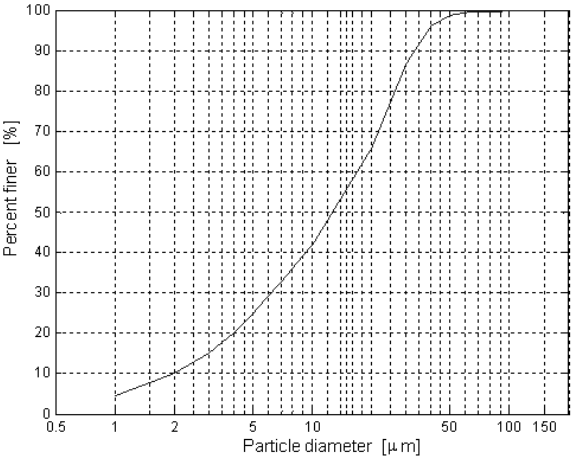

Figure 3. Particle size distribution of snail soil.

2.6 PHYSICAL CHARACTERISTICS

Physical characteristics (Table 3) show that snail soil is saturated in nature, highly porous and almost liquid.

Table 3. Physical characteristics of snail soil.

Soil property	Symbol	Unit	Value
Water content	w	%	75
Plastic limit	w_P	%	37
Liquid limit	w_L	%	60
Plasticity index	I_p	%	23
Consistency index	I_c	-	-0.65
Liquidity index	I_L	-	1.65
Density of solid	ρ_s	g/cm^3	2.62
Unit weight	γ	kN/m^3	15.5
Dry unit weight	γ_d	kN/m^3	8.8
Degree of saturation	S_r	%	100
Void ratio	e	-	2.1

2.7 COMPRESSIBILITY AND CONSOLIDATION

The investigation of compressibility was performed in LSM. Snail soil is markedly compressible; its volume undergoes great changes already when loaded with small changes of stress. Triaxial consolidation tests were performed at the effective stress changes σ'_0.

Consolidation parameters of snail soil in nature are given in Table 4. The values of consolidation parameters change with lower porosity, the parameters can be expressed as functions of porosity.

Table 4. Consolidation parameters (void ratio e = 2.1).

Soil property	Symbol	Unit	Value
Consolidation coefficient	c_v	m²/year	2,8 ÷ 3,2
Coefficient of volume compressibility	m_v	kPa^{-1}	1 ÷ 1,2 ·10^{-3}
Coefficient of soil permeability	k	m/s	2 ÷ 5 ·10^{-9}
Secondary compression ratio	$C_{\alpha\varepsilon}$ $C_{\alpha e}$	-	0.002 0.006

2.8 STRENGTH AND DEFORMABILITY

Strength parameters were determined in a series of triaxial tests. Strength parameters of snail soil in nature are given in Table 5. Values of parameters can also change with lower porosity; they can be expressed as functions of porosity.

Table 5. Consolidation parameters (void ratio e = 2.1).

Soil property	Symbol	Unit	Value
Consolidation coefficient	c	kPa	0
Friction angle	φ	°	21
Constrained modulus	M_c	kPa	800 ÷ 1000
Poisson's ratio	v	-	0.4

3 POROSITY – GEOMECHANICAL PARAMETERS RELATIONSHIPS

The investigation of the influence of porosity on geomechanical characteristics was performed. Tests for determining mechanical properties were performed using triaxial apparatuses. The following steps were observed in testing: preparation of the sample, procedure on the apparatus, performance of the test, and interpretation of the obtained results. The investigation included drained and undrained stress oriented triaxial tests according to the following phases:

- Saturation,
- Consolidation,
- Static loading.

In the first phase, saturation was tested by determining the coefficient $B = du/d\sigma > 0.96$. This was a relatively short-term phase because of saturation in the nature.

The saturated sample was then consolidated at the selected effective isotropic consolidation stress σ'_{3c} and selected compression stress change $\Delta\sigma_{3c}$. The effective isotropic consolidation stress is expressed as a difference between the cell pressure σ_{3c} and the back pressure u_b.

Static loading was performed so that the sample was loaded with the selected compression stress $d\sigma_{3c}$ or the axial stress $\Delta\sigma_a = \Delta\sigma_z$.

Sixty-two triaxial tests were performed. The investigation was based on a series of tests in which the below conditions varied:

- Void ratio e = 2.1 ÷ 1.2 (Δe is calculated),
- Initial effective pressures $\sigma_0' = \sigma'_{3c}$ = 0, 50, 100, 150 kPa,
- Variations of effective pressures $\Delta\sigma'$ = 50, 100, 150 kPa,
- Variations of axial pressures $d\sigma_z$ (depending on axial deformation).

The below pressures were measured during the test:

- Cell pressure σ_{3c} (kPa),
- Back pressure u_b (kPa),
- Pore water pressure u_w (kPa),
- Axial vertical stress in compression σ_z (kPa),
- Axial vertical and radial strain ε_z (-), ε_r (-),
- Volume deformation ε_v (-).

For undrained test ε_v (-)=0.

Constants in the research are:

- Specific surface,
- Chemical composition,
- Mineral composition,
- Grain property,
- Natural humidity, density and coefficient of porosity,
- Liquid limit, plasticity index, consistency index,
- Density of a solid mass,
- Dry volume weight,
- Saturation.

The following strength parameters were calculated: coefficients of permeability k (m/s), consolidation c_v (m²/s) and volume compressibility m_v (kPa^{-1}), constrained modulus M_c (kPa), Young's modulus E (kPa) and Poisson's ratio v (-), or compression modulus K (kPa), and shear modulus G (kPa).

Standard oedometer tests and direct shear tests of snail soil were also performed.

Snail soil has the void ratio e = 2.1 in nature, which is an extremely high value. Values of mechanical parameters change with lowering the void ratio.

Porosity (void ratio e) is in linear correlation with water content w. Density (ρ) or unit weight (γ) is in nonlinear correlation with void ratio e.

$$w = \frac{1}{D_r} \cdot e = \frac{\gamma_w}{\gamma_s} \cdot e \qquad \gamma = \frac{D_r + (S_r \cdot e/100)}{1+e} \cdot \gamma_w \quad (1)$$

where:

γ_w, γ_s unit weight of water and solids,
D_r relative density of soil,
S_r=1 degree of saturation.

Figures 4 show the correlation between void ratio e and water content w, and the correlation between void ratio e and density ρ. Therefore, the snail soil was in liquid or plastic consistency, for different tests.

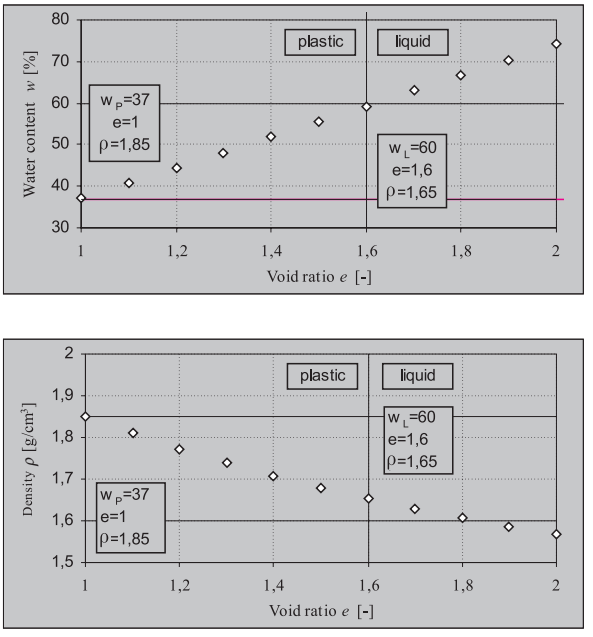

Figure 4. The correlation between void ratio e and water content w, and correlation between void ratio e and density ρ.

3.1 COEFFICIENT OF PERMEABILITY

The coefficient of permeability is expressed with equation

$$k = c_v \cdot m_v \cdot \gamma_w \qquad (2)$$

The coefficient of permeability of snail soil in nature is $k = 2 \cdot 10^{-9}$ m/s. The value of the coefficient of permeability decreases with decreasing void ratio e as shown in Fig. 5. The permeability can be expressed similar to a known expression of Ahuja et al. [3].

$$K_s = B \cdot \phi_e^n \qquad (3)$$

where:

K_s hydraulic conductivity,
ϕ_e effective porosity,
B, n are constants.

The relationship of the coefficient of permeability k vs. void ratio e for all tests is:

$$k(e) = B_1 \cdot e^n \qquad (4)$$

where

e void ratio
B_1, n_1 are coefficients.

We obtained the expression $k = 4 \cdot 10^{-11} \cdot e^{5,5019}$ for a series of all tests (where e is void ratio). Fig. 5 shows the relationship of the coefficient of permeability vs. void ratio for all tests. Deviation of the results (R = 0.3) from the above function is high because the function does not include stress conditions or pore pressure gradients, respectively. However, a more detailed description of the coefficient of permeability can be made with the functions of void ratio and stress states σ_0' = 50, 100, 150 kPa or with pertaining pore pressure gradients.

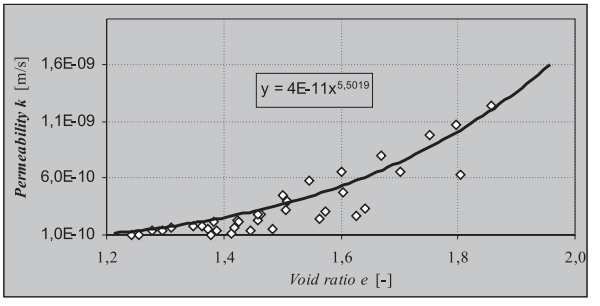

Figure 5. The coefficient of permeability k vs. void ratio e.

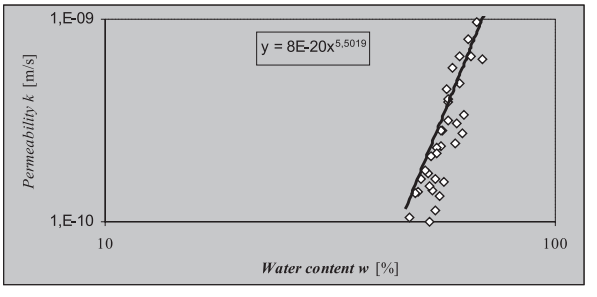

Figure 6. The coefficient of permeability k vs. water content w.

If the relationship of the coefficient of permeability k vs. void ratio e (or density ρ, or water content w) is

expressed in the logarithmic form, we can see that it is almost linear. Figure 6 shows this relationship as the coefficient of permeability k vs. water content w.

3.2 COEFFICIENT OF CONSOLIDATION

The coefficient of consolidation c_v is expressed using equation from BS 1377 [4]

$$c_v = \frac{1{,}65 \cdot D^2}{\lambda \cdot t_{100}} \qquad (5)$$

where:

D diameter of the specimen (mm),
λ coefficient which depends on the drainage,
t_{100} time of primary consolidation.

The relationship of the coefficient of consolidation c_v vs. void ratio e could be expressed similarly to the coefficient of permeability k. Fig. 7 shows the relationship of coefficient of consolidation c_v vs. void ratio e_c for all tests. We obtained the expression $c_v = 3 \cdot 10^{-8} \cdot e^{1{,}464}$ (e is void ratio).

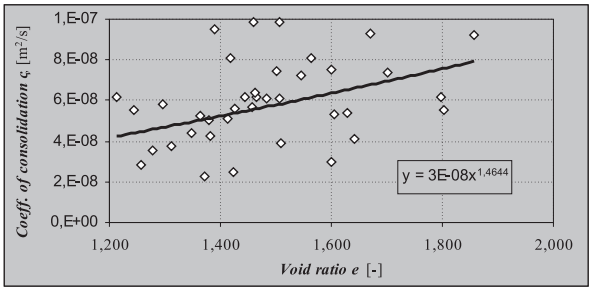

Figure 7. The coefficient of consolidation c_v vs. void ratio e.

3.3 COEFFICIENT OF VOLUME COMPRESSIBILITY

The coefficient of volume compressibility m_v is expressed with equation

$$m_v = \frac{\Delta e}{(1+e) \cdot \Delta \sigma'} = \frac{\Delta \varepsilon_v}{\Delta \sigma'} \qquad (6)$$

Fig. 8 shows the relationship of the coefficient of volume compressibility m_v vs. void ratio e for all tests. We obtained the expression $m_v = 9 \cdot 10^{-5} \cdot e^{3{,}5005}$.

The logarithmic form of relationship of volume compressibility m_v vs. water content w shows linear correlation log. $m_v = 3 \cdot 10^{-10} \cdot w^{3{,}5005}$.

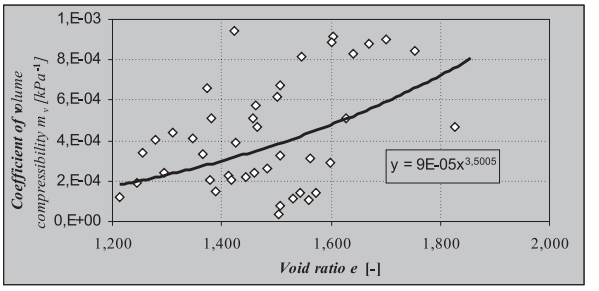

Figure 8. The coefficient of volume compressibility m_v vs. void ratio e.

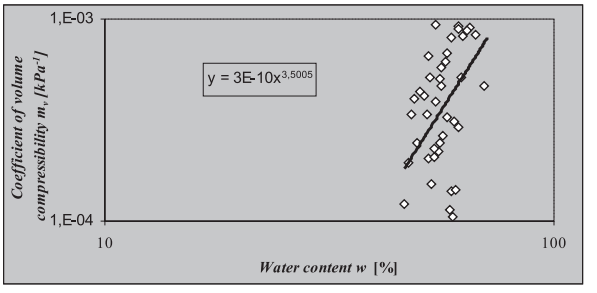

Figure 9. The coefficient of volume compressibility m_v vs. water content w.

3.4 STRENGTH PARAMETERS

To determine the relationship of strength parameters vs. void ratio an insufficient number of tests were performed therefore the results are unreliable. Fig. 8 shows Young's modulus E vs. void ratio e_c. We can see that strength does not substantially increase with increasing density or decreasing porosity; a greater difference can be only seen at higher changes of density or porosity. Poisson's ratio is $\nu = 0.4$ at void ratio $e = 2.0$ and decreases for 0.03 at void ratio $e = 1.4$.

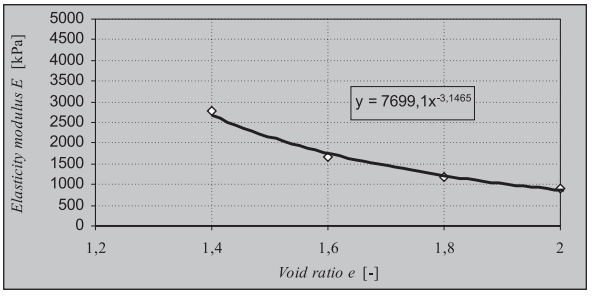

Figure 10. Young's modulus E vs. void ratio e.

If the relationship of the Young's modulus E vs. water content w is expressed in the logarithmic form, we can see that it is almost linear (Fig. 10).

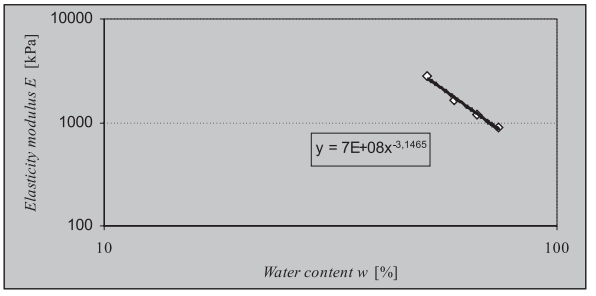

Figure 11. Young's modulus E vs. water content w.

The same is true for shear properties. Fig. 12 shows the relationship of friction angle φ vs. unit weight γ. We can see that it increases almost linearly at lower changes of density or void ratio, respectively.

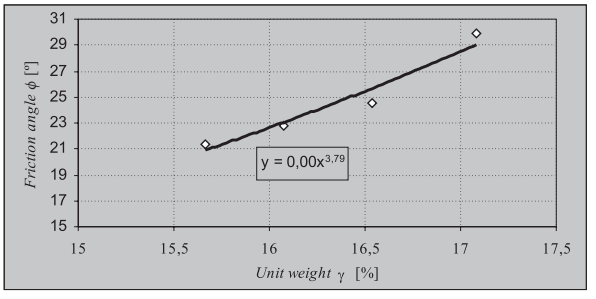

Figure 12. The friction angle φ vs. unit weight γ.

4 CONCLUSIONS

This article focuses on the investigation of snail soil and the research of its mineralogical and physical characteristics. Geomechanical characteristics were investigated for their dependence on physical characteristics. A series of triaxial tests of snail soil of different density, porosity and water content was performed. The results of the tests show that geomechanical characteristics depend on porosity.

The relationships were expressed as functions of porosity. It is evident from the results that changes of the coefficient of permeability, the coefficient of consolidation, and the coefficient of volume compressibility are non-linear with respect to void ratio. Changes of mechanical parameters such as Young's modulus, Poisson's ratio and friction angle are indistinct and almost linear at lower changes of porosity.

ACKNOWLEDGMENTS

This research is being financed by the Slovene Ministry of Higher Education, Science and Technology. The financial support of DARS, the Slovene Motorway Company, and the company Prevent is also gratefully acknowledged.

REFERENCES

[1] Trauner, L. (1982). Applicability of theory of elasticity for foundation design, *Doctoral thesis, University of Ljubljana*, 479 p., Ljubljana

[2] Trauner, L. et al. (1982). Structure soil interaction, *Research report, University of Maribor*, 67 p., Maribor

[3] Ahuja, L. R., et al. (1989). Evaluation of spatial distribution of hydraulic conductivity, using effective porosity data, *Soil Science 148*, p. 404-411

[4] British Standards Institution (1999). Consolidation, *BS 1377*, Part 8, London

METODE ZA KONTROLO PRONICANJA VODE SKOZI PREGRADE IZ VALJANEGA BETONA Z MERITVAMI VODOTESNOSTI IN DRENAŽ

YUEMING ZHU, STEPHAN SEMPRICH, ERICH BAUER, CUIPING YUAN IN DONGMEI SUN

o avtorjih

Yueming Zhu
Institute of Hydrostructure Engineering,
Hohai University
Nanjing, Kitajska
E-pošta: ym-zhu@163.com

Stephan Semprich
Institute of Soil Mechanics and
Foundation Engineering,
Graz University of Technology
Gradec, Avstrija
E-pošta: stephan.semprich@tugraz.at

Erich Bauer
Institute of Applied Mechanics,
Graz University of Technology
Gradec, Avstrija
E-pošta: erich.bauer@tugraz.at

Cuiping Yuan
Hohai University
Nanjing, Kitajska

Dongmei Sun
Hohai University
Nanjing, Kitajska
E-pošta: sundongmei@126.com

izvleček

Kitajska je v zadnjih nekaj letih močno razvila svojo tehnologijo izgradnje jezov iz valjanega betona (beton RCC). Trenutno se ta tehnologija uspešno uporablja pri izgradnji izredno visokih gravitacijskih jezov, pa tudi pri izgradnji srednje visokih in visokih ločnih jezov. Na Kitajskem trenutno projektirajo ali gradijo kakšnih sto jezov iz valjanega betona. Eden glavnih tehničnih problemov pri takšni gradnji je razumevanje pronicanja vode skozi valjani beton ter potreba po razvoju ustrezne teorije in metod za nadzor pronicanja. Prvi avtor tega članka zato že več kot deset let sodeluje v obsežni študiji o lastnostih valjanega betona in metodah za nadzor pronicanja. Študija podaja teoretične osnove ter rezultate terenskih raziskav o pronicanju vode, ukrepih za doseganje vodotesnosti, drenaži, optimalnem načrtovanju in nadzoru pronicanja. Rezultate te študije smo koristno uporabili pri izgradnji in pri povratnih analizah številnih jezov. Članek podrobno opisuje raziskovalne dosežke študije, teoretske osnove ter njihovo praktično uporabo pri visokih gravitacijskih jezovih iz valjanega betona.

ključne besede

gravitacijski jez, valjani beton, RCC, pronicanje, anizotropna prepustnost, drenaža

METHODS FOR CONTROL OF SEEPAGE IN RCC DAMS WITH WATERTIGHT AND DRAINAGE MEASURES

YUEMING ZHU, STEPHAN SEMPRICH, ERICH BAUER, CUIPING YUAN and DONGMEI SUN

About the authors

Yueming Zhu
Institute of Hydrostructure Engineering,
Hohai University
Nanjing, P.R. China
E-mail: ym-zhu@163.com

Stephan Semprich
Institute of Soil Mechanics and Foundation Engineering,
Graz University of Technology
Graz, Austria
E-mail: stephan.semprich@tugraz.at

Erich Bauer
Institute of Applied Mechanics,
Graz University of Technology
Graz, Austria
E-mail: erich.bauer@tugraz.at

Cuiping Yuan
Hohai University
Nanjing, P.R. China

Dongmei Sun
Hohai University
Nanjing, P.R. China
E-mail: sundongmei@126.com

Abstract

The technologies for construction of roller-compacted concrete (RCC) dams have been considerably developed during recent years in China. At the time being, they have been successfully applied to the constructions of even extreme-high gravity dams and medium to high arch dams. There are a few of hundreds of RCC dams (RCCD) under design and/or construction in China. One of the main concerned technical problems according to the construction is about the understanding of the property of seepage in RCCDs and the relevant theory and methods for the control of the seepage. In order to overcome the problem, the senior author has been engaged in a wide study on the property and methods for control of seepage in RCCDs for more than 10 years. The property of seepage, measures for watertightness and drainage, optimal design and construction schemes for control of seepage in the dams have been essentially understood either in theory and practice. The results have been applied for the construction and the backanalysis of several dams. The paper describes the research findings in detail with respect to the theoretical fundament and their application for a high RCC gravity dam.

Keywords

gravity dam, Roller-compacted concrete, RCC, seepage, anisotropic permeability, drainage

1 INTRODUCTION

The Horizontal Layer Method used in roller-compacted concrete (RCC) construction has been replaced by the Slope Layer Method, which importantly reduces the area of exposed young RCC and increases RCC placing rates. The intrinsic permeability of RCC is very low (it equals 1.0×10^{-9} to 1.0×10^{-12} cm/s), whilst the permeability of the lift surface including the joint lift surface is proportional to the cubic width of a hydraulic joint. Theory and engineering practice have proved that the lift surface is the main pathway of seepage, in which leakage generally occurs. According to the present technology for constructing of RCC dams, the body of a RCC dam is considered to be a strong anisotropic medium with more than 2 to 4 or even 6 to 7 orders of magnitude (for example Willew Creek RCC gravity dam, USA) of ratio of the tangential major coefficient of permeability to the normal major coefficient of permeability of the layer and lift joint surfaces. This causes the seepage properties of RCC dams to be totally different from those of conventional concrete dams.

Since the early development stages of RCC dam construction, there have been a lot of problems with seepage due to the lack of knowledge about the property of seepage in RCC dams. One problem, for example is an extremely high position of the exit point on the downstream face, so that exit-flowing discharge may be higher than expected. This is caused by the anisotropic hydraulic resistance according to the dam structure constructed by layers. So, a lot of dams were required to increase their waterproof capability by grouting during the beginning period of operation. Such was the case with Willew Creek RCC dam and Chinese Shimantan RCC gravity dam of the height of 40.5 m.

This paper analyses in detail optimal design schemes for the control of seepage. The analysis is based on a wide and in-depth study on the property and methods for the control of seepage in RCCD and on the senior author's experiences in studying characteristics of permeability and control techniques to handle problems of seepage for RCC dams.

2 PROPERTIES OF SEEPAGE OF RCC AND RCCD

The system of RCC or RCCD consists of body layer of concrete with homogeneous and isotropy property, a layer and a lift interface of anisotropy property which becomes an inhomogeneous multi-laminated medium. Actual properties of seepage of RCC and RCCD are influenced by the properties of the body of concrete, which can be described by Darcy's coefficient of permeability k_{RCC}, and the properties of the layer and the lift interface which is related to the width of a hydraulic joint, roughness of the joint, connectivity of the joint, stress and strain behaviour of the layer surface, load history, etc. The engineering practice has already proved that the layer and the lift interface are the main pathway of seepage and represent weak surfaces according to tension and sliding. In general, RCC and RCCD can be considered as strongly anisotropic medium.

An experiment recorded in literature [1, 2] presents the model of an in-situ concrete block connected in parallel and in series within the Longtan RCC project, which is shown in Fig. 1. The experiment shows that the ratio of average coefficient of permeability in the parallel model to that in the series model is about 1 to 4 orders of magnitude. And the seepage flow mainly exits through the layer and the surrounding region of great skeletal material, which proves that the layer and the lift interface are main pathways of seepage [3].

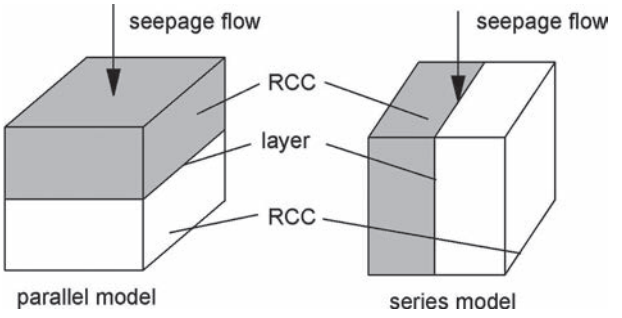

Figure 1. Parallel and series models of a rectangular RCC block in the permeability test.

Gong et al. [3] show the results of in-situ water pressure test, which includes the tests on Willew Creek RCC dam in the USA, Chinese Guanyinge and Tongzijie projects. The tangential major coefficient of permeability of the layer in Willew Creek RCC dam in the USA even surpasses 3×10^{-3} cm/s, and the average value of the tangential major coefficient of the layer permeability is in the range of 1×10^{-3} to 1×10^{-8} cm/s. So, heavy leakage occurs through layers and the location of the exit-flowing line is very high. Compared to the tangential major coefficient of layer permeability, the normal major coefficient of layer permeability is the same as the coefficient of permeability of the body of RCC. The properties of seepage of RCC and RCCD mainly depend on the tangential property of seepage. The system of RCC and RCCD should be considered as strongly anisotropic, and the ratio of anisotropy may reach 1 to 4 or even more orders of magnitude.

Theoretically, the properties of flow through layer and lift joint surfaces agree with the properties of fissure flow. The properties of seepage flow through layer and lift joint surfaces in RCC and RCCD can be usually described by the cubic law of an advective fissure flow, which has been proved by home and foreign engineering experts and which is in accordance test with results in various countries [3, 4].

The property of RCC considered as inhomogeneous multi-laminated medium can be described by tangential and normal major coefficients of the permeability of the layer which depend on the body coefficient of permeability, cubic law and the thickness of the layer. Eqs. (1) and (2) show the tangential and normal major coefficients of the permeability of the layer.

$$k_t = \frac{1}{B}[(B-d_f)k_{RCC} + \frac{g}{12\mu}d_f^3] \qquad (1)$$

$$k_n = \frac{Bk_{RCC}}{B-d_f} \qquad (2)$$

where k_t and k_n are average tangential and normal major coefficients of permeability of the layer, respectively, B denotes the thickness of the layer including the body thickness of the layer and the width of the hydraulic joint d_f, k_{RCC} denotes body coefficient of permeability of RCC, μ denotes the kinematic viscosity of water with $\mu \approx 0.013$ cm^2/s at 10° C.

Because d_f is much smaller than B, the normal major coefficient of the permeability of the layer mainly depends on the body coefficient of permeability of RCC and also on the coefficient of bedding cushion, when there is one, whilst the tangential major coefficient of permeability mainly depends on the width of a hydraulic joint.

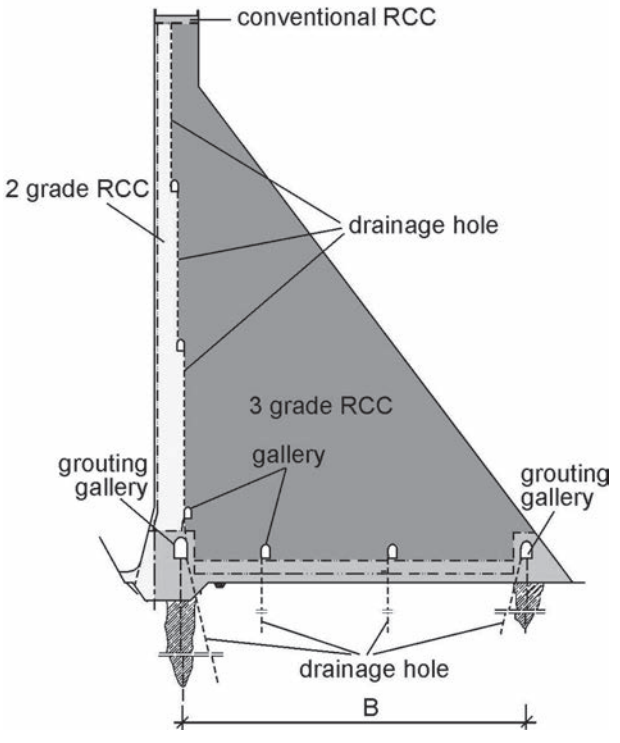

Figure 2. Cross section of seepage control measures for RCCD.

Due to a strong anisotropic property of RCC, the seepage control measures for RCCD become more difficult than conventional concrete. Fig. 2 shows the general layout of measures for watertightness and material zones. It will be a reliable anti seepage structure of a distorted concrete layer with a thickness of 0.3 to 1.0 m on the upstream face, which plays an important role of water-resistance in the front of the dam. Other forms of anti seepage structure on the upstream face of RCCDs are available, such as a RCC layer, a reinforced concrete slab, an asphalt concrete layer, and a combination of different anti-seepage structures. The majority of all projects under construction or under design adopt a distorted concrete layer as the anti seepage structure. Some infiltrating flow through the anti-seepage structure will be drained by drainage holes behind a distorted concrete layer, in which the uplift pressures in the layer and lift surface are almost zero. In order to prevent the seepage flow from exiting on the downstream face, a thin distorted concrete layer is also required on the downstream face. When the upstream water level is very high, a curtain of drainage holes hanging upward the datum plane is needed. Sometimes horizontal drainage holes are alternatively arranged in the layer and the lift surface additionally helps drainage and pressure relief. The principles of seepage control for RCCDs foundation mostly agree with conventional concrete dams which mainly depend on a curtain of watertightness and drainage holes.

3 NUMERICAL ANALYSIS ON THE RCCD SEEPAGE FIELD WITH FEM

3.1 NUMERICAL MODEL OF SEEPAGE FIELD

Due to special inhomogeneous and strongly anisotropic multi-laminated structures in RCCDs, the system of RCC should be considered as fractured rock masses medium according to the property of the layer seepage, which can be simulated by an equivalent continuum model, a discrete fractured network model and a dual porosity model [4-7].

Equivalent continuum models based on the balance equation of mass consider layer and lift surfaces as equivalent continuum porous media, which are analyzed by a mature theory of continuum porous media. But the equivalent seepage discharge and seepage pressure cannot be obtained with this method. A discrete fractured network model assumes that the body of RCC is impervious, so that the properties of RCC mainly depend on the widths of hydraulic joints, location and connectivity of the layer, and the coefficient tensor of permeability is determined by the cubic law and Darcy's law. This method is able to actually simulate the behaviour of seepage flow between layers, but due to the uncertainty of the joint and lift surface, it is more difficult to simulate fractures. The objects within a dual porosity model involve seepage behaviour both in porous media and fractured media.

Combining the merits and faults of three models mentioned above, the authors proposed inhomogeneous multi-laminated media elements model, which unifies the equivalent continuum model and the non-continuum mixed model, and which has the advantages of an equivalent continuum model involving fewer elements needed in the calculation [8].

3.2 INHOMOGENEOUS MULTI-LAMINATED MEDIA ELEMENT

An inhomogeneous multi-laminated media element model assumes that the dam body consists of a body layer of roller-compacted concrete, a lift interface, a lift joint interface of the course of one continuous construction of lifts, a bedding plane and normal concrete materials, which become inhomogeneous multi-laminated media elements. The element conductivity matrix is expressed with Eq. (3).

$$k_{ij}=\int_{-1}^{1}\int_{-1}^{1}\int_{-1}^{1}B_i^T K B_j |J| d\xi d\eta d\zeta=\sum_{k=1}^{N}\int_{\zeta_{k-1}}^{\zeta_k}\left(\int_{-1}^{1}\int_{-1}^{1}B_i^T K_k B_j |J| d\xi d\eta\right)d\zeta \quad (3)$$

Here we introduce the integral variable transformation shown in Eq. (4).

$$\zeta=\frac{\zeta_k-\zeta_{k-1}}{2}\zeta'+\frac{\zeta_k-\zeta_{k-1}}{2} \qquad (4)$$

So we have Eq. (5).

$$k_{ij}=\sum_{k=1}^{N}\int_{-1}^{1}\frac{\zeta_k-\zeta_{k-1}}{2}\left(\int_{-1}^{1}\int_{-1}^{1}B_i^T K_k B_j |J| d\xi d\eta\right)d\zeta' \qquad (5)$$

Here N is the number of layers of inhomogeneous multi-laminated media, K_k is the coefficient tensor of permeability of the k th layer, Eqs. (9), (10) and (11), B_i, B_j and $|J|$ are functions of the local coordinates of ξ, η and ζ'.

3.3 PLANAR ELEMENT WITHOUT THICKNESS FOR FISSURES

Bearing in mind numerous lift interfaces and lift joint interfaces and occurrence of horizontal cracks and cleavage cracks in case of emergency of a dam, the authors proposed the planar element without the thickness model ([9] and [10]), which can be used to simulate the exact behaviour of the seepage flow in RCC and which has been proved to be a successful model up to now.

Because the normal major coefficient of the permeability of a RCC body and the width of the joint are so small that normal head loss in the joint lift surfaces is almost zero, the seepage flow through joint lift surfaces can be considered as a two dimensional flow model (index f). We then have Eq. (6).

$$-\frac{\partial}{\partial x_i^f}\left[k_{ij}^f\frac{\partial h}{\partial x_j^f}\right]=0 \qquad i,j=1,2 \qquad (6)$$

where x_i^f is the corresponding local coordinate, k_{ij}^f is a two dimensional coefficient tensor of permeability in the planar element without the thickness model, and k_{rs}^{fe} is the element conductivity matrix which can be calculated from the below Eq. (7):

$$k_{rs}^{fe}=\int_{s^f}\left[k_{11}^f\frac{\partial N_r}{\partial x_1^f}\frac{\partial N_s}{\partial x_1^f}+2k_{12}^f\frac{\partial N_r}{\partial x_1^f}\frac{\partial N_s}{\partial x_2^f}+k_{22}^f\frac{\partial N_r}{\partial x_2^f}\frac{\partial N_s}{\partial x_2^f}\right]ds \qquad (r,s=1\cdots m) \qquad (7)$$

where s^f is a subdomain of a joint lift surface element, N_r and N_s are interpolating functions of the joint lift surface element, m is the number of nodal points in the joint lift surface element.

According to balance equation of mass [11], we obtain the below FEM governing equation for a seepage field

$$\sum_e (Q_i^{RCC}+Q_i^f)=0 \qquad i=1,2,\cdots,n \qquad (8)$$

where n is the total number of nodal points, Q_{RCC} and Q_F are nodal fluxes of the point i which are contributed by a 3-D equivalent continuum media element of RCC and a 2-D planar element without the thickness element.

3.4 COEFFICIENT TENSOR OF PERMEABILITY IN THE RCCD SEEPAGE FIELD

In the study of seepage properties in RCCDs, if the layer of RCC is horizontal, the coefficients of permeability can be described by major coefficients of permeability shown in Eqs. (1) and (2). In a sloped layer the direction of major coefficients of permeability are not the same as a coordinate axis and the properties of seepage should be expressed by the coefficient tensor of permeability shown as Eqs. (9), (10) and (11). Eq. (9) is suitable for the layer incline to the upstream, whilst Eqs. (10) and (11) are suitable for the layers' incline to the left bank and the right bank, respectively.

$$[K]=k_n\begin{bmatrix} r\cos^2\theta+\sin^2\theta & 0 & \frac{1}{2}(r-1)\sin 2\theta \\ 0 & r & 0 \\ \frac{1}{2}(r-1)\sin 2\theta & 0 & r\sin^2\theta+\cos^2\theta \end{bmatrix} \quad (9)$$

$$[K]=k_n\begin{bmatrix} r & 0 & 0 \\ 0 & r\cos^2\theta+\sin^2\theta & \frac{1}{2}(1-r)\sin 2\theta \\ 0 & \frac{1}{2}(1-r)\sin 2\theta & r\sin^2\theta+\cos^2\theta \end{bmatrix} \quad (10)$$

$$[K]=k_n\begin{bmatrix} r & 0 & 0 \\ 0 & r\cos^2\theta+\sin^2\theta & \frac{1}{2}(r-1)\sin 2\theta \\ 0 & \frac{1}{2}(r-1)\sin 2\theta & r\sin^2\theta+\cos^2\theta \end{bmatrix} \quad (11)$$

where θ is the slope angle, k_t and k_n are tangential and normal major coefficients of permeability, respectively, $r=k_t/k_n$ is the ratio of tangential major coefficient of permeability to normal major coefficient of permeability, $[K]$ is the coefficient tensor of permeability.

4 THE DESIGN METHODS FOR WATERTIGHT AND DRAINAGE MEASURES

4.1 WATERTIGHT STRUCTURES ON THE UPSTREAM FACE

Lift surfaces on the upstream face are probably a pathway of leakage, so it is important to take watertight measures in the upstream. The distorted RCC and 2-grade RCC are mostly used as watertight measures on the upstream face in present RCCDs. 2-grade RCC represents a defined RCC quality, which is higher than the 3-grade RCC. Based on the authors' experiences about methods of seepage control in RCCDs, the following schemes for the control of seepage are proposed. First, a thin layer of distorted RCC and additional 2-grade RCC are arranged on the upstream face, and seepage control treatment is done on the lift surfaces within the width of 2m. Second, a thin layer of distorted RCC and additional 3-grade RCC are arranged on the upstream face, and seepage control treatment is done on the lift surface within the width of 2 m (i.e. to spread a layer of mortar of the thickness of 1.0 ~ 1.5 cm in time). Different projects will take different schemes of control of seepage. Temperature control and crack prevention are very important on the upstream face to prevent the occurrence of penetrating cracks. Quality of structure of seepage control is more important than its width.

Uplift pressure tolerances in the lift surface, the joint lift surface and the datum plane are shown in Figs. 3 and 4, where H_u and H_d are depths of upstream and downstream respectively and γ unit weight of water.

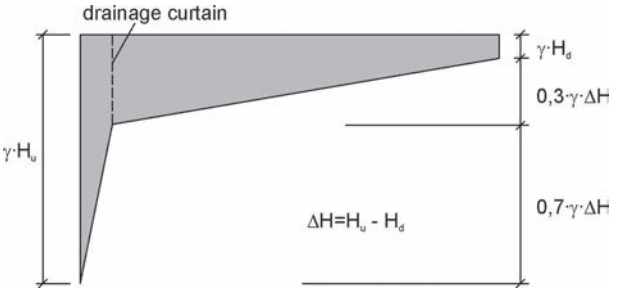

Figure 3. Cross section of design uplift pressure in the dam body.

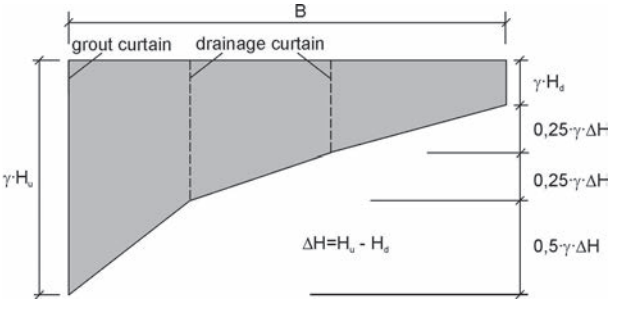

Figure 4. Cross section of design uplift pressure on the datum plane.

4.2 WATERTIGHT STRUCTURES ON THE DOWNSTREAM FACE

Due to the strong permeability of the lift surface on the downstream face of RCCDs, the location of the exit-flowing line may be very high and the leakage of seepage may be so great that it will endanger stability safety of the dam. A layer of distorted RCC with a thickness of 0.30~0.50 m will be arranged on the downstream face. Inside the distorted RCC layer, the seepage control treatment will be performed to the depth of 1 to 2 m of the

lift surfaces below the water level of downstream; alternatively; 2-grade RCC can follow inside the distorted RCC layer.

4.3 DRAINAGE HOLES CURTAINS IN THE DAM BODY

Drainage holes are required both in a conventional dam and a RCC dam to discharge the seepage flow. The curtains of exit-flowing drainage holes will be arranged in the zone of 3-grade RCC following 2-grade RCC in the upstream region, in which the intervals of drainage holes are about 4 to 5 m. In the downstream region of a 2-grade RCC zone or within the RCC, treated by seepage control, a curtain of exit-flowing drainage holes can be also arranged, in which the interval between drainage holes is recommended to be 6 m. For a high dam with a wide datum plane, the curtains of overflowing drainage holes are needed on the datum plane near the upstream region.

4.4 BEDDING PLANE OF CONCRETE ON THE DATUM PLANE

Due to cracks generated frequently, difficulties in construction and more cement used in conventional concrete, the bedding plane built of conventional concrete has been replaced by bedding plane built with 2-grade RCC of the thickness of 0.5 m to play the role of providing flat and resisting water. The bedding plane and watertight structures together form a watertight structure.

4.5 WATERTIGHT STRUCTURES AND DRAINAGE MEASURES ON THE DATUM PLANE

Watertight structures and drainage measures are also required in the zones of the dam heel and the dam toe on the datum plane. Engineering practices have proved that curtain's relative watertightness just needs to be 3 times lower than of the surrounding rock masses. The grout curtain must be complete and the curtain drainage holes should be unblocked. The interval of drainage holes on the datum plane is 4 to 5 m, the same as in the dam body.

4.6 TRANSVERSE JOINT SEAL AND WATERTIGHT STRUCTURES ON SIDES OF JOINTS

Compared to conventional concrete dams, the RCCDs need better transverse joint seal because there are lift surfaces in RCCDs. In order to prevent water from infiltrating into the dam through the sides of the transverse joint, watertight structures on the sides of the joint are strongly required. This can be realized by a distorted concrete layer of a thickness between 0.3 and 0.5 m and should be connected very well with the bedding plane.

4.7 DESIGN PRINCIPLES FOR THE WATERTIGHT STRUCTURE AND DRAINAGE MEASURE

Briefly, the design principle of a watertight structure and the drainage measure is to resist in front and to drain at the back in the upstream region of the dam as well as in the zone of the dam toe in dam foundation, whilst in the downstream region of the dam the principle is to drain in front and to block at the back as well as in the zone of the dam heel in dam foundation. Here, to resist in front in the upstream region means to arrange a layer of distorted RCC and 2-grade RCC or the zone of lift surface and lift joint surface treated by seepage control method of the width of 2 to 3 m; and to drain at the back means to arrange the main curtain of drainage holes. To drain in front in the downstream region means to arrange the main curtain of drainage holes near the upstream, and to drain at the back means to arrange a layer of distorted RCC.

In the zone of the dam toe in dam foundation, to resist in front means to arrange the main grouting and the watertight curtain, and to drain at the back means to arrange the main curtain drainage holes behind the grouting and watertight curtain. In the zone of the dam heel in dam foundation, to drain in front means to arrange the curtain of drainage holes behind the watertight curtain near downstream, and to resist in the back means to arrange the watertight curtain near downstream.

In fact, the function of water-resisting of the watertight curtain and the function of drainage and pressure relief of the curtain of drainage holes are not independent. If there is only a watertight curtain and no curtain of drainage holes in dam foundation, the uplift pressure will be very high unless the permeability of the watertight curtain is very small, for example 2 orders of magnitude smaller than that of surrounding rock masses. This is difficult to perform in engineering practices. If there is only a curtain of drainage holes and no watertight curtain in dam foundation, though the uplift pressure can be greatly reduced, the rock masses in foundation may be destroyed by a great hydraulic gradient surrounding the drainage holes, which is absolutely irrational for the long-term safety of dam.

5 APPLICATION

5.1 STUDY ON THE ENTIRE SEEPAGE FIELD

We have taken the 6th segment of Guangzhao RCCD as a case study, which is located in the middle reaches of the Longtan River in the Guizhou province. On the face of upstream, there is a layer of distorted concrete of different thickness along the height, 0.8m above the elevation of 615.0 m and 1.0 m below the elevation of 615.0 m. The watertight structure in the upstream region is composed of a layer of distorted concrete and additional 2-grade RCC and 3-grade RCC, except for the zone above the elevation of 710.0 m, where there is a layer of distorted concrete and an additional 3-grade RCC. The depth of 2-grade RCC is in the range of 3 to 13m according to the water head on the face of upstream. There is a drainage curtain in the dam body, and the watertight curtain and the main drainage curtain are arranged in the zone of the dam toe because the water level in downstream is lower than the elevation of the datum plane. The normal water levels are 745.0 m and 583.5 m in the upstream and downstream, respectively. Empirical coefficients of permeability of various watertight materials in the dam, the watertight curtain in dam foundation and the grout curtain are shown in Table 1.

According to the seepage control methods proposed in this paper, Fig. 5 and Fig. 6 show the distributions of water head contour lines and uplift pressure head contour lines, respectively, in a short form.

The entire seepage field presents exact seepage property and obvious regularity, which indicates that the seepage control method proposed in this paper plays the role of

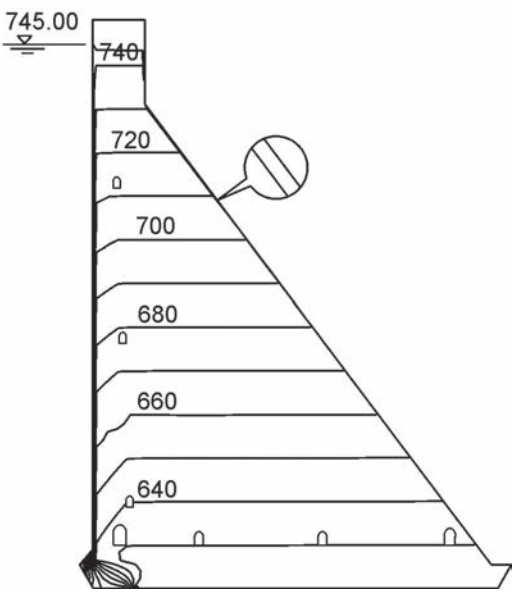

Figure 5. Water head contour lines.

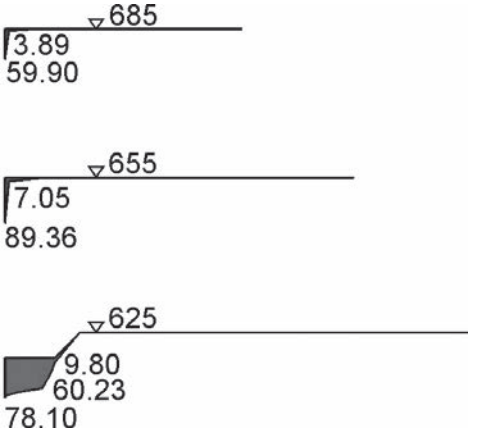

Figure 6. Uplift pressure head contour lines.

Table 1. Coefficients of permeability of body material and various watertight materials.

Type of concrete	Body coefficient of permeability (cm/s)	Normal coefficient of permeability of lift surface (cm/s)	Tangential coefficient of permeability of lift surface (cm/s)	notes
Conventional concrete	1×10^{-10}			anisotropic
Distorted concrete	1×10^{-9}			anisotropic
2 grade RCC	1×10^{-9}	1×10^{-9}	1×10^{-7}	
3 grade RCC	1×10^{-9}	1×10^{-9}	5×10^{-7}	
Watertight curtain	1×10^{-5}			isotropic
Consolidated grouting	1×10^{-4}			isotropic

resisting in front and draining at the back. In the dam body, the potential of high water head is mostly lost through the isotropic layer of distorted concrete. Though the coefficient of permeability of distorted concrete is the same as the normal major coefficient of permeability of 2-grade RCC and 3-grade RCC behind the layer of distorted concrete, it is watertight compared to the tangential major coefficient of permeability of 2-grade RCC, because the coefficient of permeability of layer of distorted concrete is 2 orders of magnitude smaller than the tangential major coefficient of permeability of 2-grade RCC. Contour lines in the layer of distorted concrete are probably parallel to the face of upstream. In the layer of distorted concrete above the datum plane about 1 m the potential of water head is reduced about over tens meters, in which the cracks always occur and quality of the layer of distorted concrete should be paid more attention. In the adjacent zone of 2-grade RCC and 3-grade RCC the contour lines have a distinctly horizontal kink towards downstream, which is caused by the fact that hydraulic gradients in 2-grade RCC and 3-grade RCC are much smaller than those in the layer of distorted concrete. Due to the easiness of seepage flow through 3-grade RCC, the quality of a watertight structure ahead 3-grade RCC should be paid more attention to ensure the safety of RCCDs.

Some seepage flow moves around the drainage holes, and it will exit from the face of downstream if there is no watertight structure arranged. Fig. 5 shows a layer of distorted concrete on the face of downstream shown in enlargement. Due to no resistance on this seepage flow in the lift surface and lift joint surface, the value of uplift pressure will be near zero. A drainage hole is another useful seepage control structure, by which almost all of the seepage flow is discharged. So, in order to ensure that the drainage hole performs successfully, the quality of the drainage hole should be paid more attention to the construction phase and the drainage hole should be checked regularly during the operation phase.

The uplift pressure contour lines at the elevation of 685.0 m, 655.0 m and 625.0 m are shown in Fig. 6. In these typical elevations, the uplift pressure is low, and the drainage curtain in the dam body, the grout curtain and the main drainage curtain in dam foundation play an important role for pressure relief.

Briefly, the seepage control methods proposed in this paper work very well. Different watertight structures play different roles and also depend on each other. From the results mentioned above we can see that the layer of distorted concrete and drainage holes play an important role of water-resisting and pressure relief. A big deal of discharge will be drained by the drainage holes. The uplift pressure will be very high if there are no drainage holes. From the distribution of uplift pressure on the datum plane, we can conclude that the grout curtain and the drainage curtain in dam foundation are very important for water-resisting.

5.2 SENSITIVITY ANALYSIS ON SEEPAGE CONTROL METHODS

5.2.1 Water-resisting function of 2-grade RCC

Fig. 7 shows the computed result when the 2-grade RCC on the face of upstream is removed on the basis of seepage control structures mentioned above, from which we can conclude that there are no obvious changes in the entire seepage field. We can so come to the same conclusions as those obtained by engineering practice. First, the water-resisting function of 2-grade RCC can be ignored. Second, the layer of distorted concrete on the face of upstream only works in the function of water resisting. Third, the arrangement of 2-grade RCC will make the construction more difficult, reduce the construction rate and make the advantages of RCCD fade away. Fig. 8 shows the distributions of uplift pressure heads, from which the same conclusions can be obtained.

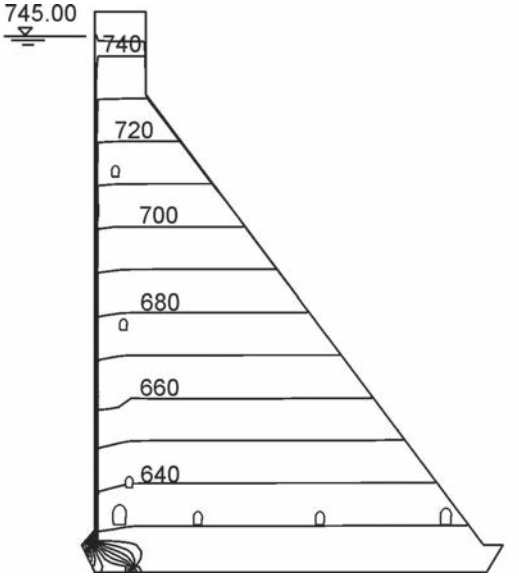

Figure 7. The contribution of hydraulic head contour lines in the dam body when 2-grade RCC is removed.

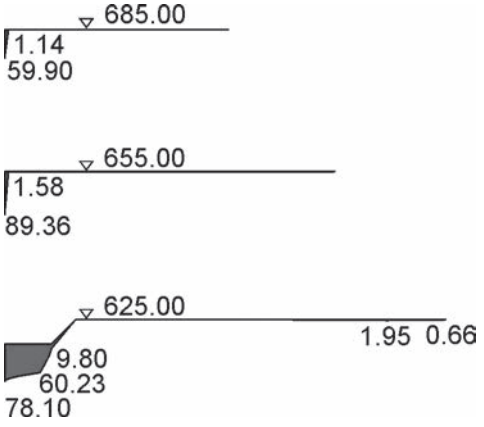

Figure 8. The distribution of uplift pressure head contour lines in different elevations when 2-grade RCC is removed.

5.2.2 The study of cracks in the dam body

Cracks in the dam body are of the key importance for the safety in hydraulic engineering. Figs. 9 and 10 show the computed results when there is a vertical cleavage crack in the layer of distorted concrete on the face of upstream. The width of this cleavage crack is 0.2 mm and it is located in the middle plane between two drainage holes. Figs. 11 and 12 show the computed results when there is a horizontal penetrating crack at intervals of 20 m only in the layer of distorted concrete on the face of upstream. The width of this horizontal penetrating crack is 0.1 mm.

When there is a vertical cleavage crack in the layer of distorted concrete on the face of upstream, the function of water-resisting of the layer of distorted concrete disappears and the main watertight structures are 2-grade RCC and drainage holes behind the layer of distorted concrete. The hydraulic head contour lines in 2-grade RCC are parallel to the face of upstream, and the uplift pressure head in the dam body is still small. But due to the anisotropic property of 2-grade RCC, the uplift pressure in 3-grade RCC is a somewhat higher compared to the distribution of uplift pressure shown in Fig. 6.

Fig. 11 shows the distribution of hydraulic head contour lines when there are several horizontal cracks on the face of upstream. The values of uplift pressure meet the demands desired. Except for the zones near the cracks, the influence of the cracks on the seepage field can be ignored. Under the watertight function of 2-grade RCC and drainage holes, the uplift pressure head contour lines are horizontal and small enough. Because there is a horizontal crack in the elevation of 685.0 m, the watertight function of the layer of distorted concrete vanishes, so the uplift pressure contour line is horizontal in the layer of distorted concrete.

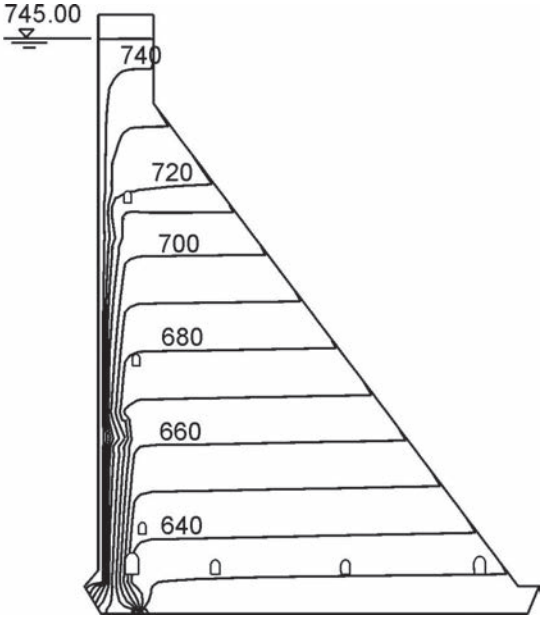

Figure 9. Distribution of hydraulic head contour lines when there is a vertical cleavage crack on the face of upstream.

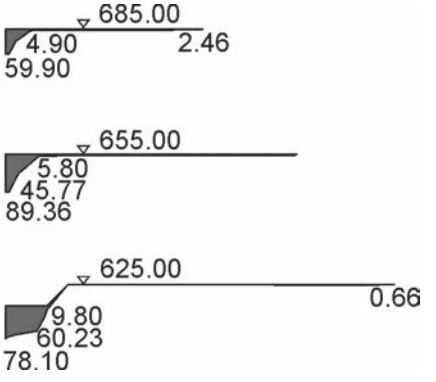

Figure 10. Distribution of uplift pressure head contour lines in different elevations when there is a vertical cleavage crack on the face of upstream.

Fig. 9 to 12 show the computed results which take into account of various adverse conditions. We can conclude that under the protection of other watertight structures there are no fatal uplift pressures in the seepage field, and the dam is in a temporary safe state. But we are all aware that the tendency of cleavage cracks and horizontal cracks is difficult to predict, so we have to pay more attention to the temperature control and cracks prevention measures, especially to the quality of the layer of distorted concrete.

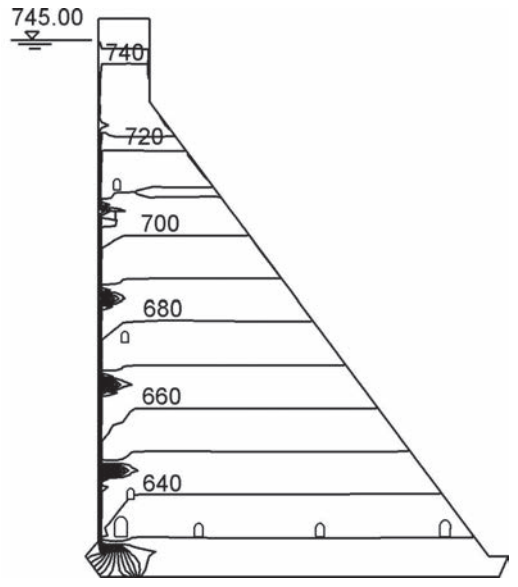

Figure 11. Distribution of hydraulic head contour lines when there is a horizontal penetrating crack at intervals of 20m in the layer of distorted concrete on the face of upstream.

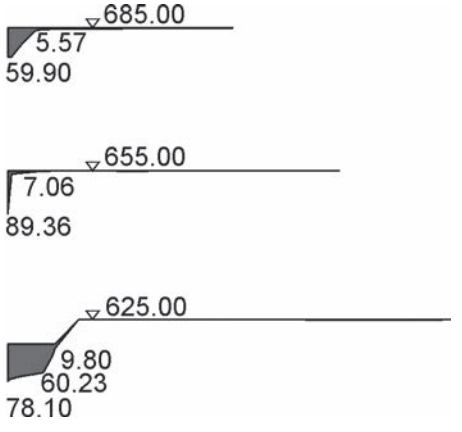

Figure 12. Distribution of uplift pressure head contour lines in different elevations when there is a horizontal penetrating crack at intervals of 20m in the layer of distorted concrete on the face of upstream.

6 CONCLUSIONS AND SUGGESTIONS

This paper generalizes the properties of seepage in RCC and RCCDs. Constructive suggestions of seepage control methods in various zones of the dam are proposed, and they have been applied to engineering practice. Because the RCC can be considered as inhomogeneous multi-laminated medium with strong anisotropy, the property of seepage of RCC are mainly depends on the property of the lift surface, in which the coefficient of permeability is 2 to 3 orders of magnitude higher than that of the RCC body. In construction stages the quality of the lift surface should be paid more attention.

Due to the anisotropy of RCC, the property of seepage of RCC is more difficult than that of conventional concrete. The design principles of watertight structures in RCCDs are to resist in front and drain at the back. On the face of upstream the arrangement of a watertight structure is strongly required, such as reinforced concrete slab, a conventional concrete slab and other forms. In present engineering practice the layer of distorted concrete and additional 2-grade RCC are recommended: the layer of distorted concrete plays the primary role in the watertight function, whilst 2-grade RCC plays the secondary role in the watertight function. In order to drain a small amount of seepage flow through watertight structures, drainage holes should be arranged behind the watertight structure in the upstream. In order to ensure that drainage hole play a permanent role in pressure relief, the diameter of a drainage hole should be greater and the distance between two drainage holes can reach 4 to 6m. In order to prevent the seepage flow from exiting too high on the face of downstream, a layer of distorted concrete is strongly required. The design of watertight control in the dam foundation is the same as that in conventional dam foundation, in which the grout curtain and main drainage curtain are absolutely needed. Based on the study of RCC for over ten years, the design of seepage control methods and the numerical model in RCCDs have been completely solved. The problem of temperature control and crack prevention is still to be researched in future.

REFERENCES

[1] Su, B. et al. (2002). Statistical features of permeability coefficients of Jiangya RCCD core samples. *Journal of Hohai University*, Vol. 30(2), 1-5.

[2] Su, B. et al. (2000). Research of permeability of roller compacted concrete of Jiangya Dam. *Journal of Hohai University*, Vol. 28(2), 7-11.

[3] Gong, D., Zhu, Y. (2002) Research on seepage of RCC Dams. *International Journal Hydroelectric Energy*, Vol. 20(2), 23-25.

[4] Wittke, W. (1990). *Rock Mechanics* – Theory and Applications with Case Histories. Springer-Verlag Berlin Heidelberg.

[5] Schrader, E.K., Namikas, D. (1988). Performance of roller compacted concrete dams. *Proceedings of the Sixteenth Congress on Large Dams*, Vol. 2, 339-364.

[6] Iwai, K. (1976). Fundamental studies of fluid flow through a single fracture. Ph.D. Thesis. Univ. of California, Berkeley, USA.
[7] Sheng, J. (2000). Studies on 3-D numerical simulation of fractured rock masses taking into account the coupling of seepage and stress and application. Ph.D. Thesis. Hohai University, Nanjing, P.R. China.
[8] Zhu, Y. et al. (2002). Analysis of seepage control characteristics of the optional scheme of Three Gorges or RCC gravity dam on the Yangtze River. *Journal of Hohai University*. Vol.28(2), 1-6.
[9] Zhu, Y., Gong, D., Zhang H. et al. (2003). Plane element simulation of fracture seepage for analyzing seepage in RCCD. *Journal of Hydraulic Engineering*, Vol 3, 63-68.
[10] Zhu Y., Liu C., Li J. (2005). Study on seepage control methods and watertight and drainage measures in RCCDs. *Guizhou Water Power*, Vol. 19(3), 5-11.
[11] Zhu Y. (1997). The computing method of equivalent nodal virtual discharge in Darcy's equation. *Journal of Hohai University*. Vol. 25(4), 105-108.
[12] Zhu Y., Zhang, L., Pang Z. (1999). Study on permeability properties of RCC Dams and Longtan gravity RCCD (1). *Hongshui River*. Vol. 18(1), 2-8.
[13] Zhu Y., Zhang L., Pang Z. (1999). Study on permeability properties of RCC Dams and Longtan gravity RCCD (2). *Hongshui River*. Vol. 18(2), 8-11.

NAVODILA AVTORJEM

Članki so objavljeni v angleškem jeziku s prevodom izvlečka v slovenski jezik.

VSEBINA ČLANKA

Članek naj bo napisan v naslednji obliki:

- Naslov, ki primerno opisuje vsebino članka in ne presega 80 znakov.
- Izvleček, ki naj bo skrajšana oblika članka in naj ne presega 250 besed. Izvleček mora vsebovati osnove, jedro in cilje raziskave, uporabljeno metodologijo dela, povzetek izidov in osnovne sklepe.
- Uvod, v katerem naj bo pregled novejšega stanja in zadostne informacije za razumevanje ter pregled izidov dela, predstavljenih v članku.
- Teorija.
- Eksperimentalni del, ki naj vsebuje podatke o postavitvi preiskusa in metode, uporabljene pri pridobitvi izidov.
- Izidi, ki naj bodo jasno prikazani, po potrebi v obliki slik in preglednic.
- Razprava, v kateri naj bodo prikazane povezave in posplošitve, uporabljene za pridobitev izidov. Prikazana naj bo tudi pomembnost izidov in primerjava s poprej objavljenimi deli.
- Sklepi, v katerih naj bo prikazan en ali več sklepov, ki izhajajo iz izidov in razprave.
- Literatura, ki mora biti v besedilu oštevilčena zaporedno in označena z oglatimi oklepaji [1] ter na koncu članka zbrana v seznamu literature.

OBLIKA ČLANKA

Besedilo naj bo pisano na listih formata A4, z dvojnim presledkom med vrstami in s 3.0 cm širokim robom, da je dovolj prostora za popravke lektorjev. Najbolje je, da pripravite besedilo v urejevalniku Microsoft Word. Hkrati dostavite odtis članka na papirju, vključno z vsemi slikami in preglednicami ter identično kopijo v elektronski obliki.

Enačbe naj bodo v besedilu postavljene v ločene vrstice in na desnem robu označene s tekočo številko v okroglih oklepajih.

ENOTE IN OKRAJŠAVE

V besedilu, preglednicah in slikah uporabljajte le standardne označbe in okrajšave SI. Simbole fizikalnih veličin v besedilu pišite poševno (npr. *v*, *T* itn.). Simbole enot, ki sestojijo iz črk, pa pokončno (npr. Pa, m itn.).

Vse okrajšave naj bodo, ko se prvič pojavijo, izpisane v celoti.

SLIKE

Slike morajo biti zaporedno oštevilčene in označene, v besedilu in podnaslovu, kot sl. 1, sl. 2 itn. Posnete naj bodo v kateremkoli od razširjenih formatov, npr. BMP, JPG, GIF. Za pripravo diagramov in risb priporočamo CDR format (CorelDraw), saj so slike v njem vektorske in jih lahko pri končni obdelavi preprosto povečujemo ali pomanjšujemo.

Pri označevanju osi v diagramih, kadar je le mogoče, uporabite označbe veličin (npr. *v*, *T*). V diagramih z več krivuljami mora biti vsaka krivulja označena. Pomen oznake mora biti razložen v podnapisu slike.

Za vse slike po fotografskih posnetkih je treba priložiti izvirne fotografije ali kakovostno narejen posnetek.

PREGLEDNICE

Preglednice morajo biti zaporedno oštevilčene in označene, v besedilu in podnaslovu, kot preglednica 1, preglednica 2 itn. V preglednicah ne uporabljajte izpisanih imen veličin, ampak samo ustrezne simbole. K fizikalnim količinam, npr. *t* (pisano poševno), pripišite enote (pisano pokončno) v novo vrsto brez oklepajev.

Vse opombe naj bodo označene z uporabo dvignjene številke[1].

SEZNAM LITERATURE

Vsa literatura mora biti navedena v seznamu na koncu članka v prikazani obliki po vrsti za revije, zbornike in knjige:

[1] Feng, T. W. (2000). Fall-cone penetration and water content ralationship of clays. *Geotechnique 50*, No. 2, 181-187.

[2] Ortolan, Ž. and Mihalinec, Z. (1998). Plasticity index-Indicator of shear strength and a major axis of geotechnical modelling. *Proceedings of the Elev-*

enth Danube-European conference on soil mechanics and geotechnical engineering, Poreč, 25 –29 May 1998.
[3] Toporišič, J. (1994). *Slovenski pravopis*. 2nd.ed., DZS, Ljubljana.

PODATKI O AVTORJIH

Članku priložite tudi podatke o avtorjih: imena, nazive, popolne poštne naslove, številke telefona in faksa, naslove elektronske pošte. Navedite kontaktno osebo.

SPREJEM ČLANKOV IN AVTORSKE PRAVICE

Uredništvo si pridržuje pravico do odločanja o sprejemu članka za objavo, strokovno oceno mednarodnih recenzentov in morebitnem predlogu za krajšanje ali izpopolnitev ter terminološke in jezikovne korekture.

Avtor mora predložiti pisno izjavo, da je besedilo njegovo izvirno delo in ni bilo v dani obliki še nikjer objavljeno. Z objavo preidejo avtorske pravice na revijo ACTA GEOTECHNICA SLOVENICA. Pri morebitnih kasnejših objavah mora biti AGS navedena kot vir.

Rokopisi člankov ostanejo v arhivu AGS.

Vsa nadaljnja pojasnila daje:

Uredništvo
ACTA GEOTECHNICA SLOVENICA
Univerza v Mariboru
Fakulteta za gradbeništvo
Smetanova ulica 17
2000 Maribor
Slovenija
E-pošta: ags@uni-mb.si

INSTRUCTIONS FOR AUTHORS

The papers are published in English with a translation of the abstract into Slovene.

FORMAT OF THE PAPER

The paper should have the following structure:

- A Title that adequately describes the content of the paper and should not exceed 80 characters;
- An Abstract, which should be viewed as a mini version of the paper and should not exceed 250 words. The Abstract should state the principal objectives and the scope of the investigation and the methodology employed, it should also summarise the results and state the principal conclusions;
- An Introduction, which should provide a review of recent literature and sufficient background information to allow the results of the paper to be understood and evaluated;
- A Theoretical section;
- An Experimental section, which should provide details of the experimental set-up and the methods used for obtaining the results;
- A Results section, which should clearly and concisely present the data using figures and tables where appropriate;
- A Discussion section, which should describe the relationships shown and the generalisations made possible by the results and discuss the significance of the results, making comparisons with previously published work;
- Conclusions, which should present one or more conclusions that have been drawn from the results and subsequent discussion;
- References, which must be numbered consecutively in the text using square brackets [1] and collected together in a reference list at the end of the paper.

LAYOUT OF THE TEXT

The text should be written in A4 format, with double spacing and margins of 3 cm, to provide editors with space to write in their corrections. Microsoft Word for Windows is the preferred format for submission. One hard copy, including all figures, tables and illustrations and an identical electronic version of the manuscript must be submitted simultaneously.

Equations should be on a separate line in the main body of the text and marked on the right-hand side of the page with numbers in round brackets.

UNITS AND ABBREVIATIONS

Only standard SI symbols and abbreviations should be used in the text, tables and figures. Symbols for physical

quantities in the text should be written in Italics (e.g. *v*, *T*, etc.). Symbols for units that consist of letters should be in plain text (e.g. Pa, m, etc.).

All abbreviations should be spelt out in full on first appearance.

FIGURES

Figures must be cited in consecutive numerical order in the text and referred to in both the text and the caption as Fig. 1, Fig. 2, etc. Figures may be saved in any common format, e.g. BMP, JPG, GIF. However, the use of CDR format (CorelDraw) is recommended for graphs and line drawings, since vector images can be easily reduced or enlarged during final processing of the paper.

When labelling axes, physical quantities (e.g. *v*, *T*) should be used whenever possible. Multi-curve graphs should have individual curves marked with a symbol; the meaning of the symbol should be explained in the figure caption.

Good quality black-and-white photographs or scanned images should be supplied for illustrations.

TABLES

Tables must be cited in consecutive numerical order in the text and referred to in both the text and the caption as Table 1, Table 2, etc. The use of names for quantities in tables should be avoided if possible: corresponding symbols are preferred. In addition to the physical quantity, e.g. *t* (in Italics), units (normal text), should be added on a new line without brackets.

Any footnotes should be indicated by the use of the superscript[1].

LIST OF REFERENCES

References should be collected at the end of the paper in the following styles for journals, proceedings and books, respectively:

[1] Feng, T. W. (2000). Fall-cone penetration and water content ralationship of clays. *Geotechnique 50*, No. 2, 181-187.

[2] Ortolan, Ž. and Mihalinec, Z. (1998). Plasticity index-Indicator of shear strength and a major axis of geotechnical modelling. *Proceedings of the Eleventh Danube-European conference on soil mechanics and geotechnical engineering*, Poreč, 25 –29 May 1998.

[3] Toporišič, J. (1994). *Slovenski pravopis*. 2nd.ed., DZS, Ljubljana.

AUTHOR INFORMATION

The following information about the authors should be enclosed with the paper: names, complete postal addresses, telephone and fax numbers and E-mail addresses. Indicate the corresponding person.

ACCEPTANCE OF PAPERS AND COPYRIGHT

The Editorial Committee of the Slovenian Geotechnical Review reserves the right to decide whether a paper is acceptable for publication, to obtain peer reviews for submitted papers, and if necessary, to require changes in the content, length or language.

Authors must also enclose a written statement that the paper is original unpublished work, and not under consideration for publication elsewhere. On publication, copyright for the paper shall pass to the ACTA GEOTECHNICA SLOVENICA. The AGS must be stated as a source in all later publication.

Papers will be kept in the archives of the AGS.

For further information contact:

Editorial Board
ACTA GEOTECHNICA SLOVENICA
University of Maribor
Faculty of Civil Engineering
Smetanova ulica 17
2000 Maribor
Slovenia
E-mail: ags@uni-mb.si

NAMEN REVIJE

Namen revije ACTA GEOTECHNICA SLOVENICA je objavljanje kakovostnih teoretičnih člankov z novih pomembnih področij geomehanike in geotehnike, ki bodo dolgoročno vplivali na temeljne in praktične vidike teh področij.

ACTA GEOTECHNICA SLOVENICA objavlja članke s področij: mehanika zemljin in kamnin, inženirska geologija, okoljska geotehnika, geosintetika, geotehnične konstrukcije, numerične in analitične metode, računalniško modeliranje, optimizacija geotehničnih konstrukcij, terenske in laboratorijske preiskave.

Revija redno izhaja dvakrat letno.

AVTORSKE PRAVICE

Ko uredništvo prejme članek v objavo, prosi avtorja(je), da prenese(jo) avtorske pravice za članek na izdajatelja, da bi zagotovili kar se da obsežno razširjanje informacij. Naša revija in posamezni prispevki so zaščiteni z avtorskimi pravicami izdajatelja in zanje veljajo naslednji pogoji:

Fotokopiranje

V skladu z našimi zakoni o zaščiti avtorskih pravic je dovoljeno narediti eno kopijo posameznega članka za osebno uporabo. Za naslednje fotokopije, vključno z večkratnim fotokopiranjem, sistematičnim fotokopiranjem, kopiranjem za reklamne ali predstavitvene namene, nadaljnjo prodajo in vsemi oblikami nedobičkonosne uporabe je treba pridobiti dovoljenje izdajatelja in plačati določen znesek.

Naročniki revije smejo kopirati kazalo z vsebino revije ali pripraviti seznam člankov z izvlečki za rabo v svojih ustanovah.

Elektronsko shranjevanje

Za elektronsko shranjevanje vsakršnega gradiva iz revije, vključno z vsemi članki ali deli članka, je potrebno dovoljenje izdajatelja.

ODGOVORNOST

Revija ne prevzame nobene odgovornosti za poškodbe in/ali škodo na osebah in na lastnini na podlagi odgovornosti za izdelke, zaradi malomarnosti ali drugače, ali zaradi uporabe kakršnekoli metode, izdelka, navodil ali zamisli, ki so opisani v njej.

AIMS AND SCOPE

ACTA GEOTECHNICA SLOVENICA aims to play an important role in publishing high-quality, theoretical papers from important and emerging areas that will have a lasting impact on fundamental and practical aspects of geomechanics and geotechnical engineering.

ACTA GEOTECHNICA SLOVENICA publishes papers from the following areas: soil and rock mechanics, engineering geology, environmental geotechnics, geosynthetic, geotechnical structures, numerical and analytical methods, computer modelling, optimization of geotechnical structures, field and laboratory testing.

The journal is published twice a year.

COPYRIGHT

Upon acceptance of an article by the Editorial Board, the author(s) will be asked to transfer copyright for the article to the publisher. This transfer will ensure the widest possible dissemination of information. This review and the individual contributions contained in it are protected by publisher's copyright, and the following terms and conditions apply to their use:

Photocopying

Single photocopies of single articles may be made for personal use, as allowed by national copyright laws. Permission of the publisher and payment of a fee are required for all other photocopying, including multiple or systematic copying, copying for advertising or promotional purposes, resale, and all forms of document delivery.

Subscribers may reproduce tables of contents or prepare lists of papers, including abstracts for internal circulation, within their institutions.

Electronic storage

Permission of the publisher is required to store electronically any material contained in this review, including any paper or part of the paper.

RESPONSIBILITY

No responsibility is assumed by the publisher for any injury and/or damage to persons or property as a matter of product liability, negligence or otherwise, or from any use or operation of any methods, products, instructions or ideas contained in the material herein.